5-12-2023

Advancements in geospatial monitoring of structures

Jordan Keith Baldwin
Mississippi State University, jordanbaldwin81@gmail.com

Advancements in geospatial monitoring of structures

By

Jordan Keith Baldwin

Approved by:
Isaac L. Howard (Major Professor)
Philip M. Gullett
Stanley Woodson
Wenmeng Tian
Farshid Vahedifard (Graduate Coordinator)
Jason M. Keith (Dean, Bagley College of Engineering)

A Dissertation
Submitted to the Faculty of
Mississippi State University
in Partial Fulfillment of the Requirements
for the Degree of Doctor of Philosophy
in Civil Engineering
in the Richard A. Rula School of Civil and Environmental Engineering

Mississippi State, Mississippi

May 2023

Name: Jordan Keith Baldwin

Date of Degree: May 12, 2023

Institution: Mississippi State University

Major Field: Civil Engineering

Major Professor: Isaac L. Howard

Title of Study: Advancements in geospatial monitoring of structures

Pages in Study: 146

Candidate for Degree of Doctor of Philosophy

The need for advancements in geospatial monitoring of structures has evolved naturally as structures have become larger, more complex, and technology has continued to rapidly develop. Greater building heights generally lead to greater challenges for surveyors, limiting the practical use of traditional measurement methods. For this reason, a new complimentary method was developed and implemented to support elevation monitoring activities during construction of the Salesforce Tower in San Francisco, California. While some studies have explored the use of strain gauges to monitor strain development within individual members, the primary contribution of this work is that it presents a practical and proven to be implementable approach to estimating elevation changes throughout a multi-story reinforced concrete core wall tower during construction while utilizing strain measurements acquired at intermittent levels.

Construction in urban landscapes has the potential to impact existing infrastructure. Identifying and mitigating any associated construction impacts is critical to public safety and construction progress. The development of Automated Motorized Total Stations (AMTS) has provided an effective means to monitor deformations in structures adjacent to construction activity. AMTS provides real time results so that movements may be immediately identified and addressed. However, the design, implementation, management, and analysis of these systems

has frequently been problematic. Inadequate monitoring specifications have led to systems that fail to perform as intended even when project requirements were satisfied. A collection of monitoring specifications and AMTS projects have been reviewed to identify why certain problems have occurred and recommendations have been made to increase the probability of success on monitoring projects. A deformation monitoring approach that defines location specific threshold values based on a statistical analysis of baseline measurements is also presented in this dissertation. Identifying potential causes for monitoring specifications to fail to perform as intended and a deformation monitoring approach that defines location specific threshold values are secondary contributions of this dissertation.

DEDICATION

This dissertation is dedicated to my family. Specifically, my fun-loving and carefree wife Jessica, who helps me realize balance when my obsession with organization and structure consumes me; my son Stetson, a smarter and soon to be taller version of myself who reminds me that games and play are indeed an important part of life; and finally, my beautiful, caring, creative, and intelligent daughter Hayden, who has blessed me with a new understanding of love, kindness, and life itself.

Thank you all for supporting me and enduring the seemingly endless nights and weekends that this process unapologetically demanded of me. I promise the time apart will be made up for and then some. *– January 2020*

ACKNOWLEDGEMENTS

First and foremost, I would like to express sincere gratitude to my major professor, Dr. Isaac L. Howard. His genuine support, encouragement, and guidance was given selflessly at a time it was needed the most, and I am eternally grateful. I would also like to thank my committee members, Dr. Philip Gullett, Dr. Stanley Woodson, and Dr. Wenmeng Tian, for contributing their valuable time, feedback, and support.

Additionally, I would like to thank to the Salesforce Tower core wall project surveyor Kevin Stein and project manager Jim Klinger for supporting the design, installation, and validation of the strain-based elevation monitoring system.

TABLE OF CONTENTS

LIST OF TABLES

LIST OF FIGURES

CHAPTER I

INTRODUCTION

1.1 Introduction and Background

Continuous advancements have been made, particularly over the past three decades, in monitoring infrastructure; including effectiveness, technologies employed, and frequency of implementation. In general, structural monitoring is an activity that utilizes sensors to better understand behavior and identify inconsistencies or changes that may otherwise be unrecognizable early on. If deficiencies are appropriately identified, precautions may be implemented to protect the structure, surrounding infrastructure, and the public. The metrics derived from various sensors and instrumentation may be categorized as either *localized* or *geospatial*. *Localized* sensors and instrumentation, such as strain gauges, inclinometers, and accelerometers, provide metrics for a discrete location, whereas *geospatial* sensors and instrumentation, such as Global Navigation Satellite Systems (GNSS), total stations, and laser scanners, provide reference to positional relativity between measured locations. Implementation of sensors and instrumentation of varying types is often favorable so that redundancy and output validation is available.

There are structures being built in present day that are larger and more complex than any before, limiting the practical use of traditional measurement methods. For this reason, a new complimentary method that combines localized and geospatial monitoring was developed and implemented to support elevation monitoring activities during construction of the Salesforce

Tower in San Francisco, California. While some studies have explored the use of strain gauges to monitor strain development within individual members, the primary contribution of this work is that it presents a practical and implementable approach to estimating elevation changes throughout a multi-story reinforced concrete core wall tower during construction while utilizing strain measurements acquired at intermittent levels.

Construction in urban landscapes has the potential to impact existing infrastructure. Identifying and mitigating any associated construction impacts is critical to public safety and construction progress. The development of Automated Motorized Total Stations (AMTS) has provided an effective means to monitor deformations in structures adjacent to construction activity. AMTS provide real time results so that movements may be immediately identified and addressed. However, the design, implementation, management, and analysis of these systems has frequently been problematic. Inadequate monitoring specifications have led to systems that fail to perform as intended even when project requirements were satisfied. A collection of monitoring specifications and AMTS projects have been reviewed to identify why certain problems have occurred and recommendations have been made to increase the probability of success on monitoring projects as a second and lesser contribution of this work. A deformation monitoring approach that defines location specific threshold values based on a statistical analysis of baseline measurements is also presented in this dissertation.

1.2 Organization of Study

This dissertation is organized into eight chapters. The first is an introduction to the general area of focus of the dissertation and the last presents overall conclusions and recommendations for future work. The second chapter is a general introduction to a variety of monitoring systems and methods. Chapters 3 through 5 are considered the first content

component, focusing on the use of sensors to monitor deviations within a construction project. Chapters 6 and 7 are considered the second content component, focusing on the use of sensors to monitor deviations outside a construction project.

Chapter 3 reviews a strain-based approach to support elevation monitoring efforts during construction of tall buildings. Limitations are discussed and recommendations are made to improve data reliability. Chapter 4 investigates the theoretical development of strains within segments of a reinforced concrete core wall. Since sensors are not likely to be installed within every level of a tower, the implications of approximating changes between instrumented levels are considered. Chapter 5 presents the implementation of an elevation monitoring system during construction of the 1,070 foot (326 m) tall Salesforce Tower in San Francisco, California. Results are presented and compared with conventional survey measurements. Content in Chapter 5 was presented at the American Concrete Institute (ACI) convention in Las Vegas, Nevada in October of 2018. A manuscript containing content from Chapters 3 through 5 has been submitted to a peer reviewed journal for consideration.

Chapter 6 investigates current trends and deficiencies in deformation monitoring practices adjacent to construction activity. Based on these observations, guidelines for increased effectiveness when utilizing Automated Motorized Total Station (AMTS) instrumentation are presented. Chapter 7 reviews AMTS derived monitoring data acquired during excavation operations for a project in Brooklyn, NY, discusses how it may be effectively used, and presents a method to statistically model baseline behavior. A manuscript containing content from Chapters 1 and 7 has been submitted to a peer reviewed journal for consideration.

CHAPTER II

OVERVIEW OF STRUCTURAL MONITORING SYSTEMS

2.1 Introduction

Structural monitoring has been identified as a useful and important activity in a variety of situations. Performance monitoring (PM) during and after construction provides valuable feedback to engineers, demonstrating if a structure is behaving as expected. Design model limitations or simplifications may lead to full-scale performance that differs from design (Li et al, 2006). In-service monitoring (IM) of structures, such as bridges and dams, may assist with identifying deficiencies that need attention. Of the more than 617,000 bridges that currently exist across the United States, 42% are at least 50 years old and 7.5% are considered structurally deficient while approximately 17% of the more than 91,000 dams nationwide have been labeled as having high-hazard-potential (ASCE 2021). Construction monitoring (CM) can be especially crucial since new construction has the potential to unintentionally impact existing infrastructure, particularly in urban environments (Moss and Mathews, 1995). A Zone of Influence (ZOI) emerges when construction activity commences, and stresses are applied to the surrounding environment. The extent and magnitude of influence depends on the proximity of the proposed activity, the type of activity, local environmental and geological parameters, as well as the location and type of existing infrastructure. Each component of infrastructure may be affected differently within the ZOI and therefore needs to be individually evaluated. When the degree of influence is great enough, negative, or even damaging effects may result. Whether the type of

construction involves tunneling, excavating, pile driving, blasting, or some other influential activity, adjacent structures, roads, bridges, railways, slopes, pipelines, or other infrastructure may have serviceability or safety compromised. Examples of influence include ground loss and ground movements resulting from changes in the state of stress within the ground mass. Such construction induced disturbances may cause structures to settle and shift, roads and railways to misalign and deform, pipelines to bend, displace or rupture, or slopes to weaken and fail (Attewell et al., 1986; Boscardin et al., 1989).

Events from recent years demonstrate the need for continually broadened monitoring applications. Fatal collapses such as the De la Concorde overpass in Canada, the I-35W Mississippi Bridge in Minnesota, the Florida International University pedestrian bridge, and the Champlain Towers South condominium in Surfside, Florida could be examples for effective use of monitoring systems. Perhaps not catastrophic but certainly significant is the settlement and tilt of the Millennium Tower in San Francisco, California. Recent analyses suggest adjacent dewatering activity may have contributed to the problem (Wagner et al, 2022). A carefully designed and implemented monitoring system that correlated movement with adjacent activity in real-time may have provided more understanding earlier on.

2.2 Monitoring System Applications

The necessity of early monitoring programs becomes particularly apparent when construction activities presented a hazard to sensitive heritage type buildings. For instance, the Mansion House, the official residence of the Lord Mayor of London, developed cracks on the east wall following excavation of a pedestrian tunnel underneath the building in 1988. Subsequent tunneling near the building in 1989 also caused a large piece of plaster to fall from the ballroom ceiling. It was at this time that officials decided that it would be beneficial to

implement a monitoring plan prior to additional nearby tunneling activities associated with a planned underground railroad extension. Crack widths were monitored, and a water-leveling system was put in place to monitor differential building movement (Price et al., 1994). Over the years, monitoring system methods and applications have expanded greatly. The following sections detail some performance, in-service, and construction monitoring applications that have transpired over the past couple of decades, as summarized in Table 2.1.

Table 2.1 Monitoring System Application Examples

Monitoring Category / Authors	Structure Monitored	Sensor Category	Sensors/Instruments Utilized	Evaluation Reference
Performance Monitoring (PM)				
Watson et al. (2007)	Bridge	Geospatial	GNSS; total station	Model
Abdelrazaq (2012)	Building	Localized & Geospatial	GNSS; total station; inclinometer; strain gauge	Model
Ha and Lee (2016)	Building	Localized & Geospatial	Total station; laser scanner; strain gauge	Model
Leica Geosystems (2019)	Building	Localized & Geospatial	GNSS; total station; inclinometer	Model
In-Service Monitoring (IM)				
Li et al. (2006)	Building	Localized & Geospatial	GNSS; accelerometer	Model
Alba et al. (2006)	Dam	Geospatial	Total station; laser scanner	N/A
Eschmann and Wundsam (2017)	Bridge	Geospatial	Camera; laser scanner	N/A
Yang et al. (2016) and Weissgerber et al. (2017)	Building	Geospatial	InSAR; total station; strain gauges	N/A
Whitlow et al. (2019)	Bridge	Localized	Infrasound; accelerometer	N/A
Construction Monitoring (CM)				
Koutsoftas et al. (2000)	Building	Localized & Geospatial	Total station; inclinometer; strain gauge	Model
Kaalberg et al. (2003)	Building	Geospatial	AMTS	N/A
Roy and Gouvin (2007)	Building; rail; tunnel; bridge	Geospatial	AMTS	N/A
Bao et al. (2018)	Building	Geospatial	GNSS	N/A

2.2.1 Performance Monitoring (PM)

Watson et al. (2007) used GNSS receivers to monitor the performance of a 206-meter-long cable-stayed bridge in northern Tasmania, Australia. Deflections of both the bridge deck and tower were monitored during vehicular loading and compared to modeled responses. Bridge deck deflections agreed well with the model, but tower deflections were nearly double in magnitude. Conventional total station survey measurements were also collected and validated the deflections observed. Further investigation revealed the model did not adequately account for increases in bridge deck stiffness due to prestressing, underestimated the vehicular load mass, and overestimated the rigidity of the tower frame. The observed deflections provided a means to identify and validate these discrepancies, highlighting the value of performance monitoring.

Abdelrazaq (2012) designed, implemented, and reported on an extensive monitoring program during construction of the Burj Khalifa, currently the tallest building in the world, standing 828-meters tall and situated in Dubai, UAE. The program consisted of monitoring foundation settlement, concrete strain development, wall and column shortening, lateral displacement of the tower, dynamic characteristics, and weather conditions. Substantial tower movement was expected due to wind excitations, large and concentrated crane loads, foundation settlement, column shortening due to elastic, creep, and shrinkage effects along with daily temperature fluctuations (150mm change in building height over 6-hour period), uneven solar effects causing tilt, and lateral drift of the building under gravity loads due to asymmetrical load distribution relative to the tower center of rigidity. A combination of localized and geospatial sensors and instrumentation were applied to the comprehensive monitoring program. A GNSS system in combination with inclination sensors assisted in providing a real-time position of the tower relative to the theoretical design position. Total stations and targets were used in

conjunction with the GNSS system to monitor tower settlement and shortening. Strain gauges were embedded within select concrete members so that strain development could be compared with predicted values. A three-dimensional finite element model was also developed to compare measured settlement and displacements. The monitoring program was generally regarded as a useful source of information throughout the construction process that provided a continuous indication of structural response and a basis for modifications to construction techniques to ensure expected performance was maintained.

Ha and Lee (2016) instrumented and monitored strain development during construction of the Ilham Baru Tower, a 274-meter-tall building in Kuala Lumpur, Malaysia. Strain gauges were embedded into multiple columns at the base of the tower to capture localized strain development so that it could be compared with predicted values. Geospatial monitoring of tower movement and settlement of the mat foundation was accomplished by periodic total station surveys. Laser scans of the tower were also conducted to compliment the conventional survey results. Predicted tower movement was modeled and compared with monitoring data. The predicted performance model was updated multiple times throughout construction based on actual measurement values and concrete testing. The construction team was provided continuous feedback on tower movement and compensation plans were adjusted accordingly.

Leica Geosystems (2019) reported on performance monitoring methods that were utilized during construction of the 426-meter-tall tower located at 432 Park Avenue in New York City. What makes this tower particularly unique is its slender profile. Although it barely stands half as tall as the Burj Khalifa, the 814 square meter footprint is only about one-tenth of Burj Khalifa. Responses from imposed forces, such as lateral wind pressures and eccentric crane loads, cause slender towers to experience significant lateral movement, complicating construction along a

vertical alignment. A system that combined localized inclinometer and geospatial GNSS monitoring provided surveyors regular feedback on positions at the top of the tower. Continuous movement compensation was then used when laying out new levels of the tower with total station instrumentation, allowing for construction to proceed along the intended alignment.

2.2.2 In-Service Monitoring (IM)

Li et al. (2006) explored the complimentary characteristics of a GNSS receiver and an accelerometer sensor, when monitoring a 108-meter steel tower in Tokyo, Japan. Accelerometers are useful for understanding the dynamic response of structures but are limited when it comes to identifying static and quasi-static displacements. Several applications have shown that GNSS receivers can successfully measure dynamic motion (Lovse et al., 1995; Ashkenazi et al., 1997; Celebi, 2000; Im et al., 2011), but become limited at higher frequencies. Tower performance was monitored during loading from a typhoon event and an earthquake event. As expected, the results indicated that the GNSS receiver was able to monitor static displacements that were not identified by the accelerometer readings, and that the GNSS receiver generally registered lower-end frequencies while the accelerometer readings registered higher-end frequencies, with some overlap. The results validated the complementary nature of the system, while indicating some level of redundancy. Anticipated structural response of the tower was also modeled and generally agreed when compared with monitoring results. This GNSS-accelerometer hybrid sensor approach has also been noted as benefiting the monitoring of bridges (Raziq and Collier, 2007; Roberts et al., 2004).

Alba et al. (2006) monitored the Lake Cancano dam located in Valtellina, Italy using a terrestrial laser scanner. Scans of the downstream face of the 136-meter tall and 381-meter-long concrete arch dam were completed in October and again the following May. Unlike traditional

total station measurements that collect positions of discrete targets, laser scanners collect a dense cloud of points over a surface. Since individual point measurements cannot be easily compared to previous measurements, point cloud data must first be processed into a surface mesh through computer modeling. Differences between these models indicated horizontal deformations inward toward the lake, primarily concentrated near the dam's center. The water surface elevation was reported to be lower during the second scan, resulting in reduced pressures. Total station measurements taken at the crest of the dam also validated the scan results. However, errors were identified within the scan data, particularly when incidence angles between the instrument and dam surface were small.

Eschmann and Wundsam (2017) explored use of unmanned aircraft systems (UAS) for bridge inspection and monitoring. Bridge height, span, and location often make access for inspection difficult. UAS may be equipped with high-resolution cameras, infrared sensors, and laser scanners. To demonstrate the capabilities of such a system for inspection and monitoring, a UAS was used to collect data on a 43-meter tall, 319-meter-long segmental box girder bridge. Post-processing was required to stitch together thousands of photographs captured and develop a three-dimensional model. The model illustrated the detection of cracks that could be periodically monitored as well as the associated intrusion of moisture by use of the infrared sensor. Although there were no follow up inspections presented, the author demonstrated the potential use of this method for ongoing monitoring purposes.

Yang et al. (2016) and Weissgerber et al. (2017) presented on an emerging use of a satellite-based measurement method called Interferometric Synthetic Aperture Radar (InSAR). Imagery is generated by measuring the time it takes to reflect radar signals off a targeted area and back to the satellite. Multiple images of the same area acquired over time can then be

compared to identify changes (Zebker & Villasenor, 1992). This technology has primarily been used to monitor land movement over large areas for the past two decades, but recent developments in analysis techniques has prompted research into the use of InSAR in modeling and monitoring structures. Yang et al. (2016) monitored the Bohai Building and the China Theater, two landmark buildings in Tianjin, China, over the course of six months. Targets were concurrently installed and measured using conventional total station methods for comparison. Agreement between the two methods was observed, although the InSAR data presented a lower level of accuracy when compared to conventional survey results. Weissgerber et al. (2017) similarly used InSAR data to monitor the Eiffel Tower along with several other towers in Paris, France over a four-year period. General agreement was observed when compared with deformation estimates derived from strain gauges.

Whitlow et al. (2019) investigated the feasibility of using infrasound technology to uniquely perform non-contact and nonline-of-sight monitoring of bridge dynamic characteristics. Infrasound involves acoustics below 20 Hz, which makes it useful for monitoring natural frequencies of structures. Three multi-sensor infrasound arrays were used to monitor behavior of the Feather River bridge in northern California. Frequency data packets were processed and filtered to estimate the direction from which the signals originated. Concurrent processing from the three stations allowed for triangulation of the signals, which corresponded with bridge location. Accelerometers were also installed along the bridge span for comparison. Agreement was observed, although some of the lower frequencies were overwhelmed by higher frequencies in the accelerometer dataset, indicating a unique benefit to infrasound monitoring. Additionally, multiple sources were detected during data collection, indicating the potential for broader range

monitoring (Whitlow et al., 202). However, multiple source detection also presented challenges and limitations when analyzing competing frequencies.

2.2.3 Construction Monitoring (CM)

Koutsoftas et al. (2000) reported on a comprehensive monitoring plan developed during deep soft soil excavations for the MUNI Metro Turnback (MMT) project in downtown San Francisco, California. The excavations planned to pass near a block of old and historic buildings that could be sensitive to ground movement. The structures were modeled, ground deformations were estimated, and a shoring plan was designed to limit negative impacts. A testing section was heavily instrumented to compare estimations with actual results. If necessary, adjustments could be made to the program to keep deformations within tolerable limits. A variety of sensors and instrumentation were utilized in an effort to understand the potential impact from the excavation and pile driving activities. Surface and subsurface settlement markers were installed and conventionally surveyed to monitor vertical ground deformation and the buildings were also outfitted with inclinometers and strain gauges. Results generally confirmed that deformation estimates from the design phase were reasonable and that excessive deformations were not encountered during construction.

Kaalberg et al. (2003) reported on a 3.8-km long underground railway project in Amsterdam, Netherlands, which consisted of excavation and tunneling activity throughout a historic part of the city. Due to the scale of the project and sensitivity of older infrastructure, more than 1,200 buildings were designated to be monitored for structural deformations. Monitoring of structural deformations has been observed to be one of the most effective ways to understand structural response, particularly due to external influence (Ding et. al., 2000). Deformations of a structure can be defined as a relative change in form or position with respect

to its original state, requiring repeated observations over time. Conventional surveying methods have historically been used to acquire these types of measurements but are prohibitive at this scale. Kenchington (2003) observed that automated and autonomous monitoring systems may incur higher upfront costs, but when implemented and managed appropriately, can produce large quantities of high accuracy data at low cost. Automated Motorized Total Stations (AMTS) were implemented on this project for this purpose. AMTS instruments acquire measurements in the same fashion as their unautomated counterparts, except that they are permanently stationed and programed to repeatedly observe a list of targets. The target positions can be wirelessly transmitted and graphed in real-time, allowing for near-immediate deformation recognition. Ultimately 74 AMTS instruments were used to monitor 7,500 targets throughout the project area. Twelve months of baseline measurements were recorded prior to construction to identify natural fluctuations, settlement, and seasonal movement.

Roy and Gouvin (2007) reported on multiple projects that utilized AMTS for construction monitoring. Residential buildings situated above a sewage tunnel that were originally constructed in 1924 in Los Angeles, were monitored during rehabilitation efforts. A rail line in Minnesota was monitored during construction of an underpass. Track positions were transmitted hourly and multiple early warnings of movement were provided. Foundation construction above and adjacent to the Queens Midtown Tunnel required monitoring of tunnel movement. Accurate and repeatable measurements were observed but the instrument scope required periodic cleaning. A new rail line below the Dulles International Airport Main Terminal in Virginia required underpinning and monitoring of the existing foundation. The AMTS instrument was mounted on the control tower to maximize line of sight and measurements were collected over the three-year project duration. The historic Bellevue Hospital in New York City was monitored after adjacent

construction caused settlement of two adjoining buildings. Fifty targets along the building façade were monitored for both settlement and upward movement as previous settlement was jacked and stabilized. The construction of the Memorial Sloan Kettering Cancer Center, located New York City, required a 25-meter-deep excavation within 50 millimeters of an adjacent 80-year-old brick and masonry church as well as a nine-story apartment building. An AMTS was mounted on the roof top of a four-story building directly across the street from the site and 50 targets were mounted to the three adjacent buildings and monitored. Movement of the AMTS instrument was observed, reinforcing the importance of a stable pedestal when monitoring.

Bents of an existing bridge required monitoring during pile driving activities for a replacement bridge in Long Island, New York. Since the project duration exceeded six months, results of a cost analysis by the contractor led to the implementation of an AMTS monitoring system in lieu of repeated manual surveys. Ten targets were installed and monitored multiple times per day. Monitoring data was consistent and useful, but the instrument was not well protected and suffered damage from salty air. Four active subway tunnels required monitoring during excavation operations in New York City. Multiple targets were monitored from each instrument for 12 months before operations were paused for a period of three years due to a lack of funding. Upon resuming the monitoring program, the instruments required calibration and cleaning after subway car break dust had been found to have worked through the seals. A tunneling project that connected two major subway lines between Chicago's Midway and O'Hare airports required monitoring of pre-1900 historic buildings and adjacent tunnels and excavations. Cost savings for an automated versus manual monitoring approach in this case was estimated to be at least 60%. Lastly, the renovation of a 100-year-old masonry building prompted monitoring of a wall, emphasizing the usefulness of AMTS on small scale projects.

Measurements were taken at short distances and were observed every 15 minutes to provide rapid feedback.

Bao et al. (2018) installed GNSS receivers on the two 100-meter-tall Kunlun Towers in Beijing, China, when an adjacent development located within meters of the west tower's pile foundation initiated a 250-meter-long, 130-meter-wide, and 20-meter-deep excavation. This application of GNSS receivers for monitoring purposes is particularly unique because they were installed as stand-alone units. Monitoring with GNSS receivers has traditionally been accomplished by a relative positioning approach, which uses simultaneous observations from a monitoring receiver and a stable reference receiver. Since no stable reference exists in a stand-alone scenario, long-term tectonic drift must be accounted for. Historical and present data from three local GNSS stations in Beijing were analyzed to develop a local reference frame. Two years of measurements were collected and adjusted for movement identified in the reference frame. Seasonal motions were also identified in the measurement datasets, likely resulting from variations in ground water level, surface water loading, snow loading, soil moisture, and bedrock thermal expansion. The fluctuations were subsequently identified and removed by fitting sinusoidal trends to the observations. The results indicated a maximum tilt in the tower foundations of less than 10-mm with a horizontal accuracy of 2- to 3-mm.

2.3 Monitoring System Advancements

Challenges faced during tall building construction prompted the development of a unique performance monitoring approach that utilizes both localized and geospatial measurements. The following three chapters detail the review, development, and implementation of a strain-based elevation monitoring system during construction of the Salesforce Tower in San Francisco, California.

As indicated in Table 1, reference modeling is not often practical or feasible for in-service and construction monitoring. The general purpose of these types of monitoring applications is to identify changes in structural behavior that may eventually prove problematic. When modeled references do not exist, results are sometimes evaluated against arbitrarily defined threshold values that do not necessarily consider the distinctive and natural behavior of the structure or component. Chapters 6 and 7 of this dissertation review critical components of monitoring specifications and explores the statistical evaluation of baseline measurements to define what constitutes abnormal or significant changes in behavior while monitoring.

CHAPTER III

REVIEW OF STRAIN-BASED ELEVATION MONITORING DURING TALL BUILDING CONSTRUCTION

3.1 Introduction

This chapter provides a review of a strain-based elevation monitoring system that was developed during construction of the Salesforce Tower in San Francisco, California. The project required frequent measurements throughout a narrow core of a tower that peaked nearly 300 m above ground level. Anticipated complexities associated with this process prompted interest in an additional measurement tool that could complement conventional total station measurements. The following paragraphs highlight the need for work of this nature.

Tall buildings serve an obvious functional purpose as population density continues to rise in cities, but are also a symbol of economic growth, status, and power (Domosh, 1988). As a result, tall building construction continues to expand worldwide in both frequency and height. According to the Council on Tall Buildings and Urban Habitat [CTBUH] Skyscraper Center (2022), nearly half of the 100 tallest buildings standing today were constructed within the past five years and the number of buildings constructed per year that reach heights of 300 m or more, known as 'supertall' buildings, has grown significantly over the past the two decades from a five-year rolling average of one in 2003 to twenty-one in 2022 (Figure 3.1).

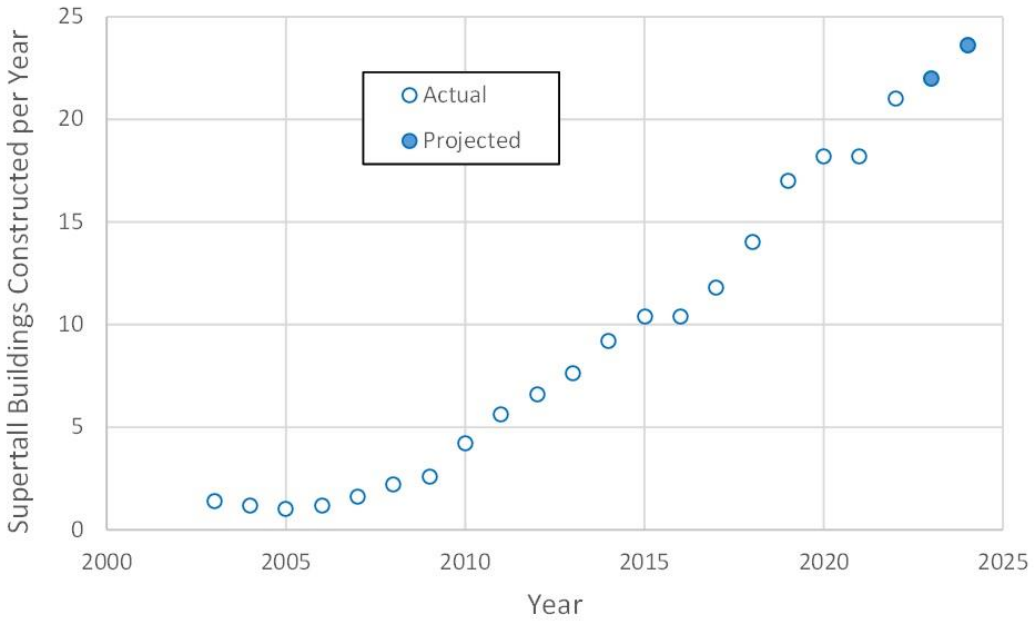

Figure 3.1 Number of Supertall Buildings Constructed per Year, based on a 5-year rolling average (CTBUH Skyscraper Center, 2022).

Additionally, the incredible feat of 'megatall' construction, reaching 600 m or more, is gaining traction with three fully constructed buildings to date, two currently under construction, six planned for construction, and 52 more in conceptual design. These statistics indicate that the design and construction of 'supertall' and even 'megatall' buildings is not only relatively new but is rapidly developing. Conventional approaches to elevation monitoring during construction of tall buildings are becoming increasingly complex, suggesting additional measurement methods may be useful. Review of a strain-based approach is presented herein, and recommendations are made to improve measurement reliability.

3.2 Background

Accurate measurements are critical to the successful completion of any building project. Dimensional inconsistency can lead to structural members not fitting as designed or may lead to serviceability problems with architectural components. For instance, if a core wall level is constructed too high or low, exterior column heights may not match resulting in uneven floor levels. Even if constructed as intended, building elements will inevitably deviate from their initial constructed dimension or position, further complicating the measurement process. Vertical shortening occurs when members are stressed, and as concrete matures. Shortening is also cumulative so that a given floor level is subjected to changes in elevation caused by the sum of shortening occurring within all lower levels. Shortening on the order of 1 to 3 mm per story is commonly observed during construction. Differential shortening may also occur between the core of a tower and the perimeter frame, generally caused by differences in stresses, geometry, and material properties (Heiman et al., 1980). Differential shortening may cause distortions in partition walls and damage to elevator guide rails, facades, claddings, finishes, mechanical, and plumbing components (Fintel et al., 1987).

To avoid undesirable consequences, frequent adjustments to story heights must be made (Choi et al., 2013). Compensation plans, based on estimates or prediction modeling, are often incorporated into the design so that floor or column heights may be incrementally adjusted (Fragomeni et al., 2014). Since estimates and prediction modeling have been found to produce variability when compared to experimental results, conventional measurements are still generally necessary (Goel et al., 2007; Habrah & Abu-Tair, 2017).

During construction of tall buildings, elevations are benchmarked at intermittent levels throughout the height of the tower. As construction proceeds upward, benchmarks are used as

reference to ensure each new story is correctly built to the designed elevation. The accuracy of benchmark elevations is affected throughout construction as a building shortens due to the development of axial strain. Conventional methods, such as steel tape, total station, and GNSS (Global Navigation Satellite System) have traditionally been used to monitor benchmark elevations (Ghilani, 2018). The practical application of these methods is limited by tower height. The labor necessary to repeatedly traverse up and down a tall tower with steel tape or total station instruments can become extensive and line of sight and visibility complications become more pronounced. Conversely, due to reduced obstructions, GNSS receivers generally perform better at greater heights. Strain-based elevation monitoring is not necessarily limited by height and was developed to compliment these current methods during construction of the Salesforce Tower in San Francisco, CA. While some studies have explored the use of strain gauges to monitor axial strain development within individual members, the primary contribution of this case study is that it presents a practical approach to estimate elevation changes throughout a multi-story reinforced concrete core wall tower during construction.

3.2.1 Complexities of Concrete Structures

All buildings will experience some degree of shortening due to the compression of supporting structural elements. This response in steel structures, for example, presents a challenge for surveyors but is reasonably predictable (Greulich & Rober, 1988). Conversely, concrete structures have a response that evolves over time.

Concrete has become a critical component to constructing sustainable and resilient buildings (Hajek & Fiala, 2018). Concrete is a non-homogenous mixture primarily consisting of cement, water, and aggregates; supplementary cementitious materials such as fly ash and additives such as water reducers are also often present in modern concrete mixtures (American

Concrete Institute [ACI] Committee 212, 2016). Concrete continues to mature through a process of chemical reactions between the cementitious particles and water, called hydration. Although most of the process transpires within weeks, it can continue for years, and concrete may never attain full maturity. Water particles also slowly evaporate to the environment over time causing the volume of the member to reduce. This process is known as drying shrinkage and generally follows a logarithmic trend, meaning the rate of change slows over time. Drying shrinkage is generally responsible for the majority of shortening that occurs during the first few months after placement. Creep also contributes to a reduction in volume and can be defined as the time-dependent deformation of concrete under a sustained stress (Neville, 2011).

Shrinkage and creep effects are complex and difficult to predict since they depend on several parameters such as concrete composition, concrete age when loaded, magnitude of load, temperature, humidity, volume-to-surface ratio, and time. Any variations in these parameters can affect the shrinkage and creep behavior. Unless the members are contained, fluctuating environmental conditions are particularly difficult to anticipate (Schindler & Folliard, 2005).

Vertical shortening of concrete members is a cumulative process consisting of immediate and time-dependent strains which begin during construction and extend throughout the lifetime of the building. Shrinkage strain development is independent of load, begins when the member is cast, and continues to develop over time in a logarithmic fashion. When loaded, immediate compressive strains occur, and creep strains begin to develop over time. The total effects contributing to shortening in concrete members may be considered the sum of elastic strain (compressive), ε_e, shrinkage strain, ε_{sh}, and creep strain, ε_c (Bazant, 1988).

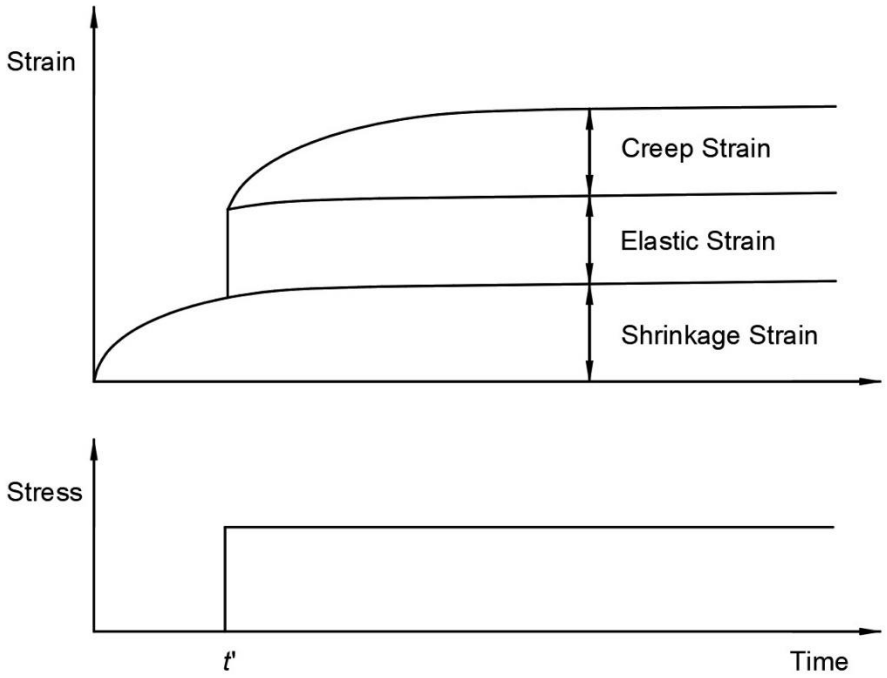

Figure 3.2 Concrete Strain Development.

Figure 3.2 illustrates the cumulative effect of each contribution of strain as a function of time with a load applied at a time equal to *t*'. If multiple instances of loading occurred, separate loading histories and creep strain curves would develop. The magnitudes of each strain contribution may be similar but are not necessarily equal (Bazant, 1988). Steel reinforcement will restrain some of these effects since the concrete and reinforcement strains must remain approximately equal. This is achieved through bonding of the reinforcement to the concrete. The amount of restraint depends on the amount of reinforcement that is present (Gribniak et al., 2013).

The majority of concrete shortening has been observed to occur within the first few months of placement (Fintel et al., 1987; Swamy & Arumugasaamy, 1978). Since much of this movement takes place during construction, adjustments must be made to member heights and

elevations throughout this period. While performing displacement monitoring during construction of the Burj Khalifa, Abdelrazaq (2012) observed shortening averaged approximately 2 to 3 mm per story, which required intermittent elevation adjustments to compensate for the recorded movements. Matar and Faschan (2017) reported on an incident where adjustments to column heights and elevations were neglected as construction proceeded upward. Consequently, the elevation of the upper floors of the 60-story building were found to vary by as much as 100 mm between individual columns.

3.2.2 Measurement Methods

The field of surveying and associated measurement methods are constantly evolving (Wolf, 2002). A variety of measurement methods have been implemented to establish and verify elevations during the construction of tall buildings. Benchmarks are often set incrementally throughout the height of a tower so they can be used as a convenient reference while avoiding measurements back down to the base. Due to tower shortening, the benchmark elevations need to be regularly updated. This can be accomplished by periodically measuring the height of the benchmark relative to the base of the tower. A change in height between two periodic measurements would indicate the magnitude of shortening that had occurred. The benchmark elevation can then be updated by applying the magnitude of shortening to the previously computed elevation.

Steel measuring tape has been long recognized as an accurate and reliable measuring tool. Elevator shafts are typically used to acquire these types of measurements since multiple floors can be spanned at a time. Measurement cycles, often conducted monthly, start from the base and span the height of the tower. Elevation benchmarks, typically set in the core wall every four floors or so, can then be updated based on measurement results. The entire measurement cycle

can take several days to complete, depending on the height of the tower at the time. Temporary obstructions, such as construction scaffolding, can impede the process. Temperature adjustments must also be made since the steel tape will contract and expand with thermal changes (Cronin, 2020; Ghilani, 2018; Sullivan, 2020).

Control networks, which contain a series of reference points, are typically established around the perimeter of a tower prior to construction and serve as the basis of control throughout construction. These reference points are primarily set at ground level but may also be attached to adjacent buildings. Direct observation between ground control and the tower can be made using total station instrumentation. This type of observation becomes limited as visibility is reduced. This limit was reached at approximately 275 m during construction of the Salesforce Tower.

Modern tower construction commonly consists of a reinforced concrete core with a steel framed skeleton covered in glazing. Construction of the core typically leads the steel by about ten levels, trailed by the glazing about another ten levels. Since exterior observation is no longer possible once the glazing is in place, lower levels in the tower cannot be remeasured using this method unless a survey is traversed internally through the tower. This process can be time intensive due to the narrow confines of the shaft.

Global Navigation Satellite Systems (GNSS) specifically tailored to improve horizontal positioning capabilities have been developed and implemented on several projects with reported success (Hayes et al., 2006; Baker et al., 2007; van Cranenbroeck et al., 2009; Abdelrazaq, 2012; Leica Geosystems, 2019). The GNSS receivers are typically attached to the form system and advance upward as each level of the core is poured. These systems provide an additional level of redundancy to ensure tower plumbness is maintained. Another benefit of these systems is that each measurement is independent of the last, meaning error propagation is not a factor.

However, accuracy in the vertical component is limited since satellites cannot be observed below the horizon. Wide and opposing angles between satellite signals and a receiver is considered a key component to accuracy in positional solutions. This can often be accomplished in the horizontal plane but is considered weaker in the vertical since opposing signals cannot be obtained from the opposite side of the earth's core (Ghilani, 2018). These differences lead to measurement errors in the vertical that are approximately double the horizontal, which is commonly observed to be on the order of ± 5 mm to ± 15 mm (Oh, 2020). Consistent and accurate solutions may also be limited in dense urban environments. Satellite signals may bounce off adjacent buildings or may be blocked entirely. Due to minimal obstructions, a GNSS system was successfully implemented during construction of the Salesforce Tower as the primary measurement source of horizontal positioning of each new constructed level as well as a secondary measurement source for elevation control.

Another emerging satellite-based measurement method called Interferometric Synthetic Aperture Radar (InSAR) has been used for the past two decades primarily to monitor land movement over large areas. Imagery is generated by measuring the time required to reflect radar signals off a targeted area and back to the satellite. Multiple images of the same area acquired over time can then be compared to identify changes (Zebker & Villasenor, 1992). InSAR measurements detected approximately 2 mm of subsidence between 1992 and 1999 in the vicinity of a condominium building located in Surfside, Florida which ultimately collapsed in 2021 (Tejedor, 2021). Developments in analysis techniques has prompted research into the use of InSAR in modeling and monitoring structures (Li et al., 2020; Weissgerber et al., 2017; Yang et al., 2016). Technological advancements in aerial photogrammetry, unmanned aircraft system (UAS), and terrestrial imagery have also led to developments in structural monitoring (Kwak et

al., 2013; Eschmann and Wundsam, 2017; Lu & Lee, 2017). Similar approaches may also be beneficial when monitoring shortening within buildings during construction.

3.3 Strain-Based Measurements

Commensurate with the proverb "measure twice, cut once," there is a consensus among surveyors that measurement redundancy is crucial. Multiple sources are often necessary to ensure confidence in measurement results, particularly when inconsistencies are observed. Additionally, as project conditions change, some sources may become limited or entirely unusable, requiring a toolkit of measurement options.

Strain gauges have been periodically used to monitor strain development within concrete members and may also be a useful measurement source for surveyors. The three primary types of strain gauges produced are based on electrical, optical, or mechanical principles. Vibrating wire strain gauges are based on mechanical principles and have been commonly utilized in concrete applications. Changes in strain are measured by detecting frequency changes when the wire is tightened or relaxed. These gauges may be either embedded within a member or externally mounted. When installed appropriately, embedded gauges can maintain long-term stability (Potocki, 1958; van Oosterhout, 2003; Neild et al., 2005; Yu & Gupta, 2005). However, damage to embedded sensors is common during concrete placement. Encasing the sensors in briquettes has been suggested to provide a layer of protection, although these briquettes consume a larger volume which may lead to voids below them (Bakoss et al., 1977).

The elastic modulus of the briquette will almost always differ from the surrounding concrete even if it is made up of the same mix since it will be offset in age. Bakoss et al. (1977) estimated a 10% difference in elastic moduli would produce approximately 3% of error in strain readings, whereas a 30% difference in elastic moduli would produce approximately 8% of error

in strain readings. Reducing the time between casting briquettes and the structural member helps to minimize these effects. Externally mounted gauges avoid damage due to concrete placement, but can be susceptible to measurement error since the surface is more prone to cracking and greater strain variations as a result of direct environmental exposure (Beresford, 1970). These gauges are also exposed to potential damage by general construction operations.

Acquisition of field measurements utilizing strain gauges in tall concrete buildings began around the 1970s (Beresford, 1970). Studies conducted since then have primarily focused on comparing measured strain development with predicted values. In some cases, survey measurements and other sensors were concurrently implemented.

3.3.1 Strain Gauge Studies

Several studies have compared measured strains and displacements with predicted values. Creep and shrinkage development can be predicted using modeling criteria developed by Bazant & Baweja (2000) (B3), Gardner & Lockman (2001) (GL), American Concrete Institute Committee 209 (2008) (ACI), Comité Euro-International du Béton (1999) (CEB), and Bazant et al. (2015) (B4). Predictions are assumed to represent the average strain developed throughout a member. Parameters that are considered by each criteria vary but generally evaluate concrete mix or strength, member size, age at loading, humidity, and curing time. Prediction formulas were developed by each group by fitting specified parameters to databases of experimental results. Since the databases consist of specimens containing a wide array of properties, a similarly wide range of variability is generally observed when comparing predictions to experimental values. Statistical comparisons between prediction criteria indicate that each exhibit varying dependencies and sensitivities to input parameters (Goel et al., 2007). Zou et al. (2014) observed that prediction formulas are primarily based on testing of one-dimensional

prismatic or cylindrical specimens with small volume to surface ratios which may not directly apply to large volume to surface ratio members, such as core walls. The acquisition of core wall strain measurements within a variety of buildings may contribute to this body of work.

Heiman et al. (1980) and Brady (1985) reported on data collected over several years from embedded vibrating wire strain gauges in a reinforced concrete column of a 24-story tower in Sydney, Australia. The gauges were installed along the same column line at Levels 8, 12, and 20. Each instrumented level consisted of two gauges set within the outer thirds horizontally and at approximately mid-point vertically of the rectangular column. Survey targets were installed at Levels 9 and 14 and shortening between these levels was measured over time.

Due to significant construction delays, labor disputes, and accessibility issues, the first survey measurements were not captured until Level 12 was aged 476 days, where the strain gauge measurements were logged shortly after placement. Shortening values were then divided by the initial measured distance between targets so that averaged change in strain values could be compared to Level 12 measured changes in strain. A total of 19 measurements were made until Level 12 was aged 3,683 days at which time the change in strain of 702 με (microstrain) was recorded by gauges and the change in strain value determined by survey measurements was 784 με. Strain gauge measurements at Level 8 were also compared with ACI prediction values. At an age of approximately 1,600 days, a value of approximately 600 με was predicted and compared to a gauge measured value of 545 με. The gauges were considered durable, reliable, and provided sensible and accurate data. The strain data was beneficial since survey accessibility was difficult at times.

Abdelrazaq (2012) designed, implemented, and reported on an extensive monitoring program during construction of the Burj Khalifa, an 828 m reinforced concrete tower in Dubai,

UAE. The program primarily consisted of monitoring strains and shortening in vertical members. Wall and column shortening was monitored using conventional surveying methods, and strain development was monitored using embedded vibrating wire strain gauges. Wall and column shortening averaged 2 to 3 mm per story and measured strain development generally agreed with predictions.

Fragomeni et al. (2014) instrumented several reinforced concrete columns over multiple levels of an 80-story building on the Gold Coast of Australia using externally mounted vibrating wire strain gauges. The gauges were epoxied to the side of the columns near the top, bottom, and middle of the member. Measurement data collected from each column was scattered and varied approximately +/- 15%, on average. No consistent trends were identified in relation to the location of the gauges. Measured strains at each column resembled a logarithmic curve over time. The basement column gauge measurements averaged approximately 800 με between ages of 10 and 900 days. Total shortening of the basement column was estimated to be 1.8 mm by applying the average strain to the 2,250 mm column height.

Ha and Lee (2016) instrumented and monitored strain development during construction of the Ilham Baru Tower, a 274 m tall reinforced concrete building in Kuala Lumpur, Malaysia. Vibrating wire strain gauges were embedded at ground level within six columns along the perimeter, three columns beside the core, and five locations within the core region. Gauge measurements began shortly after placement and ranged between approximately 100 με and 280 με after 15 months. Higher strains were observed in columns at the front of the tower which corresponded with an observed lean. Prediction models were also developed based on ACI criteria coupled with shrinkage and creep test data. Modeling results were periodically compared

with gauge measurements so adjustments could be made to refine predictions. The final adjusted model predicted a total axial shortening of 144 mm.

Historically, strain gauges have generally been utilized to compare measured strain development with predicted values. When gauges were used to estimate wall or column shortening, either a single measured strain value or an average strain value obtained from multiple gauges within the member was applied to the total length.

3.3.2 Strain Profile

To better understand how strain gauge measurements may be interpreted to estimate shortening, the development of strain along the profile of a member will be examined. Due to self-weight, *q*, a vertically aligned member experiences greater total strain at its base than its top. If a simplified one-dimensional case of elastic strain is considered, the displacement, *u*, along the height of the member, *H*, with an applied stress, σ, would need to satisfy the following differential equation and boundary conditions:

$$\frac{d}{dz}\left(AE_c\frac{du}{dz}\right) + q(z) = 0 \tag{3.1}$$

$$\left(E_c\frac{du}{dz}\right)_{z=H} = \sigma \tag{3.2}$$

$$u(z=0) = 0 \tag{3.3}$$

If the density of the member is denoted as γ, and both the cross-sectional area, *A*, and elastic modulus, E_c, are considered constant, then strain and displacement profiles can be derived as:

$$\varepsilon(z,\sigma) = \frac{\sigma + \gamma H}{E_c} - \frac{\gamma}{E_c} z \tag{3.4}$$

$$u(z,\sigma) = \frac{\sigma + \gamma H}{E_c} z - \frac{\gamma}{2E_c} z^2 \tag{3.5}$$

These equations show the approximated strain profile exhibits a linear change with *z* while the displacement profile exhibits a non-linear change with *z*. The displacement at the top of the member can be related to strain by combining Equations [3.4] and [3.5] while setting *z* equal to *H*:

$$u(H) = \varepsilon(H)H + \frac{\gamma}{2E_c} H^2 \tag{3.6}$$

When a tower story is initially constructed, *p* equals zero since no loads have yet been applied, resulting in the strain (ε) equaling zero at *H*, per Equation [3.4]. Per Equation [3.6], initial member displacement becomes:

$$u(H,0) = \frac{\gamma}{2E_c} H^2 \tag{3.7}$$

Because concrete members are poured to fit a form with specific dimensions, initial shortening due to self-weight is inherently compensated through the form-fitting process. Construction of additional levels causes incremental increases of stress, strain, and displacement given by:

$$\Delta\varepsilon(z,\sigma) = \varepsilon(z,\sigma) - \varepsilon(z,0) = \frac{\sigma}{E_c} \tag{3.8}$$

$$\Delta u(z,\sigma) = u(z,\sigma) - u(z,0) = \frac{\sigma}{E_c} z \tag{3.9}$$

Combining, the column shortening becomes:

$$\Delta u(H,\sigma) = \Delta\varepsilon \cdot H \tag{3.10}$$

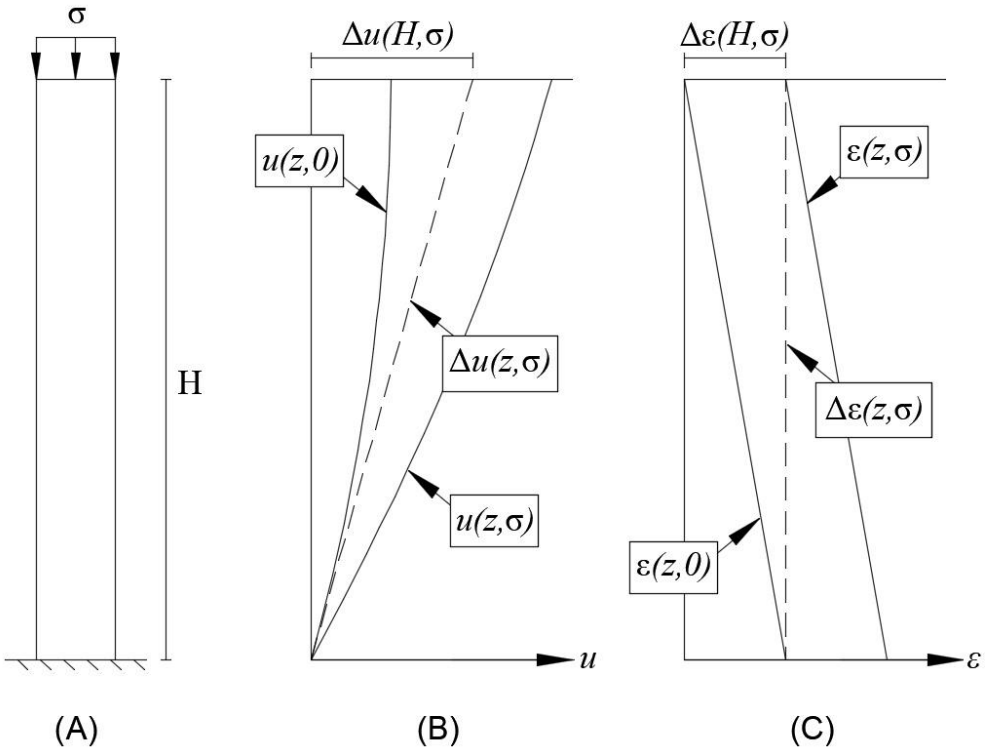

Figure 3.3 (A) Member profile, (B) displacement profile, and (C) strain profile

Figure 3.3 illustrates the displacement and strain profiles. Although incremental strain increases appear to be approximately linear, some variations are expected to exist throughout the

member. Zou et al. (2014) investigated and confirmed the existence of strain variations by fabricating and instrumenting a reinforced concrete wall in a laboratory. Both embedded and externally mounted strain gauges monitored strain development throughout the wall after applying a load. Embedded gauges generally measured lower values than the surface and gauges near the sides measured lower values than the center.

3.3.3 Concrete Strain Variations

Just as an athlete's pace will fluctuate throughout a marathon for a multitude of reasons, so will strain throughout a tower. If the bottom and top of a tower is analogous to the start line and finish line of a marathon, checkpoints may be considered analogous to conventional survey measurements in between. Incremental shortening can be periodically recorded along the tower height while providing a continuous reference to the bottom.

Unlike conventional means, each strain measurement is detached from the start and is completely independent of all other measurements. Since the only strain captured is along the length of the gauge, the quantity and spacing of gauges could greatly impact results. If 0.15 m gauges are spaced approximately every 37 m (every 8 stories), only 0.4% of the overall performance is captured (0.15 m long gauge / 37 m spacing = 0.4%). This would be similar to measuring an athlete's average pace over a length of 20 m at each checkpoint (20 m / 5,000 m = 0.4%). Since these measurements would be independent of each other and detached from the start, the athlete's overall race time could only be approximated. Most simply, a runner's pace could be considered constant between checkpoints, or performance between checkpoints could be adjusted based on known variables. For instance, if consecutive checkpoints consisted of relatively flat terrain, an average would not capture the impact of a steep incline in between. Estimates may be improved by accounting for the likelihood of decreased performance

resulting from the incline. While it is likely impossible to track all variables during tower construction, identifying some of the greatest influences may prove beneficial.

Strain variations will occur within reinforced concrete members for a variety of reasons. Drying shrinkage in concrete occurs when moisture exits as concrete pore humidity attempts to match that of the surrounding environment. Moisture located deep within the section will take more time to travel and exit the member compared to moisture near the surface. As a result, a moisture gradient develops, and the surface dries and shrinks more quickly than the center of the member. Fluctuations in ambient temperatures also cause temperature gradients to develop between the center and surface of the member (Asadi et al., 2018). The material's coefficient of thermal expansion (CTE) is a property that indicates the magnitude of thermal strain that results from a temperature change. Concrete CTE has been found to vary based on moisture content. Consequently, the presence of a moisture gradient across the section would also indicate a CTE gradient. CTE will be lower within the center of the member where greater moisture content is present (Sellevold & Bjontegaard, 2006). Gauges only located within the center of the member are unable to capture variation occurring across the section resulting in readings that will underestimate the average. The magnitude of underestimation will be greater for thicker sections, will be less when exposed to higher environmental humidities and smaller temperature fluctuations, and will reduce over time as the moisture gradient flattens (Bazant & Najjar, 1972; Bazant & Wang, 1984; Kim & Lee, 1998; Zhang et al., 2012).

A temperature gradient also results as concrete hydrates and heat dissipates from the concrete surface but remains within the center. Temperatures generally return to near ambient levels within days, but the temporary opposing conditions can lead to the development of tensile stresses on the surface (Klemczak & Knoppik-Wrobel, 2014; Lawrence et al., 2012). Tensile

stresses also develop when moisture evaporates from the surface, and cracks can result. Cracking can also occur in concentrated compressive zones (Turcry et al., 2006; Niknezhad et al., 2017). Deceptive, and likely excessive, strain measurements may be encountered if cracks were to develop near a gauge.

Loads applied to the wall segment will cause stress and strain discontinuity within the loading region. Markic (2018) identified the force dispersion below an applied load to follow a bottle-shaped trajectory until the stress becomes uniform at a distance approximately equal to the thickness of the member. Zou et al. (2014) observed larger strain variations (~20% of average) near the top of an instrumented wall segment where a load had been applied and lower strain variations (~10% of average) at mid-height. Klemczak and Knoppik-Wrobel (2014) identified restraining effects near boundaries leading to reduced local compressive stresses. Some strain variation will also exist along the height of the wall due to the accumulation of self-weight. Strain gauges placed at mid-height of a wall may best represent uniform loading conditions, but this location will fail to capture the variation that exists within the loading region, which could be significant for thicker wall sections and large loads.

Strains will also vary throughout a member since placement of concrete is variable. Vibration techniques are often employed to consolidate concrete. During this process, voids are reduced, and entrapped air is released, but segregation can also occur as heavier aggregates begin to settle due to gravity. Self-compacting concrete (SCC) is a highly flowable concrete that is commonly used to reduce these effects. Still, some degree of mixture variation, regardless of best placement practices, will inevitably exist and cannot be completely controlled (Niknezhad et al., 2017; Paiovici et al., 2004). Due to such variations, conditions at the specific location of the gauge may not be representative of the average conditions that exist throughout the member.

3.3.4 Gauge Considerations

Collecting data with sensors may be considered analogous to conducting a poll amongst a population. If the selected samples are not representative of the entire population, the results will be skewed and deceptive. For instance, the largest opinion poll in the history of the United States, consisting of 2.4 million respondents (~2% of the total population), was conducted in 1936 by a magazine called the *Literary Digest* in an effort to predict which candidate would win the presidential election – Landon or Roosevelt. The results of the poll predicted Landon would win by a landslide. The opposite came true when Roosevelt won 46 of the then 48 states. The same year, another poll that used a sample on the order of 2% of the size used by the *Literary Digest* produced a prediction within 1% of the actual results. Since that time, it has been observed throughout several elections that accurate predictions can be made with sample sizes that are even substantially smaller - on the order of 0.05% (Kaplan et al., 2014). The presence of such a large sample in the *Literary Digest* poll may have created the illusion of accuracy, but was actually biased and simply not representative of the population.

A 0.15 m gauge embedded within a 4.5 m wall will only capture about 3.4% of vertical behavior (0.15 m / 4.5 m = 3.4%). In order to estimate shortening along the entire height, measurements must be extrapolated to represent the behavior of the other 96.6%. Like polls, small sets of representative data may be adequate and potentially more effective than large uncontrolled sets (McFarland & McFarland, 2015). For instance, multiple gauges could be installed throughout a core wall, but measurements may poorly represent overall conditions if gauges are of insufficient length and accuracy, if differences between concrete and gauge material properties are not accurately determined and accounted for, or if gauges are placed in locations experiencing stress discontinuity, cracking, or excess environmental exposure.

Whereas, a minimal number of optimally configured gauges, calibrated correctly, and placed in locations that closely represent average conditions may be capable of producing adequate results. Since concrete member strain varies throughout and changes over time, optimal installation locations will also likely vary depending on project specific parameters, such as wall geometry, concrete composition, and environmental conditions. Application across a variety of projects would be ideal to optimize procedures and concurrent conventional survey measurements would be useful invalidating results.

3.3.4.1 Gauge Selection

The selected strain gauges should have an appropriate range, resolution, accuracy, and length. The gauge range should at minimum match the expected magnitude of strain to be measured. If as much as 3 mm of shortening is expected within a 4.5 m story, the magnitude of measured strain would be nearly 700 με. A range of at least 1,000 με is recommended in this case to accommodate any additional variability. To limit noise within the dataset, the measurement resolution should be at least 1 με with error no greater than ± 3 με. The gauge must be long enough to closely capture the general response amid localized stress concentrations. Studies have observed measurement errors of less than ± 5% when gauge lengths are at least five times the maximum aggregate dimension. Errors rapidly increased up to ±65% when a gauge length equal to the aggregate dimension was utilized (Geymayer, 1968; Bakoss et al., 1977).

If the gauge is placed between longitudinal reinforcing bars, it will be enveloped by concrete. Since the gauge has differing material properties than that of the surrounding concrete, it tends to respond differently to thermal changes and applied stresses. This difference in material responses can lead to the development of shear stresses at the gauge to concrete interface and adequate bonding needs to be present to effectively transfer strains across this

interface. Without adequate bonding, slippage between the materials could occur leading to strain measurements that are not consistent with the surrounding concrete. Strain gauges equipped with flanges at the ends should be utilized as they promote interlocking. Studies have shown this configuration results in some stress concentrations near the flanges but greatly reduces the shear stresses along the length of the gauge (Hameed et al., 2002). Errors can also be minimized if the gauge stiffness is limited. Models have estimated transfer of strain with minimal error can be achieved when the gauge's effective modulus of elasticity is less than six times that of the concrete (Quirion & Ballivy, 2000).

3.3.4.2 Gauge Installation

Since inconsistent strains are expected near boundaries, installation of gauges at mid-height is recommended. Gauges can either be tied between vertical reinforcement bars using soft iron wire or precast within a briquette then cast with the concrete. In either case, protection of the gauge while maintaining its vertical alignment is critical to both measurement reliability and accuracy.

Since gauge protection and alignment cannot be guaranteed, concrete mixture variation is expected throughout, and cracking has the potential to influence measurements, multiple gauges should be installed throughout each story for redundancy. Additionally, thicker walls will experience greater moisture and thermal gradients. Installation of two gauges, placed at ¼ and ¾ points across the thickness, may more closely capture average conditions (Bazant & Najjar, 1972; Klemczak & Knoppik-Wrobel, 2014). These effects become more pronounced in climates that have lower humidities and greater temperature fluctuations.

3.3.4.3 Measurement Processing

Strain gauge measurements could theoretically be refined if specific conditions leading to strain variations could be identified. For instance, member moisture and thermal gradients could be measured over time, crack detection could identify discontinuities, and core samples could be taken to test for variations in concrete strength and modulus.

A relatively simple and non-invasive adjustment may also be made to strain measurements to correct for differences in CTE between the gauge and the concrete. A strain gauge made of steel may want to expand and contract differently than the surrounding concrete but since it is embedded and interlocked within the concrete, it is likely restrained from doing so (although inconsistencies may result from imperfect bonding and thermal gradient effects). The restraint can cause the gauge to be stressed as though it is being pushed or pulled. If left uncorrected, the difference in response between the materials will lead to "apparent" strains registered by the gauge even though they do not actually exist within the concrete. If the difference in CTE between the gauge and member are known, measurements may be adjusted by applying the difference to the change in temperature (Batten et al., 1999):

$$\Delta\varepsilon = \Delta\varepsilon_g - [\Delta\alpha \cdot \Delta T] \tag{3.11}$$

The relative change in strain experienced by the member at the gauge location is denoted as $\Delta\varepsilon$; the change in strain measured by the gauge as $\Delta\varepsilon_g$; and the change in temperature experienced by the gauge as ΔT. The difference in thermal expansion coefficients between the member and the gauge is denoted as $\Delta\alpha$, where a positive value indicates the member has a greater coefficient of thermal expansion than the gauge. The equation assumes compressive

strains are positive, otherwise the second term should be subtracted from the first. The gauge CTE should be easily obtained from the manufacturer, but determination of an appropriate concrete CTE is more complex.

Since concrete is a mixture, its CTE is a function of its constituents. Specimens may be tested in a laboratory to estimate a CTE value, but each batch of concrete is unique, and as an evolving material, concrete CTE is not constant. Sellevold and Bjontegaard (2006) demonstrated a strong connection between concrete CTE variations and moisture content. Moisture content not only changes as concrete ages and dries but is also affected by fluctuations in environmental humidity. Consequently, exact adjustments may not be possible. To improve results, laboratory humidity should match the average expected on site. An argument for a higher laboratory humidity could be made when a gauge is situated deep within a wall and will experience even greater humidities than the surface.

Walls are composite members consisting of concrete and steel reinforcement. As such, a theoretical effective reinforced concrete CTE may be estimated by considering the physical interaction between the two materials (Berwanger, 1971):

$$\alpha_{rc} = \alpha_s \left[\frac{\alpha_s - \alpha_c}{1 + \mathrm{n}\rho}\right] \tag{3.12}$$

The modular ratio, defined as the ratio of steel to concrete elastic moduli, is denoted as ‘n’; the reinforcement ratio, defined as the ratio of steel to total member area, is denoted as ‘ρ’; and the CTE of the steel and concrete is denoted as α_s and α_c, respectively. The effective reinforced concrete CTE is nearly equal to the plain concrete CTE for low reinforcement ratios and small differences in CTE. For instance, when considering a modular ratio equal to 6, a

reinforcement ratio equal to 0.007, and steel and concrete CTE equal to 12.0 με/°C and 13.2 με/°C, respectively, an effective CTE equal to 13.152 με/°C can be computed. The concrete modulus of elasticity is a property that develops over time, however the effective reinforced concrete CTE is relatively insensitive to changes in the modular ratio. For instance, adjusting the modular ratio in the previous example from 6 to 5, representing a 20% increase in the concrete modulus of elasticity, produces an effective CTE equal to 13.159 με/°C. It is similarly insensitive to small changes in reinforcement ratio. A 20% increase, from 0.007 to 0.010, results in an effective CTE equal to 13.143 με/°C. These calculations are meaningful to only one digit.

In general, the relative impact of CTE adjustments decreases as wall strains increase. A CTE differential of 1 με/°C results in a 1 με adjustment for each degree of temperature change. If temperature changes of +/- 5 °C are experienced, a 5% adjustment is made to a wall at 100 με versus a 1% adjustment at 500 με.

3.3.5 Shortening Estimation

Figure 3.4 illustrates an example of a predicted strain profile for the bottom eight stories of a tower between an initial reference time, t_r, and current time, t, where compressive strains are considered positive. The difference between the two strain profiles gives the incremental change in strain occurring between the two points in time, $\Delta\varepsilon$, and the solid vertical line illustrates the average change, $\overline{\Delta\varepsilon}$. Shortening within the segment, Δh, can be estimated by multiplying the average change in strain by the height, h, and the approximate elevation at time t can be found by subtracting estimated shortening from the elevation at time t_r. To measure and compute the actual average change in strain, gauges would need to be installed within each story of the tower. During construction of the Salesforce Tower, gauges were installed approximately every eight stories, requiring change in strain values for intermediate stories to be estimated.

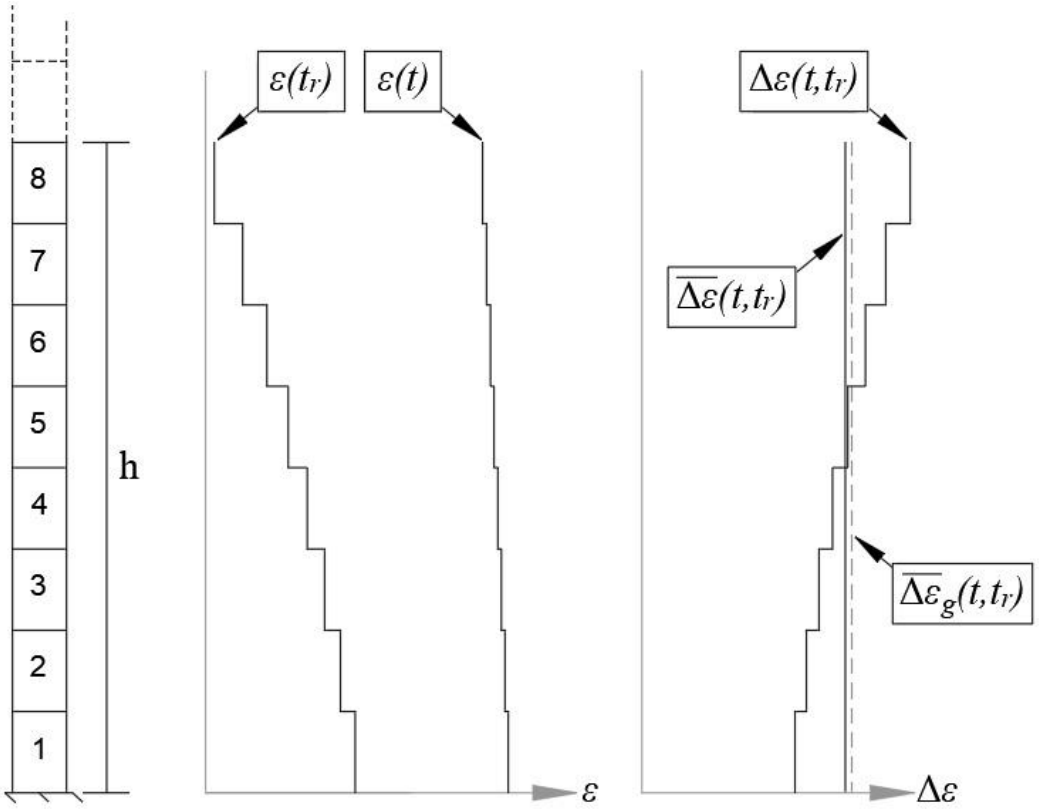

Figure 3.4 Tower Strain Profile Example

Three methods of varying complexity were developed to estimate the average change in strain, and subsequent shortening and elevation changes, within a tower using strain measurements acquired at intermittent levels. Table 3.1 indicates the change in strain estimation parameters used in each method. Because the change in strain profile of a tower segment resembles a linear trend, each method linearly interpolates gauge measured changes in strain to compute the average gauge measured change in strain, as illustrated by the dashed line in Figure 3.4. In addition, Method B incorporates a coefficient of thermal expansion (CTE) adjustment to the strain gauge measurements, while Method C attempts to approximate the non-linear change in strain (the difference between the solid and dashed vertical lines illustrated in Figure 3.4) using results from concrete strain prediction models.

Table 3.1 Summary of Parameters Associated with Tower Shortening Estimation Methods

Parameter	A	B	C
Measured strain change (Δε)	✓	✓	✓
Height between instrumented levels (h)	✓	✓	✓
Measured temperature change (Δ*T*)		✓	✓
Material CTE difference (Δα)		✓	✓
Reinforcement ratio (longitudinal)			✓
Span between instrumented levels (*m*)			✓
Concrete age when measurements begin (t_r)			✓
Concrete age when measurements end (*t*)			✓
Prediction model results (ACI, B3, CEB, GL, B4)			✓

Table 3.2 outlines parameters associated with a variety of concrete strain prediction modeling criteria developed by Bazant & Baweja (2000) (B3), Gardner & Lockman (2001) (GL), American Concrete Institute Committee 209 (2008) (ACI), Comité Euro-International du Béton (1999) (CEB), and Bazant et al. (2015) (B4). Though these modeling criteria would typically be incorporated into complex computer modeling when analyzing strain development throughout a tower, here they are used to supplement strain gauge measurements using a simplified approach detailed in the following chapter.

Table 3.2 Summary of Parameters Associated with Concrete Strain Prediction Models

Parameter	ACI	B3	CEB	GL	B4
Curing duration	✓	✓	✓	✓	✓
Curing condition	✓	✓			
Relative humidity	✓	✓	✓	✓	✓
Volume to surface ratio	✓	✓	✓	✓	✓
Cement type	✓	✓	✓	✓	✓
Concrete slump	✓				
Fine aggregate percentage	✓				
Air percentage	✓				
Cement content	✓	✓			✓
Water content		✓			✓
Aggregate content		✓			✓
Type of aggregate			✓		✓
Concrete 28-day strength		✓	✓	✓	✓
Concrete age when loaded	✓	✓	✓	✓	✓
Member shape		✓			✓
Admixtures					✓

3.4 Summary of Strain-Based Elevation Monitoring Review

This study explored the feasibility of implementing a strain-based measurement system to assist with monitoring elevation changes during construction. Limitations related to strain variability within reinforced concrete members have been reviewed and approaches to potentially increase measurement reliability through gauge selection, installation, and measurement processing has been discussed. The following is a summary of recommendations:

1) The selected gauge should be at least 150 mm long and contain flanges at the ends.
2) The selected gauge should have a range of at least 1,000 με and a resolution of 1 με with a specified error no greater than +/- 3 με.
3) At least four gauges should be installed throughout each story.

4) Walls thicker than 1 m should contain two gauges, placed at ¼ and ¾ points across the thickness.
5) Laboratory testing should be performed to estimate concrete CTE at humidity levels expected on site or greater and measurement data should be adjusted accordingly.
6) Once strain measurements are acquired, simple or more complex shortening estimation methods may be used depending on project conditions.

CHAPTER IV

APPROXIMATING STRAIN CHANGES WITHIN CONCRETE CORE WALL SEGMENTS

4.1 Introduction

During construction of the Salesforce Tower, it was proposed that strain gauges be embedded at approximately eight-level intervals to be consistent with project reporting requirements. Strain within each story of an eight-level segment develops uniquely since each is poured separately and ages independently. If gauges are only installed at the top and bottom levels of a segment, the unique behavior occurring in between will be undetected. Concrete strain development prediction criteria are presented in the remainder of this chapter and results are based on an eight-level segment that was used to estimate theoretical behavior.

4.2 Concrete Strain Development

Axially loaded members experience strain resulting from imposed stresses. Reinforced concrete members also experience time-dependent strains as a result of shrinkage due to moisture loss and creep due to sustained long-term stress.

4.2.1 Development Theory

Strain developed within a uniaxially loaded concrete member at constant temperature, as documented by Bazant (1988), may be considered the sum of elastic strain (compressive), ε_e, shrinkage strain, ε_{sh}, and creep strain, ε_c:

$$\varepsilon = \varepsilon_e + \varepsilon_{sh} + \varepsilon_c \tag{4.1}$$

When predicting strain development, it is convenient to first evaluate stress dependent strain, ε_σ. Since elastic (compressive) and creep strains are both stress dependent, they will be combined as:

$$\varepsilon_\sigma(t,t') = \varepsilon_e(t') + \varepsilon_c(t,t') \tag{4.2}$$

The initial elastic (compressive) strain resulting from a stress applied at time *t*' is denoted as $\varepsilon_e(t')$; the creep strain experienced at time *t* resulting from a stress applied at time *t*' is denoted as $\varepsilon_c(t,t')$. When stresses are applied within the concrete's linear elastic range, the elastic (compressive) strain may be approximated as (Bazant, 1988):

$$\varepsilon_e(t') = \frac{\sigma(t')}{E_c(t')} \tag{4.3}$$

The stress applied at time *t*' is denoted $\sigma(t')$. Since the concrete modulus of elasticity increases over time, the value at the time the stress is applied is considered and denoted as $E_c(t')$. The initial strain due to self-weight is not considered herein. Since the member is poured to fit a form, strains that develop after curing are of primary concern.

Experimental research indicates that creep strains may be considered approximately proportional to stress assuming the applied stresses are within service range (Bazant, 1988). Core wall stresses are expected to be well within service range while monitoring since a fraction

of operational loading is present during construction. Creep strains may then be approximated as (Bazant, 1988):

$$\varepsilon_c(t,t') = \left[\frac{\sigma(t')}{E_c(t')}\right] \varphi(t,t') \tag{4.4}$$

The creep coefficient that applies at time *t* resulting from a load applied at time *t*' is denoted as $\varphi(t,t')$. Equations [4.3] and [4.4] may then be combined to define the stress dependent strain per Equation [4.2] as (Bazant, 1988):

$$\varepsilon_\sigma(t,t') = \left[\frac{1+ \varphi(t,t')}{E_c(t')}\right] \sigma(t') = J(t,t')\, \sigma(t') \tag{4.5}$$

The concrete's compliance function, which combines both compressive and creep strains existing at time *t* per unit stress applied at time *t*', is denoted as $J(t,t')$. A given core wall segment not only experiences one instance of load application but likely multiple instances as construction progresses and additional stories are incrementally added. Experimental research indicates that stress dependent strains may be considered approximately cumulative based on the principal of superposition if there are no stress reversals (Bazant, 1988). Stress reversals are not expected as each story will be permanently constructed, and associated stresses will not be removed. To account for multiple stress histories, the results from Equation [4.5] for each instance of stress can be summed together to approximate the total stress dependent strain as (Bazant, 1988; Zou et al, 2014):

$$\varepsilon_\sigma(t,t') = \sum_{i=1}^{n} \left[\frac{1+ \varphi(t,t_i')}{E_c(t_i')}\right] \sigma(t'_i) = \sum_{i=1}^{n} J(t,t'_i)\, \sigma(t'_i) \tag{4.6}$$

Each increment of 'i' may be thought of as each additional story added above a given wall segment, with 'n' being the total number of stories added. The shrinkage strain (non-stress dependent component of Equation [4.1] may then be added to Equation [4.6] to estimate the total strain development as:

$$\varepsilon_p(t,t') = \sum_{i=1}^{n} J(t,t'_i)\,\sigma(t'_i) + \varepsilon_{sh}(t,t_0) \tag{4.7}$$

The compliance and shrinkage terms may be predicted using a variety of criteria.

4.2.2 Prediction Criteria

The first known worldwide comprehensive database of creep and shrinkage tests was assembled at Northwestern University in 1978. It was expanded with additional test data and labeled the RILEM database in 1992. By 2015, substantial expansion and restructuring led to the development of the NU database which included over 1400 creep and 1800 shrinkage curves, many of which contained admixtures (Hubler et al., 2015). Several prediction criteria have been developed using these results, including B3, GL, ACI, CEB, and B4, introduced in the previous chapter. As outlined in Table 3.1, parameters that are considered by each criteria vary but generally evaluate concrete mix or strength, member size, age at loading, humidity, and curing time. A wide range of variability has been observed in all prediction results when compared to experimental results and inconsistent results have been observed between prediction criteria since they each exhibit varying dependencies and sensitivities to parameters under consideration. For example, the CEB criteria is sensitive to relative humidity and tends to underestimate shrinkage, whereas the ACI criteria is sensitive to water content and tends to overestimate shrinkage.

A variety of statistical comparisons between criteria have been performed. When considering both RILEM and NU databases, Al-Manaseer and Prado (2015) found the ACI criteria to best predict both shrinkage and creep results followed by B3, CEB, and GL. Whereas Bazant and Li (2008) considered the NU database only and found the B3 criteria to best predict shrinkage results followed by GL and then ACI. Gardner (2004) considered the RILEM database only and found the GL criteria to best predict both shrinkage and creep results followed by B3 and CEB. The differences in evaluations may be attributed to the differing statistical methods employed and test data considered.

The most recently developed B4 criteria (Bazant et al., 2015) uniquely considers high strength concrete with supplementary cementitious materials but requires in depth computations and primarily centers on multi-decade performance predictions. Work by Kropacek et al. (2019) found the B4 and ACI criteria to similarly predict specimen shrinkage when considering fluctuating environmental conditions. Although the ACI criteria does not directly consider high strength concrete, work by Pan et al. (2011) observed insensitivity to concrete strength which led to consistent results when evaluating high strength concrete.

When considering large volume to surface ratio members, such as core walls, work by Zou et al. (2014) identified potential deficiencies in strain prediction criteria since they are primarily based on testing of one-dimensional prismatic or cylindrical specimens with small volume to surface ratios. Short-term test data from specimens containing project specific mixes may be used to calibrate and improve prediction results (Bazant et al., 1987; Bazant & Baweja, 2000). Periodic measurements may also be used to refine predictions as was performed during construction of the Jeddah Tower (Peronto et al., 2017).

Sample calculations utilizing the ACI criteria are presented in the following sub-section and results for all five criteria discussed are also summarized as follows.

4.2.2.1 ACI Shrinkage Prediction

ACI Committee 209 (2008) predicts the mean shrinkage of a member to develop over time as:

$$\varepsilon_{sh}(t,t_0) = \left[\frac{(t-t_0)^{\alpha}}{f+(t-t_0)^{\alpha}}\right] \varepsilon_{shu} \tag{4.8}$$

Recommended values for constants *f* and α are given as 35 days and 1, respectively. The average ultimate shrinkage strain is denoted as ε_{shu} and may be computed as:

$$\varepsilon_{shu} = 780\mu\varepsilon \cdot \gamma_{sh} \tag{4.9}$$

A correction factor that accounts for varying conditions is denoted as γ_{sh} and represents the cumulative product of individual correction factors resulting from variations in curing time (γ_{sh,t_o}), relative humidity ($\gamma_{sh,h}$), volume-surface ratio ($\gamma_{sh,vs}$), concrete slump ($\gamma_{sh,s}$), aggregate mix ($\gamma_{sh,g}$), cement content ($\gamma_{sh,c}$), and air content ($\gamma_{sh,a}$). Each individual factor may computed as follows:

$$\gamma_{sh,to} = 1.202 - 0.2337\log(t_o) \tag{4.10}$$

$$\gamma_{sh,h} = 1.40 - 1.02h, \text{ for } 0.40 \leq 0.80 \tag{4.11}$$

$$\gamma_{sh,h} = 3.00 - 3.0h, \text{ for } 0.80 \leq 1 \quad (4.12)$$

The length of curing, in days, is denoted as t_o; the environmental relative humidity, in decimal, is denoted as h.

$$\gamma_{sh,vs} = 1.2e^{\{U(V/S)\}} \quad (4.13)$$

The member volume-surface ratio, in inches is denoted as V/S. The constant U may be equal to -0.12 or -0.00472 for units of inches or millimeters, respectively.

$$\gamma_{sh,s} = 0.89 + U \cdot s \quad (4.14)$$

The slump of fresh concrete is denoted as s. The constant U may be equal to 0.041 or 0.00161 for units of inches or millimeters, respectively.

$$\gamma_{sh,g} = 0.30 + 0.014g, \text{ for } g \leq 50\% \quad (4.15)$$

$$\gamma_{sh,g} = 0.30 + 0.002g, \text{ for } g > 50\% \quad (4.16)$$

The ratio of fine aggregate to total aggregate within the concrete mix, expressed as a percentage, is denoted as g.

$$\gamma_{sh,c} = 0.75 + U \cdot c \quad (4.17)$$

The cement content per unit volume of concrete mix is denoted as *c*. The constant *U* may be equal to 0.00036 or 0.00061 for units of lb/yd3 or kg/m3, respectively.

$$\gamma_{sh,a} = 0.95 + 0.008a \tag{4.18}$$

The air content percentage within in the concrete mix is denoted as *a* but $\gamma_{sh,a}$ should not be less than 1.

4.2.2.2 ACI Creep Prediction

ACI Committee 209 (2008) predicts the average creep coefficient of a member to develop over time as:

$$\varphi(t,t') = \left[\frac{(t-t')^{\psi}}{d+(t-t')^{\psi}}\right] \varphi_u \tag{4.19}$$

Recommended values for constants *d* and ψ are given as 10 days and 0.6, respectively. The average ultimate creep coefficient is denoted as φ_u and may be computed as:

$$\varphi_u = 2.35 \cdot \gamma_c \tag{4.20}$$

A correction factor that accounts for varying conditions is denoted as γ_c and represents the cumulative product of individual correction factors resulting from variations in curing time (γ_c,t_o), relative humidity (γ_c,h), volume-surface ratio (γ_c,vs), concrete slump (γ_c,s), aggregate mix (γ_c,g), and air content (γ_c,a). Each individual factor may computed as follows:

$$\gamma_{c,to} = 1.25 \cdot t_o^{-0.118} \quad (4.21)$$

The curing time factor γ_c,t_o should be less than or equal to 1.

$$\gamma_{c,h} = 1.27 - 0.67h \quad (4.22)$$

$$\gamma_{c,vs} = 2/3 \cdot (1 + 1.13e^{\{U(V/S)\}}) \quad (4.23)$$

The constant *U* may be equal to -0.54 or -0.0213 for units of inches or millimeters, respectively.

$$\gamma_{c,s} = 0.82 + U \cdot s \quad (4.24)$$

The constant *U* may be equal to 0.067 or 0.00264 for units of inches or millimeters, respectively.

$$\gamma_{c,g} = 0.88 + 0.0024g \quad (4.25)$$

$$\gamma_{c,a} = 0.46 + 0.09a \quad (4.26)$$

The air content factor $\gamma_c,_a$ should not be less than 1.

4.3 Strain Development Predictions

Table 4.1 details each of the ACI correction factors and their association with parameters specific to the Salesforce Tower concrete mix, average expected relative humidity, and average member volume to surface ratio. These ultimate shrinkage strain and ultimate creep coefficient values were used to compute time specific shrinkage strain and creep coefficient values using Equations [4.8] and [4.19].

Table 4.1 ACI Ultimate Shrinkage Strain and Creep Coefficient.

Input Parameter		Shrinkage Factors			Creep Factors		
Curing time, t_o [days]	5	$\gamma_{sh,to}$ =	1.04	(4.10)	$\gamma_{c,to}$ =	1.00	(4.21)
Humidity, *h*	0.7	$\gamma_{sh,h}$ =	0.69	(4.11)	$\gamma_{c,h}$ =	0.80	(4.22)
Vol. to surf. ratio, *vs* [mm]	380	$\gamma_{sh,vs}$ =	0.20	(4.13)	$\gamma_{c,vs}$ =	0.67	(4.23)
Slump, *s* [mm]	230	$\gamma_{sh,s}$ =	1.26	(4.14)	$\gamma_{c,s}$ =	1.42	(4.24)
Fine aggregate, *g* [%]	50	$\gamma_{sh,g}$ =	1.00	(4.15)	$\gamma_{c,g}$ =	1.00	(4.25)
Cement content, *c* [kg/m3]	470	$\gamma_{sh,c}$ =	1.03	(4.17)			
Air content, *a* [%]	2.48	$\gamma_{sh,a}$ =	1.00	(4.18)	$\gamma_{c,a}$ =	1.00	(4.26)
		γ_{sh} =	0.18		γ_c =	0.76	
		ε_{shu} [με] =	**143.6**	(4.9)	**φ_u =**	**1.786**	(4.20)

The time specific shrinkage strain and creep coefficient values were used in conjunction with anticipated concrete strength, applied stresses, and construction sequencing to predict strain development within a typical wall section using Equation [4.7]. The concrete mix design test results found the average 28-day concrete compressive strength to be 11.9 ksi (81.9 MPa) with a longitudinal reinforcement ratio, defined as the ratio of steel to total member area, averaging approximately 0.008. Anticipated stresses were determined by considering a typical 15 foot (4.5

m) tall wall with an average density of 155 lb/ft^3 (2480 kg/m^3), which was expected to impose a uniaxial stress of approximately 16 psi (110 kpa) to each segment below. A new story was expected to be constructed every 5 days, on average. Table 4.2 presents the first ten time steps of strain development that is predicted to occur within the bottom story of a core wall segment as a result of both stress dependent and shrinkage strains. Sample calculations for the first two time steps are presented in the following sub-section.

Table 4.2 Typical Modeled Strain Development.

(1)	(2)	(3)	(4)	(5)	(6)	(7)	(8)	(9)	(10)
n	*t* [days]	$\varepsilon_\sigma(t,t_1')$ [με]	$\varepsilon_\sigma(t,t_2')$ [με]	…	$\varepsilon_\sigma(t,t_{10}')$ [με]	$\varepsilon_\sigma(t,t')$ [με]	$\varepsilon_{sh}(t,t_0)$ [με]	$\varepsilon_p(t,t')$ [με]	$\varepsilon_r(t,t')$ [με]
1	5	3.31				3.31	0.00	3.31	3.16
2	10	4.54	2.88			7.42	17.95	25.37	24.33
3	15	4.99	3.95	…		11.66	31.90	43.56	41.84
4	20	5.30	4.34	…		16.01	43.07	59.08	56.79
5	25	5.53	4.61	…		20.46	52.21	72.67	69.87
6	30	5.72	4.81	…		24.98	59.82	84.80	81.58
7	35	5.88	4.98	…		29.57	66.26	95.83	92.22
8	40	6.01	5.12	…		34.23	71.78	106.01	102.04
9	45	6.13	5.23	…		38.94	76.57	115.51	111.20
10	50	6.24	5.34	…	2.5	43.70	80.76	124.46	119.84

4.3.1 Sample Calculations

If the bottom story of a segment is constructed when *t* equals zero days, then according to the anticipated construction schedule, the next level is expected to be constructed when *t* equals five days. From Equation [4.6], *n* represents the number of stories that have been stacked above the bottom wall. Since this is the first and only stress applied to the wall at this time, *n* is equal to one.

4.3.1.1 First Time Step (*n*=1)

Figure 4.1a illustrates the first instance of loading.

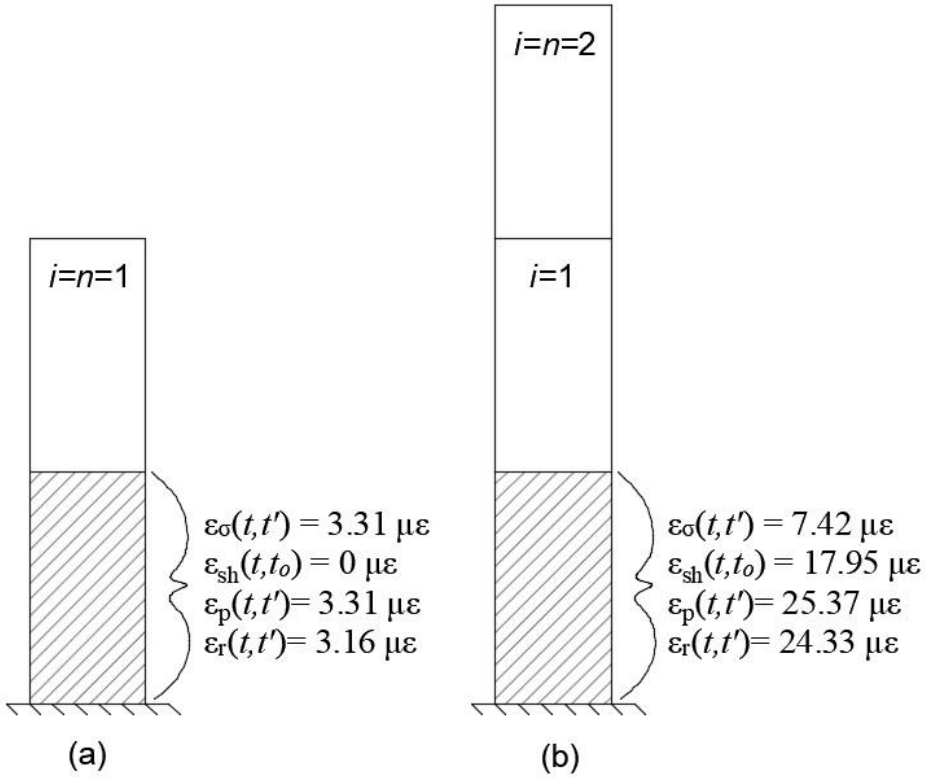

Figure 4.1 Strain Development at (a) *t*=5 and (b) *t*=10.

Since the concrete strength and elastic modulus develop with age, the current stiffness needs to be approximated at each time step. In the absence of concrete mix specific test data, current shrinkage and creep prediction models generally recommend that the development of the concrete modulus of elasticity and the 28-day value be estimated as (Bazant & Baweja, 2000; ACI Committee 209, 2008; Bazant et al., 2015):

$$E_c(t) = E_c(28)\left[\frac{t}{4+0.85t}\right]^{1/2} \quad (4.27)$$

$$E_c(28) = (57{,}000)\ f_c(28)^{1/2} \tag{4.28}$$

The concrete elastic modulus may be estimated using a *t* equal to five days for the first time step as follows:

$$E_c(28) = (57{,}000)\ (11{,}880\ \text{psi})^{1/2} = 6{,}212{,}739\ \text{psi}\ (42835\ \text{MPa}) \tag{4.29}$$

$$E_c(5) = 6{,}212{,}739\ \text{psi}\ \left[\frac{5}{4+0.85(5)}\right]^{1/2} = 4{,}836{,}611\ \text{psi}\ (33347\ \text{MPa}) \tag{4.30}$$

Per Equation [4.19], the creep coefficient will equals zero at the time the stress is applied, because both *t* and *t*' are equal to five days. The total stress dependent strain may be computed using Equation [4.5] while applying the anticipated stress of 16 psi (110 kpa) given above:

$$\varepsilon_\sigma(5,t_1') = \left[\frac{1+0}{4{,}836{,}611psi}\right] 16\ \text{psi} = 3.31\ \mu\varepsilon \tag{4.31}$$

Since *n* is equal to one, there are no other stress histories to include in the summation. Per Equation [4.8], the shrinkage strain equals zero during this time step since both *t* and t_o are equal to five days. The total predicted strain developed within the bottom wall at *t* equal to five days, may now be determined per Equation [4.7] as:

$$\varepsilon_p(5,t') = 3.31\ \mu\varepsilon + 0 = 3.31\ \mu\varepsilon \tag{4.32}$$

Since strain predictions are based on plain concrete samples, results need to be adjusted to account for reinforcement effects. Due to bonding, the longitudinal reinforcement contained in core walls will provide some level of restraint against volume reduction, reducing the magnitude of predicted strains. To quantify and adjust for these effects, predicted strains may be translated to a fictitious axial force:

$$N(t,t') = \varepsilon_p(t,t') \cdot E_c(t) \cdot A_c \tag{4.33}$$

The concrete net area is denoted as A_c. The adjusted predicted strain may then be obtained by applying the fictitious force over the concrete and steel areas while considering their respective elastic moduli (Gribniak et al, 2013):

$$\varepsilon_r(t,t') = \left[\frac{N(t,t\prime)}{E_C(t)A_C+E_SA_S}\right] = \left[\frac{\varepsilon_p(t,t\prime)}{1+n(t)\rho}\right] \tag{4.34}$$

The steel modulus of elasticity is denoted as E_s; the steel area as A_s; the modular ratio, defined as the ratio of steel to concrete elastic moduli, at time t as $n(t)$; and the reinforcement ratio as ρ. Using the average longitudinal reinforcement ratio given as 0.008, the result in Equation [4.32] may be adjusted as:

$$\varepsilon_r(5,t') = \left[\frac{3.31\ \mu\varepsilon}{1+\left(\frac{29{,}000{,}000\ psi}{4{,}836{,}611\ psi}\right)0.008}\right] = 3.16\ \mu\varepsilon \tag{4.35}$$

4.3.1.2 Second Time Step (*n*=2)

Another story is expected to be added when *t* is equal to 10 days, as illustrated by Figure 3.1b. Since this is the second instance of stress to be applied to the bottom story, *n* becomes equal to two. Per Equation [4.6], the total stress dependent strain equals the summation of strains associated with each stress history.

The creep coefficient for the first stress application (*i*=1) may now be determined based on Equation [4.19] using the ACI Committee 209 (2008) recommended value of 10 days for *d*, and 0.6 for ψ, while also applying the ultimate creep coefficient, φ_u, as given in Table 4.1:

$$\varphi(10,t_1') = \left[\frac{(10-5)^{0.6}}{10+(10-5)^{0.6}}\right](1.786) = 0.3715 \quad (4.36)$$

The stress dependent strains for the first stress application (i=1) may now be computed per Equation [4.5] as:

$$\varepsilon_\sigma(10,t_1') = \left[\frac{1+0.3715}{4{,}836{,}611psi}\right] 16\text{psi} = 4.54\ \mu\varepsilon \quad (4.37)$$

The concrete elastic modulus may again be determined based on Equation [4.27], except that *t* will now be equal to 10 days for the second stress application:

$$E_c(10) = 6{,}212{,}739\text{psi}\left[\frac{10}{4+0.85(10)}\right]^{1/2} = 5{,}556{,}843\text{ psi}\ \ (38313\text{ MPa}) \quad (4.38)$$

Per Equation [4.19], the creep coefficient equals zero at the time the second stress is applied (i=2) since both t and t' are equal to 10 days. The stress dependent strain resulting from the second stress application may be computed using Equation [4.5] as:

$$\varepsilon_{\sigma}(10,t_2') = \left[\frac{1+0}{5{,}556{,}843psi}\right] 16\text{psi} = 2.88\ \mu\varepsilon \tag{4.39}$$

Per Equation [4.6], the total stress dependent strain will be equal to the summation of strains associated with each stress history:

$$\varepsilon_{\sigma}(10,t') = \varepsilon_{\sigma}(10,t_1') + \varepsilon_{\sigma}(10,t_2') = 4.54\ \mu\varepsilon + 2.88\mu\varepsilon = 7.42\ \mu\varepsilon \tag{4.40}$$

The shrinkage strain may now be determined based on Equation [4.8] using the ACI Committee 209 (2008) recommended value of 35 days for f for moist curing conditions, and 1 for α, while also applying the ultimate shrinkage strain, ε_{shu}, as given in Table 4.1:

$$\varepsilon_{sh}(10,5) = \left[\frac{(10-5)^1}{35+(10-5)^1}\right] (143.6\mu\varepsilon) = 17.95\ \mu\varepsilon \tag{4.41}$$

The total predicted strain developed within the bottom wall at t equal to 10 days, may now be determined per Equation [4.7] as:

$$\varepsilon_{p}(10,t') = 7.42\ \mu\varepsilon + 17.95\mu\varepsilon = 25.37\ \mu\varepsilon \tag{4.42}$$

To account for reinforcement effects at the second time step, the quantity of strain that develops in plain concrete since the first time step will first need to be considered.

$$\Delta\varepsilon_p(10,t') = \varepsilon_p(10,t') - \varepsilon_p(5,t') = 25.37\ \mu\varepsilon - 3.31\ \mu\varepsilon = 22.06\ \mu\varepsilon \quad (4.43)$$

The result may then be translated to a fictitious axial force applied to the concreate and steel, similar to Equation [4.34], while using the current modulus value:

$$\Delta\varepsilon_r(10,t') = \left[\frac{22.06\ \mu\varepsilon}{1+\left(\frac{29{,}000{,}000\ psi}{5{,}556{,}843\ psi}\right)0.008}\right] = 21.17\ \mu\varepsilon \quad (4.44)$$

The result may then be added to the developed strain from the previous time step, given in Equation [4.35], to find the total predicted strain value at time step two adjusted for the reinforced section:

$$\varepsilon_r(10,t') = 3.16\ \mu\varepsilon + 21.17\ \mu\varepsilon = 24.33\ \mu\varepsilon \quad (4.45)$$

Each subsequent time step follows a similar sequence until all total predicted strain development values are determined as shown in the right-hand Column (10) of Table 4.2. Although these values represent the predicted strain development for the bottom story of a core wall segment, the values can be thought to similarly represent the strain development within any story if the same material properties, stresses, environmental conditions, and construction sequencing are expected.

If a core wall segment containing multiple stories is considered, the strain developed within a given story at time *t* would be based on an *n* value that is one less than the story below it. Column (1) of Table 4.3 demonstrates this relationship for each level in an eight-level segment, at a *t* equal to 50 days. The total predicted strain development within the first level is equal to 119.84 με at a *t* equal to 50 days and an *n* equal to 10 per Table 4.2. The total predicted strain development within the second level would be based on an *n* equal to nine since it has one less story stacked above, equaling 111.20 με per Table 4.2. Each subsequent level follows a similar pattern. Since elevation monitoring is concerned with changes in elevation between two periods of time, differences in developed strain between two periods of time are similarly examined.

Table 4.3 Modeled vs. Approximate Results (t_r=45; t=50).

	(1)	(2)	(3)
Level	$\varepsilon_r(t_{50},t')$ [με]	$\varepsilon_r(t_{45},t')$ [με]	$\Delta\varepsilon_r(t_{50}, t_{45})$ [με]
1	119.84	111.20	8.64
2	111.20	102.04	9.16
3	102.04	92.22	9.82
4	92.22	81.58	10.64
5	81.58	69.87	11.70
6	69.87	56.79	13.09
7	56.79	41.84	14.95
8	41.84	24.33	17.51
		$\overline{\Delta\varepsilon}_r(t_{50}, t_{45})$ =	11.94
		$\overline{\Delta\varepsilon}_a(t_{50}, t_{45})$ =	13.07
		$\chi(t_{50},t_{45})$ =	-1.14

4.4 Modeling Strain Changes Within Segments

From the basis of having predicted strain development for an eight-level segment computed, how strains are predicted to change within this segment over time are considered in this section. The earliest point at which changes in strain need to be considered is after construction of the segment is complete and access is available so an elevation benchmark may be set. Since the objective is to measure changes in the elevation of the benchmark, changes in strain are only referenced from this point forward. Based on anticipated construction sequencing, this point in time was estimated to be 10 days following construction of the eighth level, when t equals 45 days. This will be considered the earliest anticipated reference time, represented here as t_r. Similar to taring a scale, it is at this point in time that monitoring of changes in strain, and in turn changes in elevation of the benchmark, begins. Predicted relative changes in strain occurring between t_r and t for any given level may be computed as:

$$\Delta\varepsilon_r(t, t_r) = \varepsilon_r(t,t') - \varepsilon_r(t_r,t') \tag{4.46}$$

Table 4.3 gives the predicted relative change in strain occurring within an eight-level segment between a t_r equal to 45 days, detailed in Column (2), and a t equal to 50 days, detailed in Column (1). The average relative change in strain occurring through a given segment q, consisting of m levels, may be computed as:

$$\overline{\Delta\varepsilon}_{r,q}(t_{50}, t_r) = \frac{1}{m}\sum_{j=1}^{m} \Delta\varepsilon_{r,j}(t, t_r) \tag{4.47}$$

Table 4.3, where *m* is equal to eight stories, gives the average relative change in predicted strain, between a t_r equal to 45 days and a *t* equal to 50 days, as 11.94 με. For comparison purposes, the following equation could simulate a scenario where strain development is only measured within the top and bottom stories of the segment, where the stories in between are approximated by linear interpolation:

$$\overline{\Delta\varepsilon}_{a,q}(t, t_r) = \frac{1}{2}\left[\Delta\varepsilon_{r,1}(t, t_r) + \Delta\varepsilon_{r,m}(t, t_r)\right] \tag{4.48}$$

Using this approximation with the same data in Table 4.3 gives an average relative change in predicted strain equal to 13.07 με. By computing the difference between Equation [4.47] and Equation [4.48], the theoretical average relative change in strain occurring throughout the segment that is not captured by the gauges may be found:

$$\chi(t_{50}, t_r) = \overline{\Delta\varepsilon}_{r,q}(t, t_r) - \overline{\Delta\varepsilon}_{a,q}(t, t_r) \tag{4.49}$$

Per Table 4.3 values, the difference may be computed as -1.14 με (11.94 με – 13.07 με = -1.14 με). This result indicates the linear approximation produces an overestimation, which is apparent in Figure 4.2, where both the modeled and approximate relative changes in strain are illustrated.

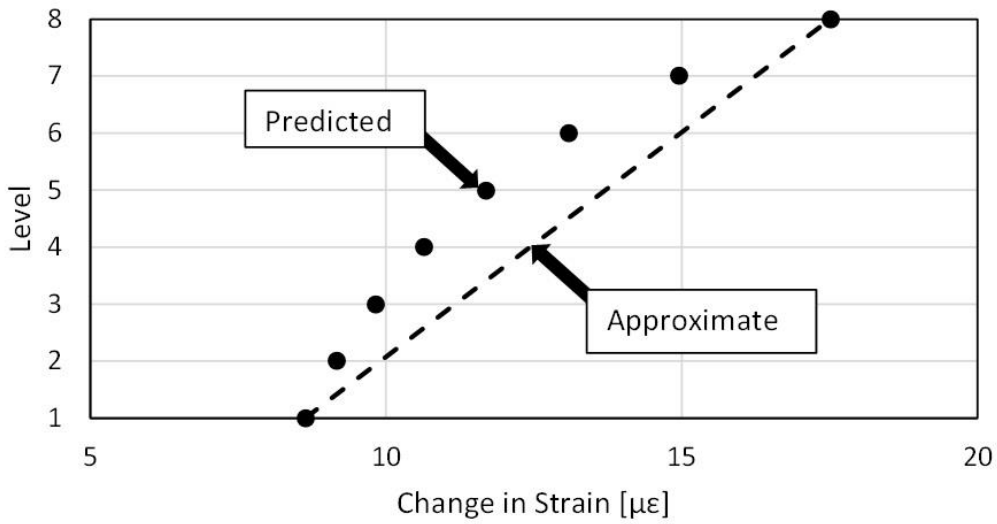

Figure 4.2 Modeled vs. Approximate Changes in Strain.

This difference varies in magnitude for all values of t and t_r and is affected by different span lengths, m. The ACI modeling criteria has been presented herein but each of the other four models will also produce varying results. Generally similar results were found when applying the CEB, B3, and GL prediction criteria, where each indicated an overestimation when applying the linear approximation. The CEB results were almost identical to ACI, whereas the B3 and GL results reflected lower magnitudes. The B4 results indicated an overestimation at later reference times but an underestimation at earlier times. The B4 criteria uniquely considers autogenous shrinkage strain separately as a delayed effect which causes an inflection point in the strain development resulting in a reversal in curvature around an age of 50 days. Strain development for each of the models is illustrated in Figure 4.3.

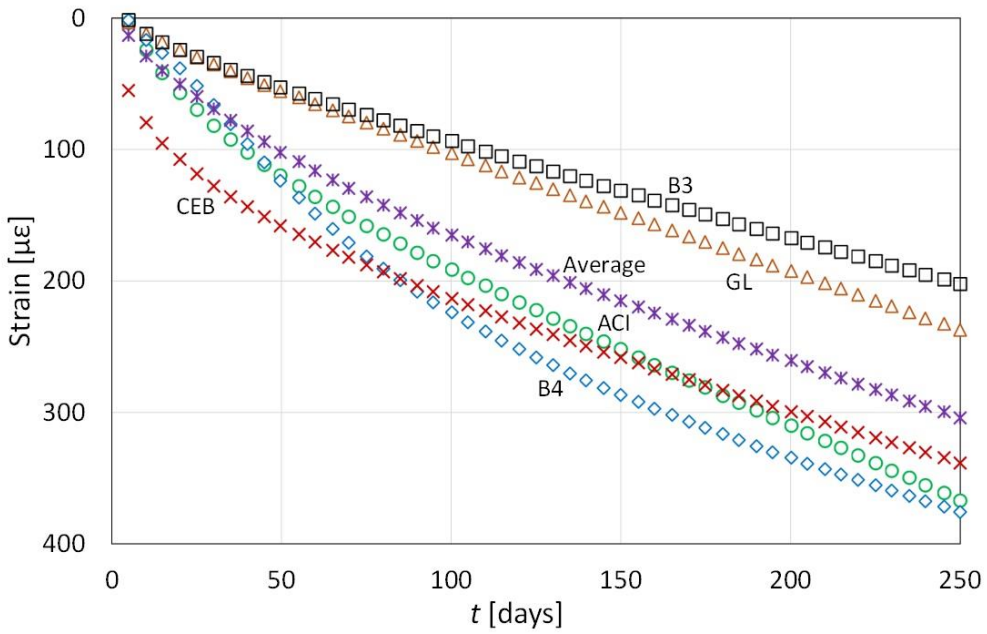

Figure 4.3 Modeled Strain Development

To capture the range of variability amongst prediction model results, as exhibited in Figure 4.3, non-linear prediction differences, χ, were calculated and compiled for ACI, B3, CEB, GL, and B4 for all expected combinations of t_r (between 10 and 115 days after the top story of a segment is poured, at 5 day intervals), t (between 10 days after t_r and 260 days after the top story of a segment is poured, at 5 day intervals), and m (between 5 and 8 stories, at 1 story intervals). The time parameter ranges were selected to encompass the expected project duration and the story range was selected to accommodate some variation in sensor spacing. The resulting 16,940 model data points are illustrated in Figure 4.4 when plotted against each of the three independent variables. Computation of the coefficient of determination (R^2) was used to estimate best fit in each case. A linear fit proved best for t_r and m, whereas a logarithmic function slightly improved fit for the t plot.

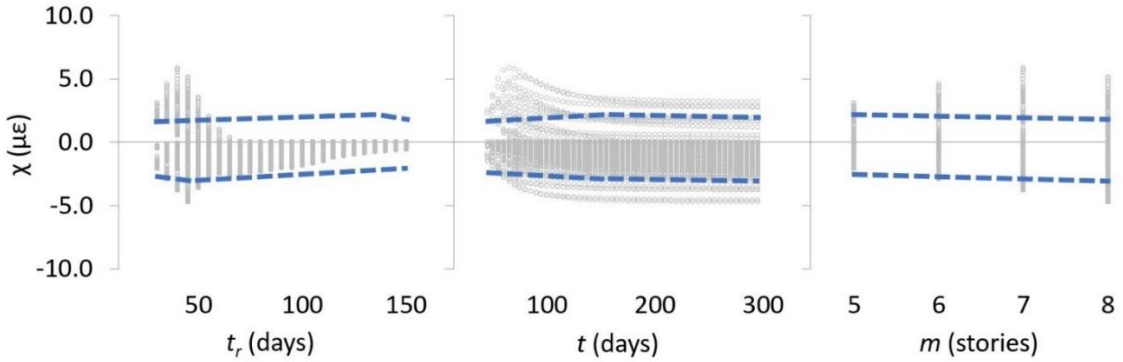

Figure 4.4 Regression Model Data

Using the method of least squares, a multivariable regression model was then developed to approximate intermediate development effects (Mendenhall & Sincich, 2012):

$$\chi_a(t_r,t,m) = 1.8 + 0.01(t_r) - 0.4ln(t) - 0.17(m) + E \quad (4.50)$$

The model accommodates small variations in stress (0.10-0.12 MPa) and reinforcement ratio (0.007-0.010) if results are considered significant to the nearest whole microstrain. The model error is represented as E with a standard error given as +/- 0.8 με and represents a coefficient of determination equal to 0.13. The dashed lines in Figure 4.4 represent the upper and lower bounds of a 95% confidence interval, which may be found by computing results for all possible combinations of the independent variable ranges and adding the standard error multiplied by 1.96 (Mendenhall and Sincich, 2012). In general, it can be observed that lower values of both t_r and t and higher values of m exhibit greater variations that extend beyond these bounds, indicating that the model may fail to capture some of these effects.

For comparison purposes, values from Table 4.3 may be applied to the model:

$$\chi_a(45,50,8) = 1.8 + 0.01(45) - 0.4ln(50) - 0.17(8) = -0.7\ \mu\varepsilon \quad (4.51)$$

If evaluated at a 95% confidence level and rounded to the nearest whole microstrain, a range between -2 με and 1 με can be computed. The result of -1.14 με from Table 4.3 can be observed to fall within this range.

4.5 Summary of Strain Approximations

To simulate a scenario where strain is measured at intermittent levels, average changes in predicted strain throughout a segment were compared with average predicted changes on either end of the segment. The difference between the two models is the theoretical unmeasured change in strain throughout the segment. ACI prediction modeling criteria was used to demonstrate the comparison, but results from CEB, GL, B3, and B4 criteria were also summarized.

Results from the ACI, CEB, GL, and B3 prediction criteria indicated the simplified linear approximation may overestimate the average strain developed throughout a tower segment. The magnitude of overestimation was found to be dependent upon the age of concrete at the time shortening consideration began. The B4 prediction criteria indicated an underestimation if shortening consideration begins when the age of the concrete is younger but an overestimation when the concrete is older. A multi-variable regression analysis was performed using all prediction criteria results to approximate these differences.

CHAPTER V

IMPLEMENTATION OF A STRAIN-BASED ELEVATION MONITORING SYSTEM DURING CONSTRUCTION OF THE SALESFORCE TOWER

5.1 Introduction

Actual strain gauge measurements obtained during construction of the Salesforce Tower project are presented and compared with results derived from ACI, B3, CEB, GL, and B4 prediction criteria. Due to time and budget constraints, it was not deemed feasible to instrument every level. Instead, it was proposed that strain gauges be embedded at approximately eight-story intervals to be consistent with project reporting requirements. Three new shortening estimation methods are also presented; Method A uses strain gauge data only and linearly interpolates changes in strain between instrumented levels; Method B is also based on a linear interpolation but includes a CTE adjustment to the strain gauge data; Method C expands on Method B by acknowledging that a linear interpolation will introduce error since each story is poured independently and develops uniquely. The regression model developed in the previous chapter is used to approximately adjust for the expected non-linear development.

5.2 Project Details

The tip of the Salesforce Tower reaches 1,070 feet (326 m) above grade. The first 961 feet (293 m) contains 63 stories below the roof while the remainder consists of an open-air screen wall. The structure also extends below grade 55 feet (17 m), housing three parking garage levels. The inner core consists of a square and biaxially centered reinforced concrete core wall

with an 88.67 feet (27.0 m) interior clear width. The core walls throughout the tower height range 48 inches (1.2 m) thick at the base to 24 inches (0.6 m) thick at the top and are comprised of the same high-strength concrete with a 28-day compressive strength of 11.9 ksi (81.9 MPa), slump of 9 in (230 mm), and 0.75 in (19 mm) maximum aggregate size. The core is split in half with a dividing wall spanning in the east to west direction (Figure 5.1).

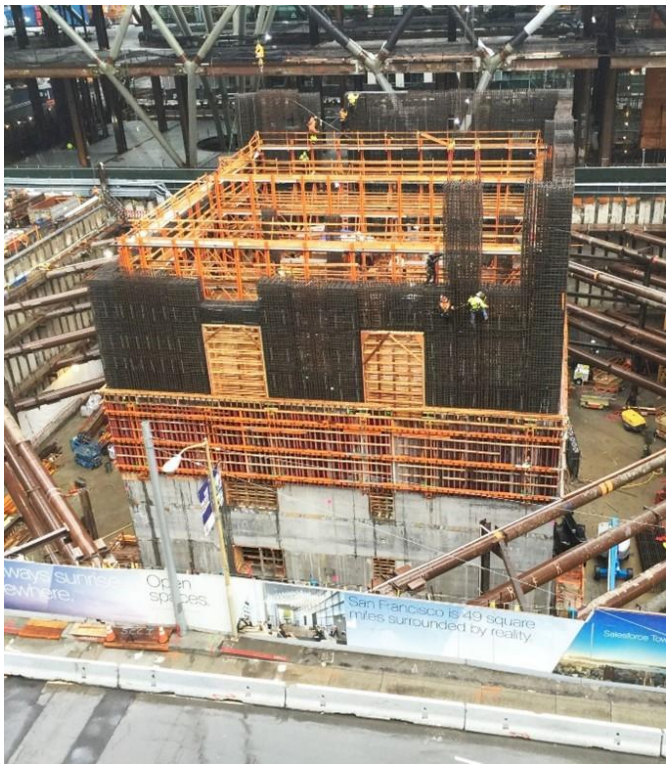

Figure 5.1 Core Wall Construction.

The exostructure is made up of steel columns and beams which support reinforced concrete decking and a glass curtain wall (Figure 5.2). Project specifications required that benchmark elevations be established and subsequent changes in elevations be periodically monitored approximately every eight stories. A strain-based elevation monitoring system was

developed to support the monitoring process. The following section details how the system was implemented.

Figure 5.2 Glass Curtain Wall Nearing Completion.

5.2.1 System Installation and Data Processing

Six-inch (150mm) long steel encased vibrating wire strain gauges, manufactured by Soil Instruments Ltd., were utilized to monitor changes in strain. Strain changes are found by measuring changes in frequency experienced by the vibrating wire within the gauge. Changes in

temperature may produce misleading change in strain values. All materials expand and contract when experiencing temperature changes. A steel gauge reacts differently than reinforced concrete experiencing the same thermal changes due to fundamental differences in material properties, defined as the coefficient of thermal expansion (CTE). For a cantilevered system, such as a concrete core wall, the following adjustment may be made to compensate for the gauge's thermal bias (Batten et al, 1999):

$$\Delta\varepsilon = \Delta\varepsilon_g - [\Delta\alpha \cdot \Delta T] \tag{5.2}$$

The relative change in strain experienced by the member at the gauge location is denoted as $\Delta\varepsilon$; the change in strain measured by the gauge as $\Delta\varepsilon_g$; and the change in temperature experienced by the gauge as ΔT. The difference in thermal expansion coefficients between the concrete member and the gauge is denoted as $\Delta\alpha$, where a positive value indicates the member has a greater CTE value than the gauge. Equation [5.1] assumes compressive strains are considered positive, otherwise the second term should be subtracted from the first.

Strain gauges were embedded at approximately mid-wall-height at nine separate levels (3, 5, 13, 21, 28, 36, 44, 48, and 55). For purposes of redundancy, gauges were installed in each of the four core walls at each instrumented level, totaling 36 gauges in the tower. Plans to embed gauges within the underground parking levels were unsuccessful due to delays in approval. The four gauges at each instrumented level were placed vertically between, and tied to, the longitudinal wall reinforcement at the wall mid-span. Cables were channeled from the gauges to a junction box where a data logger and communication device was later installed once the concrete had been poured and the forms had advanced to the next level. A Geokon LC-2x4

Datalogger (4 channel) was used to read, process, and output the vibrating wire frequency signals. These signals were then passed through a Sensemetrics X-Series Thread, which wirelessly transmitted the data in real-time to the Sensemetrics cloud-based data management and analysis interface (Figure 5.3).

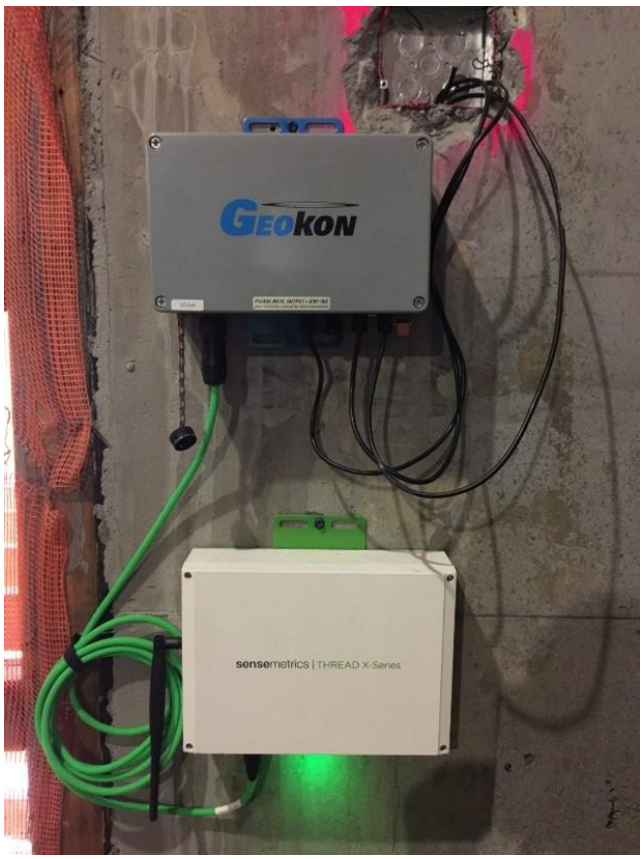

Figure 5.3 Geokon Datalogger and Sensemetrics Thread.

Corrections due to differing material CTE per Equation [5.1] were automatically applied to the gauge measurements within the data management interface. Laboratory testing approximated the concrete coefficient of thermal expansion to be 13.2 με/°C compared to 12.2 με/°C specified for the gauge, resulting in a $\Delta\alpha$ value of 1.0 $x10^{-6}$ (Soil Instruments, 2018). A

composite CTE will exist due to the presence of reinforcement. However, insignificant changes in CTE have been observed when the reinforcement ratio, defined as the ratio of steel to total member area, is low. A composite CTE was neglected in this case since the low reinforcement ratios, which ranged between 0.002 and 0.012 at gauge locations, were found to have a negligible effect.

5.3 Measurement Results

Several problems were encountered throughout the data collection process. Of the 36 gauges installed, only 16 ultimately provided usable data (Table 5.1). Lack of timely power sources led to a delay in Level 21 measurements and the inability to collect any measurements at levels 44, 48, and 55. One of the gauges reported inconsistent measurements, five others never reported any measurements, and two others stopped reporting measurements mid-project. Some of the gauge cabling potentially interfered with construction operations and was observed to have been physically cut, which likely accounts for the gauges that stopped working, whereas the gauges that never reported measurements were likely damaged during concrete placement. Some gaps in measurements were also observed periodically at all levels, likely due to temporary power interruptions. In general, gauge measurements that were successfully acquired at each level varied by about ±10% of average (Figures 5.4 through 5.9). Measurements were averaged together, gaps in data were linearly interpolated, and averaged predictions were supplemented during the period of delay at Level 21.

Table 5.1 Measurement Acquisition

Level	North Wall	South Wall	East Wall	West Wall
3	*[1]	✓	✓	✓
5	✓	✓	✓	✓
13	*[2]	✓	-[3]	✓
21	-[3]	-[3]	*[4,5]	*[4]
28	✓	✓	✓	✓
36	✓	-[3]	-[3]	✓
44	-[6]	-[6]	-[6]	-[6]
48	-[6]	-[6]	-[6]	-[6]
55	-[6]	-[6]	-[6]	-[6]

✓ Complete measurement dataset acquired
* Partial measurement dataset acquired
- No measurement dataset acquired

[1] Sensor stopped reporting measurements on day 294 of the project timeline (L3-North).
[2] Sensor measurements were inconsistent with others and stopped reporting measurements on day 294 of the project Timeline (L13-North).
[3] Sensor was likely damaged or malfunctioned and reported no measurement data (L13-East; L21-North/South; L36-South/East).
[4] Delay in early sensor measurements due to lack of power supply (L21-East/West).
[5] Sensor stopped reporting measurements on day 269 of the project timeline (L21-East).
[6] No power supply was provided within sufficient timeframe to collect measurement data (L44-All; L48-All; L55-All).

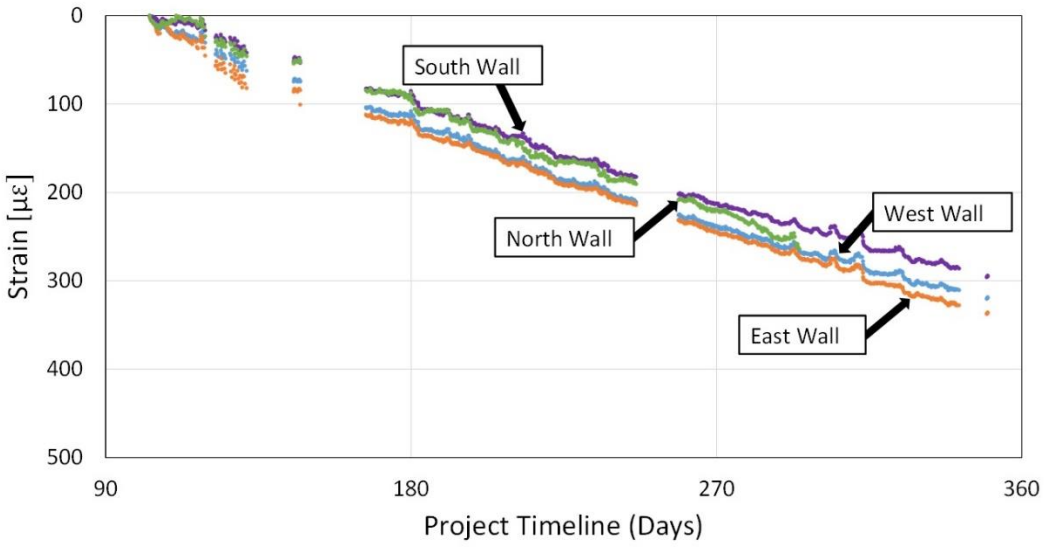

Figure 5.4 Level 3 Strain Measurements.

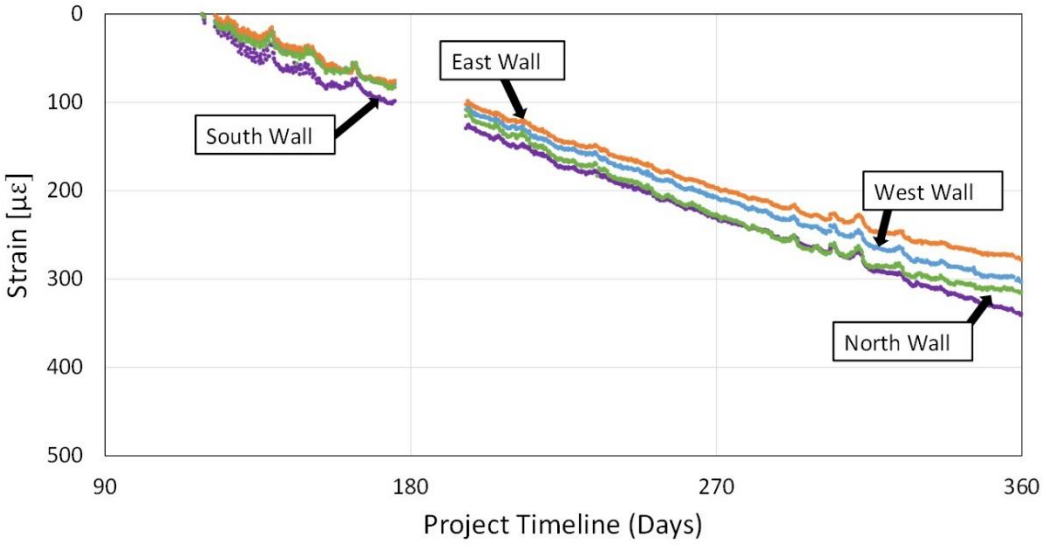

Figure 5.5 Level 5 Strain Measurements

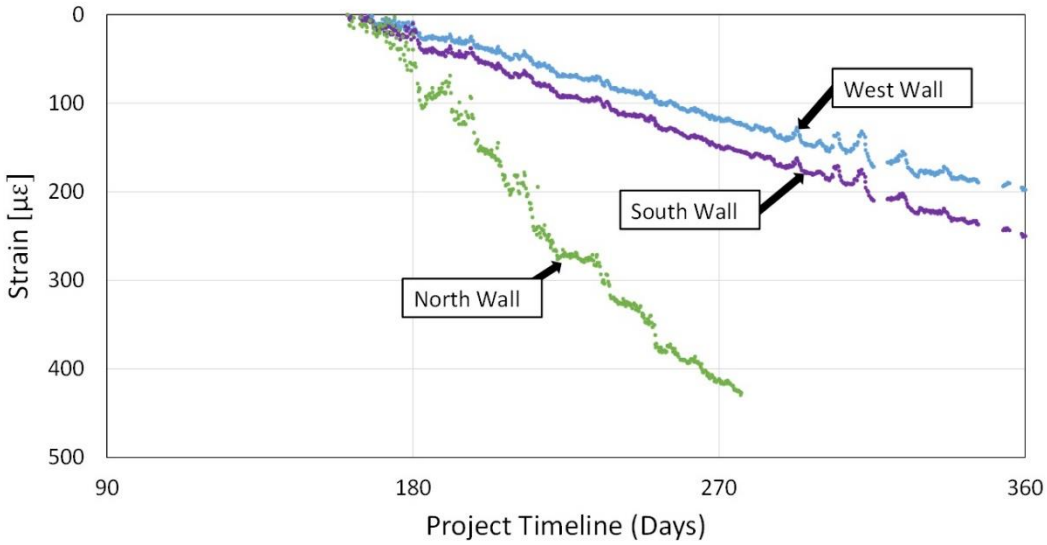

Figure 5.6 Level 13 Strain Measurements.

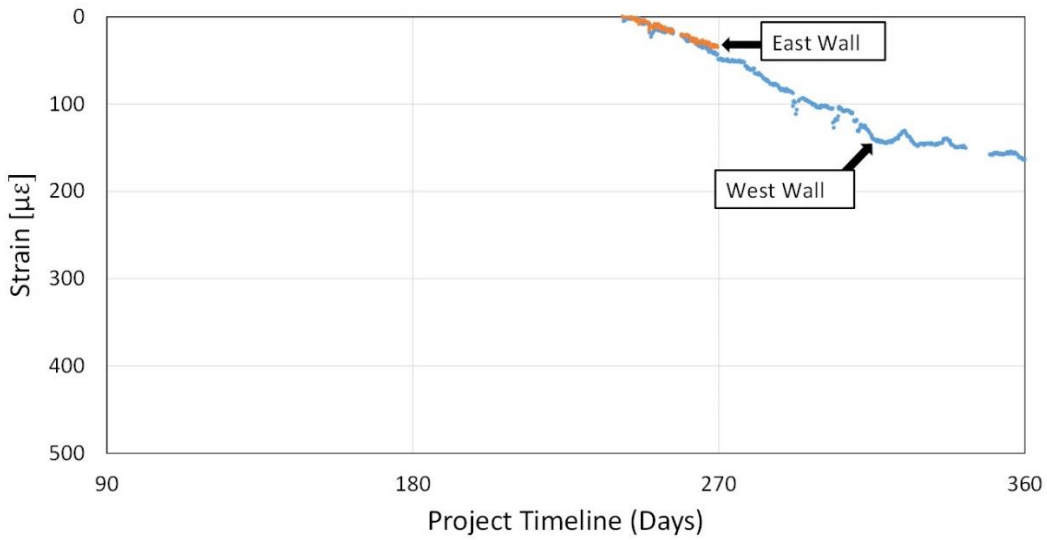

Figure 5.7 Level 21 Strain Measurements.

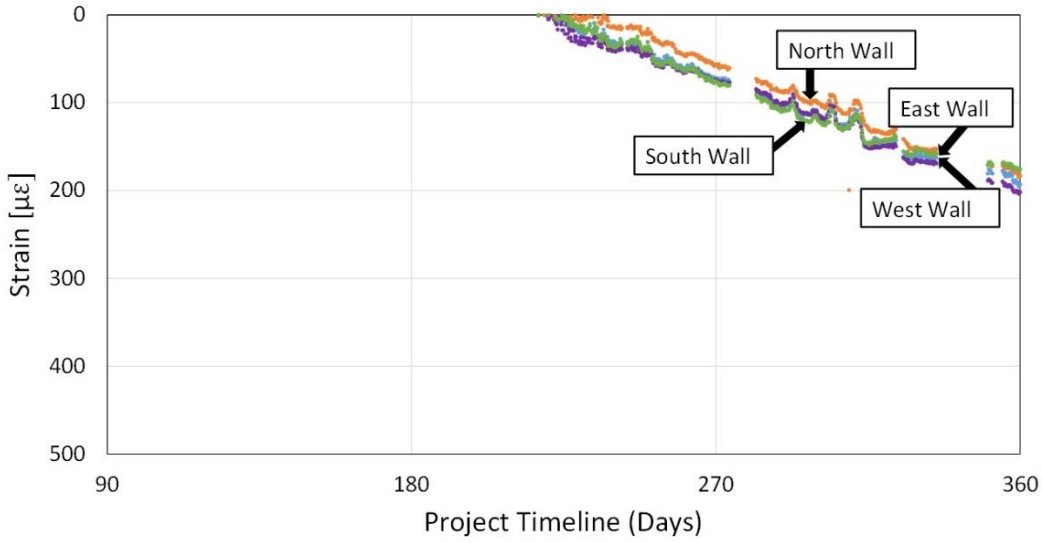

Figure 5.8 Level 28 Strain Measurements.

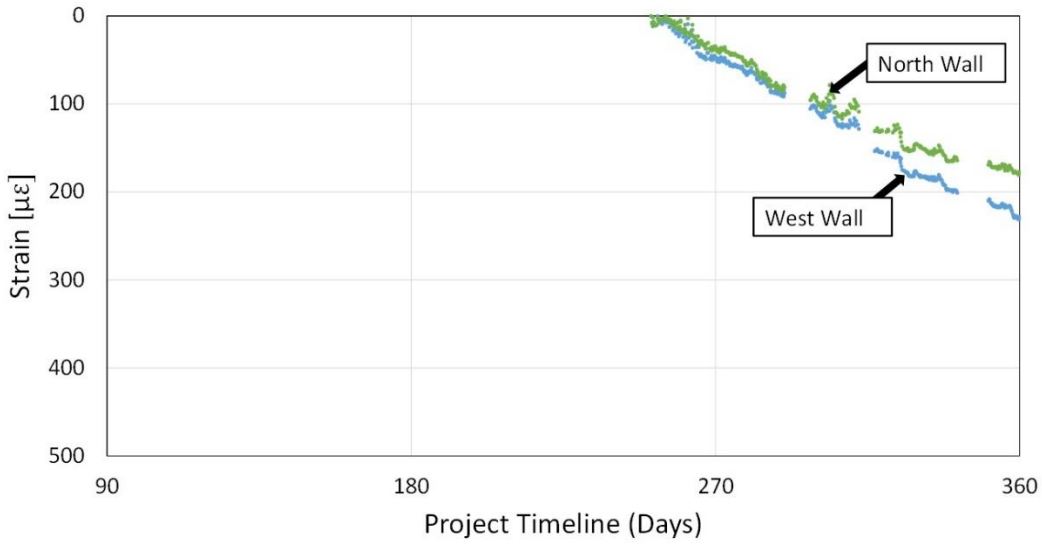

Figure 5.9 Level 36 Strain Measurements.

5.3.1 Comparison with Predictions

Strain gauge temperature readings and CTE adjusted strain measurements for Levels 3, 5, 13, 21, 28, and 36 are presented in Figures 5.11 through 5.16. Results using ACI, B3, CEB, GL, and B4 prediction models, presented in Table 3.1, were also developed and overlaid for comparison and to ensure the measurement results were reasonable. Figure 5.10 presents only prediction model results for Parking Level P3 because construction began before a gauge could be installed. This level is located three levels below grade, represents the base of the tower, and was constructed on day zero of the project timeline (x-axis). Due to a lack of measurements at this level, average predicted values were used when calculating shortening estimations.

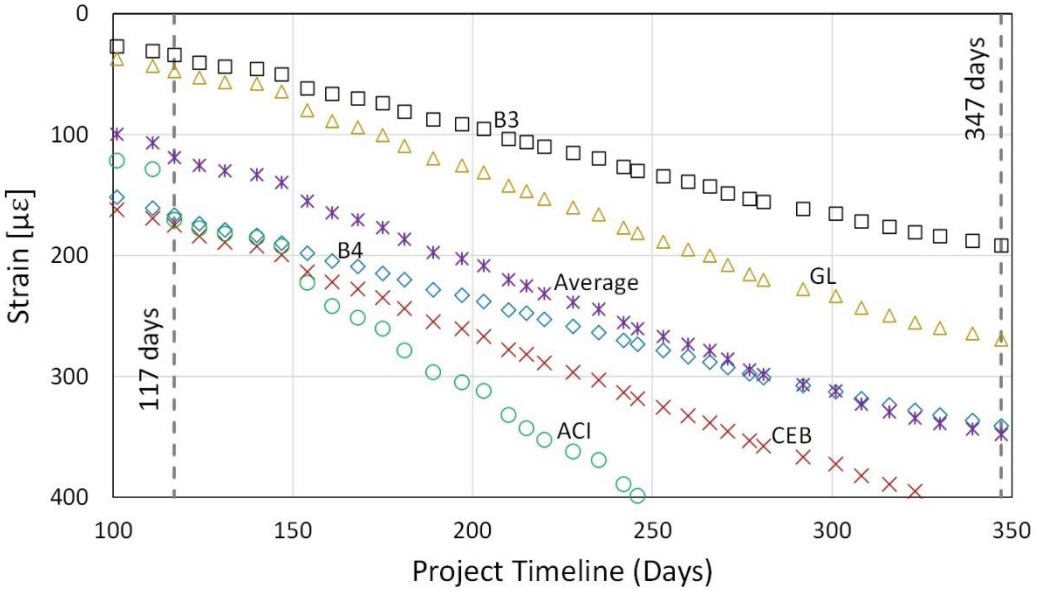

Figure 5.10 Level P3 Predictions.

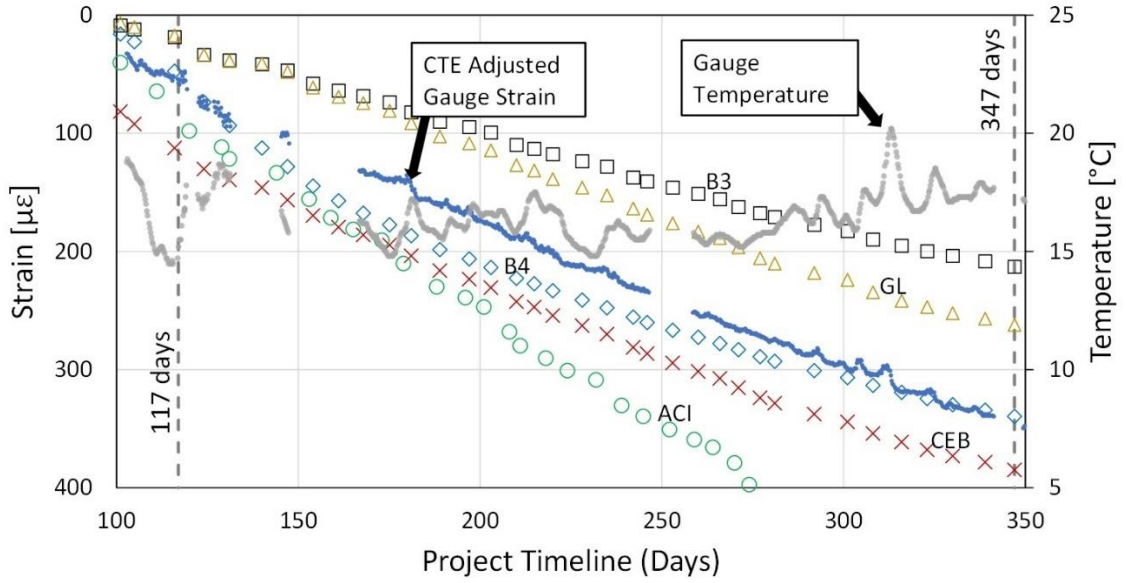

Figure 5.11 Level 3 Measurements and Predictions.

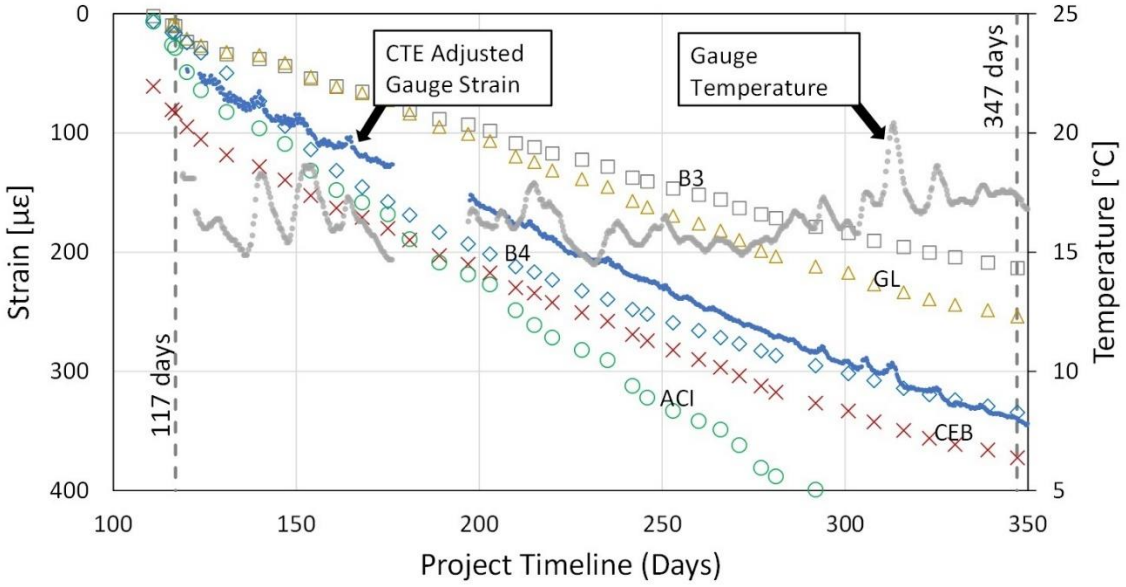

Figure 5.12 Level 5 Measurements and Predictions.

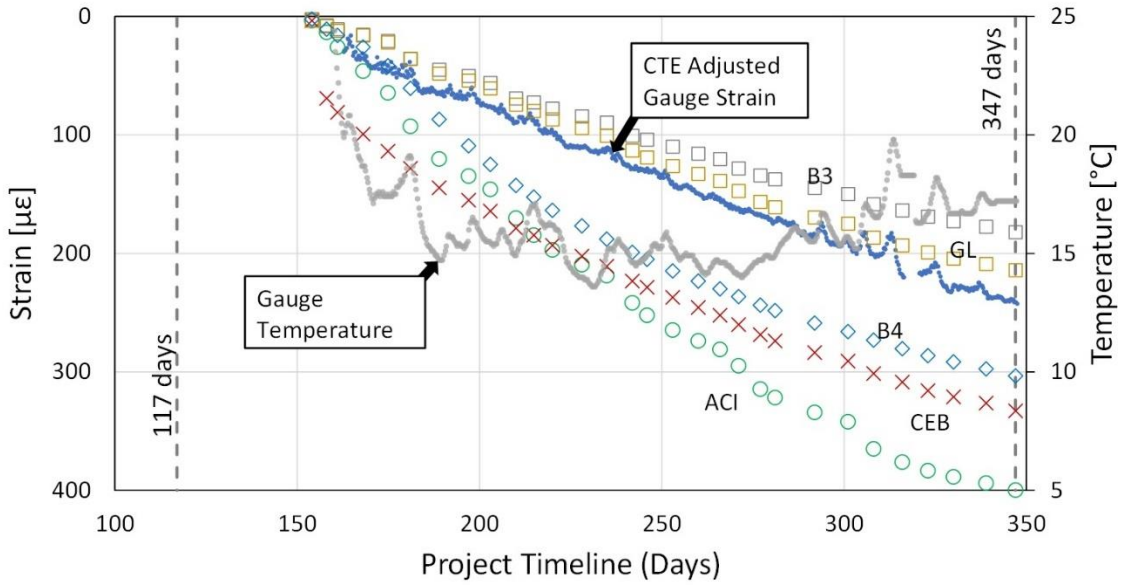

Figure 5.13 Level 13 Measurements and Predictions.

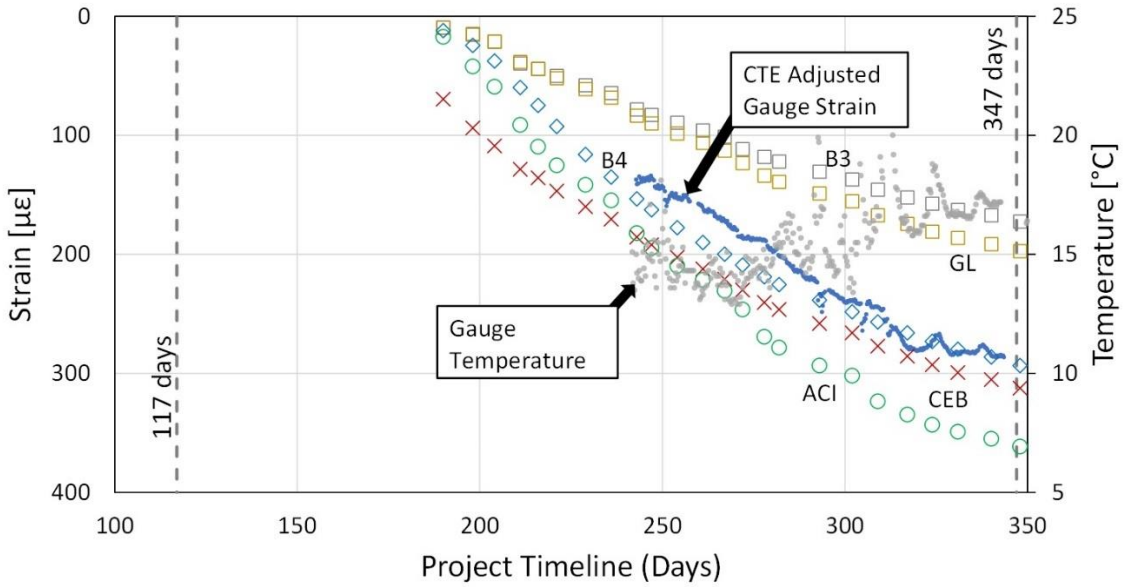

Figure 5.14 Level 21 Measurements and Predictions.

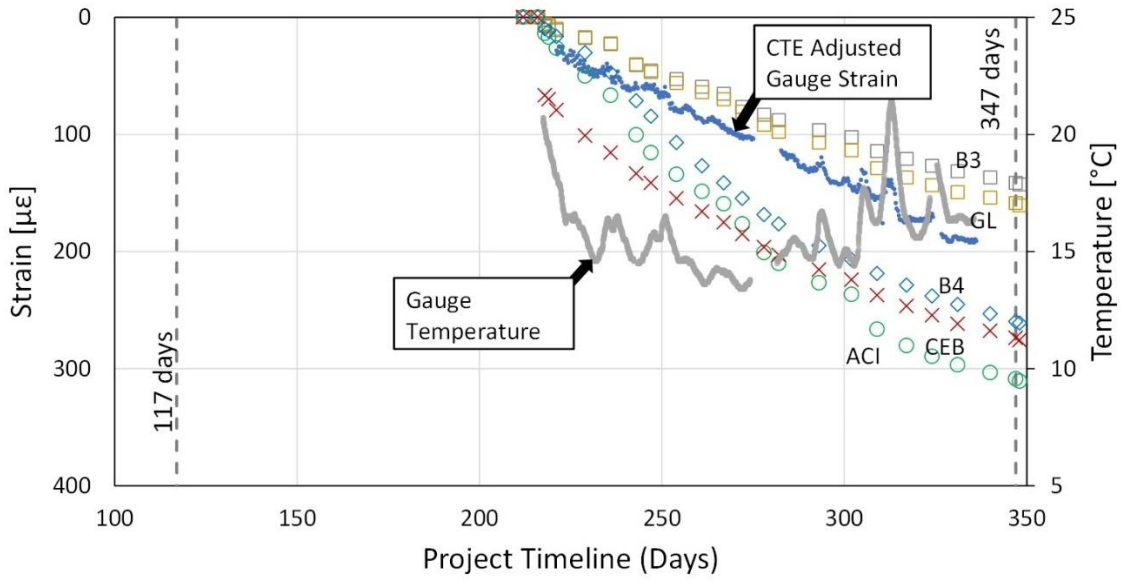

Figure 5.15 Level 28 Measurements and Predictions.

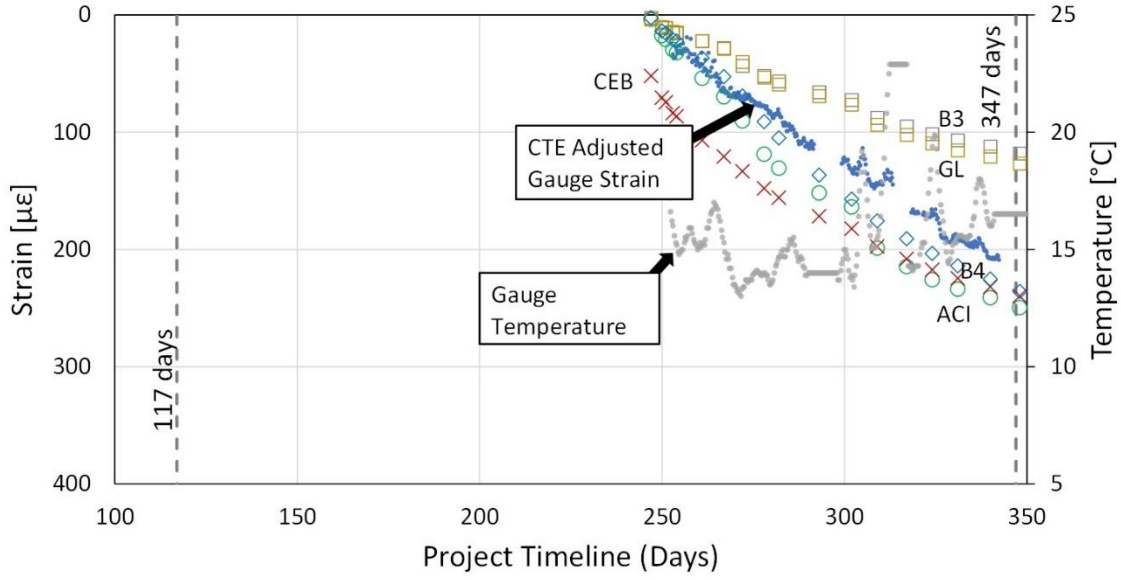

Figure 5.16 Level 36 Measurements and Predictions.

In general, strain gauge measurements acquired during construction of the Salesforce Project trended between B4 and GL predictions. Databases containing creep and shrinkage test results have expanded greatly to include thousands of specimens with some containing admixtures (Hubler et al., 2015). However, when considering large volume to surface ratio members, such as core walls, work by Zou et al. (2014) identified potential deficiencies in predictions since they are primarily based on testing of one-dimensional prismatic or cylindrical specimens with small volume to surface ratios. Measuring core wall strains within a variety of buildings may assist in further expanding this body of work.

5.3.1.1 Lumped Mass Sequencing

To simplify creep predictions, multiple story masses were lumped together. Experimental research indicates that creep strains may be considered approximately proportional to stress and may be defined as (Bazant, 1988):

$$\varepsilon_c(t,t') = \left[\frac{\sigma(t')}{E_c(t')}\right] \varphi(t,t') \tag{5.3}$$

The creep coefficient at time t resulting from a load applied at time t' is denoted as $\varphi(t,t')$; the member stress and elastic modulus are denoted as σ and E_c, respectively. Core wall segments will experience multiple instances of stress application as construction progresses and additional stories are incrementally added. Bazant (1988) indicated that the total creep strain developed within a member may be considered the sum of creep effects resulting from each instance of stress based on the principal of superposition. Since the bottom level of the Salesforce Tower would experience over 60 stories applied above it, an equal number of

prediction models would need to be constructed to represent strain development associated with each stress application.

Work by Kim et al (2012) found lumping multiple stress applications into larger groups greatly reduced the amount of processing required when predicting strain development. Results from an analysis of an 80-story building with masses lumped into 10-story groups produced an error of less than 2% at an age of 1,000 days. In a similar fashion, masses were lumped into six to 10-story groups when preparing creep prediction models for the Salesforce Tower project.

5.3.1.2 Reinforcement Adjustment

Since prediction models are based on a database of plain concrete samples, results need to be adjusted to account for reinforcement effects. Due to bonding, core wall longitudinal reinforcement provides some level of restraint against volume reduction. To quantify and adjust for these effects, predicted shrinkage and creep strains may be equated to compressive strains resulting from a fictitious axial force, *N(t)*:

$$N(t) = \varepsilon_p(t) \cdot E_c(t) \cdot A_c \tag{5.3}$$

The predicted shrinkage and creep strain at time *t* is denoted as $\varepsilon_p(t)$; the concrete modulus of elasticity at time *t* as $E_c(t)$; and the concrete net area as A_c. The adjusted predicted strain, $\varepsilon_{p,a}(t)$, may then be obtained by applying a simulated force over the concrete and steel areas while considering their respective elastic moduli (Gribniak et al, 2013):

$$\varepsilon_{p,a}(t) = \left[\frac{N(t)}{E_c(t)A_c + E_s A_s}\right] = \left[\frac{\varepsilon_p(t)}{1 + n(t)\rho}\right] \tag{5.4}$$

The steel modulus of elasticity is denoted as E_s; the steel area as A_s; the modular ratio at time t as $n(t)$; and the reinforcement ratio as ρ. The concrete modulus of elasticity was estimated as 57,000 times the square root of the reported 28-day concrete strength, in psi, per ACI Committee 209 (2008). The reported 28-day concrete strength was equal to 11,880 psi (81.9 MPa). Cylinder testing collected from the first 39 floors averaged 11,528 psi (79.5 MPa) with a low of 9,705 psi (66.9 MPa), a high of 13,645 psi (94.1 MPa), and a standard deviation of 897 psi (6.2 MPa). Due to differences in size, geometry, and curing conditions, cylinder strength does not match the structure exactly. Reinforcement ratios throughout the Salesforce Tower core walls ranged between 0.002 and 0.028 with Grade 60 bars. Higher ratios generally occurred near wall ends and adjacent to openings. Ratios also increased along lap splices. Increased ratios at such locations were neglected and typical ratios within the middle of the wall were used when making adjustments. In general, prediction model results were reduced by approximately 4% due to these effects.

5.4 Shortening Estimation Methods

For purposes of estimating elevation changes, the tower was divided into segments. Segments span between instrumented levels so that each contains strain measurements at either end. Shortening within an individual segment could theoretically be determined if the average change in strain throughout the length were known. For example, the average change in strain occurring through segment q, consisting of m levels, between some reference time t_r and current time t, could be computed as:

$$\overline{\Delta\varepsilon}_q(t, t_r) = \frac{1}{m}\sum_{j=1}^{m} \Delta\varepsilon_j(t, t_r) \quad (5.5)$$

The change in strain at each level '*j*' may be computed as:

$$\Delta\varepsilon_j(t, t_r) = \varepsilon_j(t) - \varepsilon_j(t_r) \tag{5.6}$$

However, since each segment is only instrumented at the top and bottom levels, strain measurements are only available for a *j* equal to 1 and *m*. The average change in strain within segment *q* may then be approximated by linearly interpolating between gauge measurements, computed as:

$$\overline{\Delta\varepsilon}_{a,q}(t, t_r) = \frac{1}{2}\left[\Delta\varepsilon_1(t, t_r) + \Delta\varepsilon_m(t, t_r)\right] \tag{5.7}$$

Shortening within segment *q* may then be estimated by applying the segment length, h_q, to the approximated average strain:

$$\Delta h_q(t, t_r) = \overline{\Delta\varepsilon}_{a,q}(t, t_r) \cdot h_q \tag{5.8}$$

Total cumulative shortening encompassing *p* segments can then be found by summing shortening within each individual segment:

$$\Delta H_p(t, t_r) = \sum_{q=1}^{p} \Delta h_q(t, t_r) \tag{5.9}$$

The adjusted elevation at the top of segment *p* can then be computed as:

$$EL_p(t) = EL_p(t_r) - \Delta H_p(t, t_r) \quad (5.10)$$

5.4.1 Method B Estimation Sample Calculations

Figure 5.17 illustrates the first two segments of the Salesforce Tower. Since a strain gauge sensor had not been installed within Level P3, only prediction values are illustrated in Figure 5.10. The average of all five prediction values are used in shortening estimation calculations in lieu of gauge data. Figures 5.11 and 5.12 illustrate both measured and predicted strains along with temperature readings at Levels 3 and 5, respectively. Since gauges measure changes in strain, initial values equal zero when powered on unless adjusted otherwise. Although relative changes in strain and subsequent shortening estimations are unaffected, initial values were set equal to the average of the five prediction values to allow for better comparison with predictions.

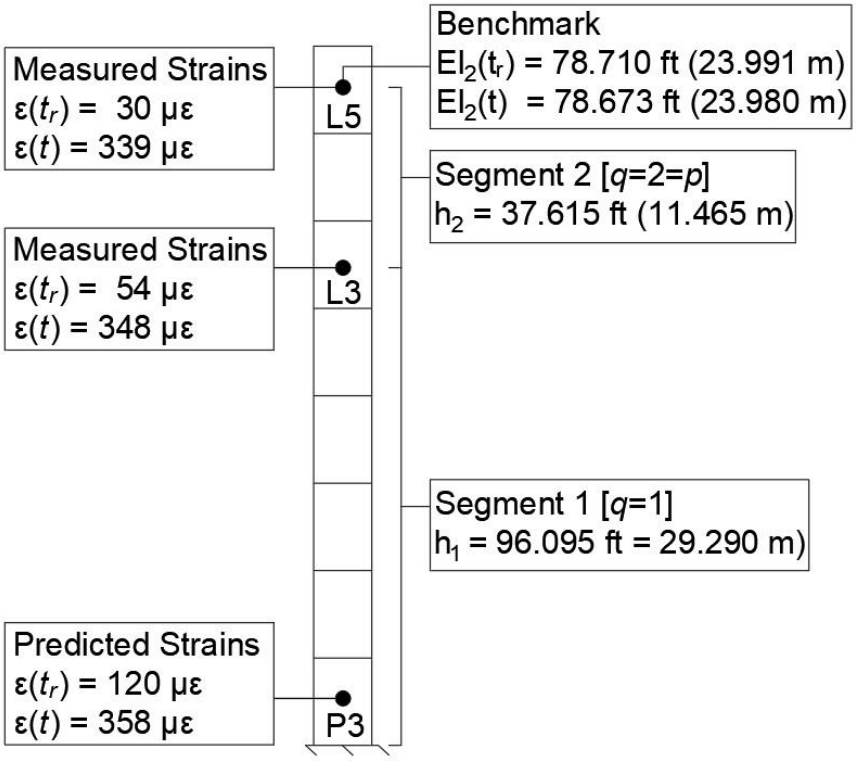

Figure 5.17 Shortening Approximation Method for Segments 1 & 2 (t_r=117 days; t=347 days)

Using the Method B estimation, change in elevation example computation results for a benchmark set within Level 5 are presented in Table 5.2. The benchmark was established approximately 10 days after the story was poured, which coincides with day 117 of the project timeline (Level P3 was poured on day zero).

Table 5.2 Change in Elevation Computations.

	Segment 1 [q=1]	Segment 2 [q=2=p]
$\varepsilon_1(t)$ [με]	358	348
$\varepsilon_1(t_r)$ [με]	120	54
$\varepsilon_m(t)$ [με]	348	339
$\varepsilon_m(t_r)$ [με]	54	30
$\Delta\varepsilon_1(t,t_r)$ [με]	238	294
$\Delta\varepsilon_m(t,t_r)$ [με]	294	309
$\chi_q(t_r,t,m)$ [με]	-0.2 ± 1.6	0.3 ± 1.6
$\overline{\Delta\varepsilon}_q(t,t_r)$ [με]	265.8 ± 1.6	301.8 ± 1.6
h_q [ft | m]	96.095 | 29.290	37.615 | 11.465
$\Delta h_q(t, t_r)$ [ft | mm]	0.0255 ± 0.0002 | 7.87 ± 0.06	0.0114 ± 0.0001 | 3.47 ± 0.03
$\Delta H_p(t, t_r)$ [ft | mm]	-	0.037 | 11.3
$EL_p(t_r)$ [ft | m]	-	78.710 | 23.991
$EL_p(t)$ [ft | m]	-	78.673 | 23.980

The following example calculations evaluate shortening between t_r equal to 117 days and t equal to 347 days. (when Level 61 was poured). Segment 1 spans between Level P3 at the base of the tower and Level 3. Using values obtained from Figures 5.10 and 5.11, the estimated change in strain occurring within Levels P3 and 3 may be computed using Equation [5.6] as:

$$\Delta\varepsilon_{P3}(t, t_r) = (358\ \mu\varepsilon) - (120\ \mu\varepsilon) = 238\ \mu\varepsilon \quad (5.11)$$

$$\Delta\varepsilon_{3}(t, t_r) = (348\ \mu\varepsilon) - (54\ \mu\varepsilon) = 294\ \mu\varepsilon \quad (5.12)$$

The approximate average change in strain for Segment 1 may then be computed using Equation [5.7] as:

$$\overline{\Delta\varepsilon}_{a,1}(t, t_r) = \frac{1}{2}[(238\ \mu\varepsilon) + (294\ \mu\varepsilon)] = 266.0\ \mu\varepsilon \quad (5.13)$$

Shortening within Segment 1 may then be estimated by applying the approximate average change in strain to the segment length using Equation [5.8] as:

$$\Delta h_1(t, t_r) = (266.0\ \mu\varepsilon) \cdot (96.095\ \text{ft}) = 0.0256\ \text{ft}\ (7.80\ \text{mm}) \quad (5.14)$$

Segment 2 spans between Level 3 and Level 5. Using values obtained from Figures 5.11 and 5.12, the estimated change in strain occurring within Level 5 may be computed using Equation [5.6] as:

$$\Delta\varepsilon_5(t, t_r) = (339\ \mu\varepsilon) - (30\ \mu\varepsilon) = 309\ \mu\varepsilon \quad (5.15)$$

The approximate average change in strain for Segment 2 may then be computed using Equation [5.7] as:

$$\overline{\Delta\varepsilon}_{a,2}(t, t_r) = \frac{1}{2}[(294\ \mu\varepsilon) + (309\ \mu\varepsilon)] = 301.5\ \mu\varepsilon \quad (5.16)$$

Shortening within Segment 2 may then be estimated by applying the approximate average change in strain to the segment length using Equation [5.8] as:

$$\Delta h_2(t, t_r) = (301.5\ \mu\varepsilon) \cdot (37.615\ \text{ft}) = 0.0113\ \text{ft}\ (3.44\ \text{mm}) \qquad (5.17)$$

Total cumulative shortening of both segments may be computed using Equation [5.9] as:

$$\Delta H_2(t, t_r) = (0.0256\ \text{ft}) + (0.0113\ \text{ft}) = 0.037\ \text{ft}\ (11.3\ \text{mm}) \qquad (5.18)$$

Finally, the updated benchmark elevation at the top of Segment 2 at time *t* may be computed using Equation [5.10] as:

$$EL_2(t) = (78.710\ \text{ft}) - (0.037\ \text{ft}) = 78.673\ \text{ft}\ (23.980\ \text{m}) \qquad (5.19)$$

The Method A estimation follows the same procedures except that strain values unadjusted for temperature are used. Equations [5.11], [5.12], and [5.15] would need to be revised using back calculated values for $\Delta\varepsilon_g$ from Equation [5.1], based on temperature readings given in Figures 4.4 and 4.5. Since temperature fluctuations were minimal between these two periods in time and the measurements are only significant to three digits, in this case, the results of the Method A estimation are equal to that of Method B.

5.4.2 Method C Estimation Overview and Sample Calculations

The Method C shortening estimation expands on Method B by also incorporating the theoretical non-linear behavior occurring between instrumented levels. In the previous chapter, ACI, B4, CEB, GL, and B3 prediction models were developed to simulate a scenario where strain is measured at intermittent levels of a core wall tower. Results were used to compare changes in concrete strain development occurring throughout multiple stories with a simplified approximation that linearly interpolates changes in strain development between either end. The difference between the two models is considered the theoretical non-linear change in strain occurring throughout the segment that is uncaptured by the gauges. A multi-variable regression equation was developed using all prediction results while considering all combinations of t_r (between 10 and 115 days after the top story is poured, at 5 day intervals), t (between 10 days after t_r and 260 days after the top story is poured, at 5 day intervals), and m (between 5 and 8 stories, at 1 story intervals):

$$\chi_{a,q}(t_r,t,m) = 1.8 + 0.01(t_r-t_s) - 0.4ln(t-t_s) - 0.17(m) + E \quad (5.20)$$

Since the time parameters are specific to an individual segment, each is adjusted by t_s, which represents the time the bottom story of the segment under consideration was poured. The model accommodates small variations in stress (0.10-0.12 MPa) and reinforcement ratio (0.007-0.010) if results are considered significant to the nearest whole microstrain. The model error is represented as E with a standard error given as +/- 0.8 με and represents a coefficient of determination equal to 0.13. Error represented at a 95% confidence level may be found by multiplying the standard error by 1.96, equating to +/- 1.6 με (Mendenhall & Sincich, 2012).

To incorporate the theoretical non-linear behavior, Equation [5.7] may be revised as:

$$\overline{\Delta\varepsilon}_{a,q}(t, t_r, m) = \frac{1}{2}[\Delta\varepsilon_1(t, t_r) + \Delta\varepsilon_m(t, t_r)] + \chi_{a,q}(t_r, t, m) \quad (5.21)$$

The theoretical non-linear change in strain behavior for Segments 1 and 2 may be computed using Equation [5.20] as:

$$\chi_{a,1}(117,347,5) = 1.8 + 0.01(117\text{-}0) - 0.4ln(347\text{-}0) - 0.17(5) \pm E = -0.2 \pm E\ \mu\varepsilon \quad (5.22)$$

$$\chi_{a,2}(117,347,2) = 1.8 + 0.01(117\text{-}107) - 0.4ln(347\text{-}107) - 0.17(2) \pm E = 0.3 \pm E\ \mu\varepsilon \quad (5.23)$$

It should be noted that an *m* equal to 2 stories falls below the 5 story model parameter lower limit. Additionally, substantial delays were encountered during construction of Segment 1, resulting in story construction averaging approximately 17 days compared to 5 days assumed in the model. The approximate average change in strain for Segments 1 and 2 may then be computed using Equation [5.21] while evaluating the model error at a 95% confidence level as:

$$\overline{\Delta\varepsilon}_{a,1}(t, t_r) = \frac{1}{2}[(238\ \mu\varepsilon) + (294\ \mu\varepsilon)] - 0.2 \pm 1.6\ \mu\varepsilon = 265.8 \pm 1.6\ \mu\varepsilon \quad (5.24)$$

$$\overline{\Delta\varepsilon}_{a,2}(t, t_r) = \frac{1}{2}[(294\ \mu\varepsilon) + (309\ \mu\varepsilon)] + 0.3 \pm 1.6\ \mu\varepsilon = 301.8 \pm 1.6\ \mu\varepsilon \quad (5.25)$$

Shortening within Segments 1 and 2 may then be estimated by applying the approximate average change in strain to the segment length using Equation [5.8] as:

$$\Delta h_1(t, t_r) = (265.8 \pm 1.6\ \mu\varepsilon) \cdot (96.095\ \text{ft}) = 0.0255 \pm 0.0002\ \text{ft}\ (7.87 \pm 0.06\ \text{mm}) \quad (5.26)$$

$$\Delta h_2(t, t_r) = (301.8 \pm 1.6\ \mu\varepsilon) \cdot (37.615\ \text{ft}) = 0.0114 \pm 0.0001\ \text{ft}\ (3.47 \pm 0.03\ \text{mm}) \quad (5.27)$$

Total cumulative shortening of both segments may be computed using Equation [5.9] as:

$$\Delta H_2(t, t_r) = (0.0255 \pm 0.0002\ \text{ft}) + (0.0114 \pm 0.0001\ \text{ft}) = 0.037\ \text{ft}\ (11.3\ \text{mm}) \quad (5.28)$$

Since the measurements are only significant to three digits, in this case, the results of the Method C estimation are equal to the Method B estimation.

5.4.3 Overview of Results

Figure 5.18 illustrates cumulative shortening that occurred at benchmark levels throughout construction based on Method C estimations. As expected, the trends indicate the rate of shortening increases with higher levels in the tower. Also overlaid on the figure are shortening values that were periodically gathered using conventional total station instrumentation, specific to benchmarks set at Levels 3 and 5. The project surveyor estimated the measurement error to be on the order of +/- 0.015 feet (+/- 4.6 mm). The strain-based estimations agree with the conventional measurements when the estimated range of error is considered.

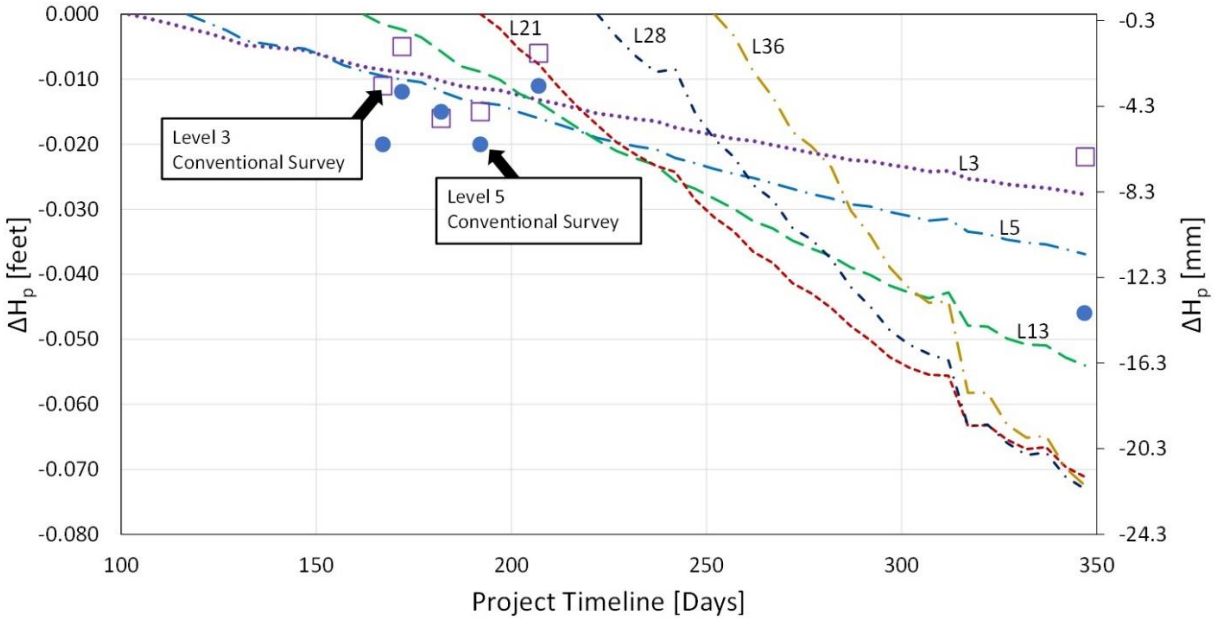

Figure 5.18 Method C Shortening Estimations at Benchmark Levels

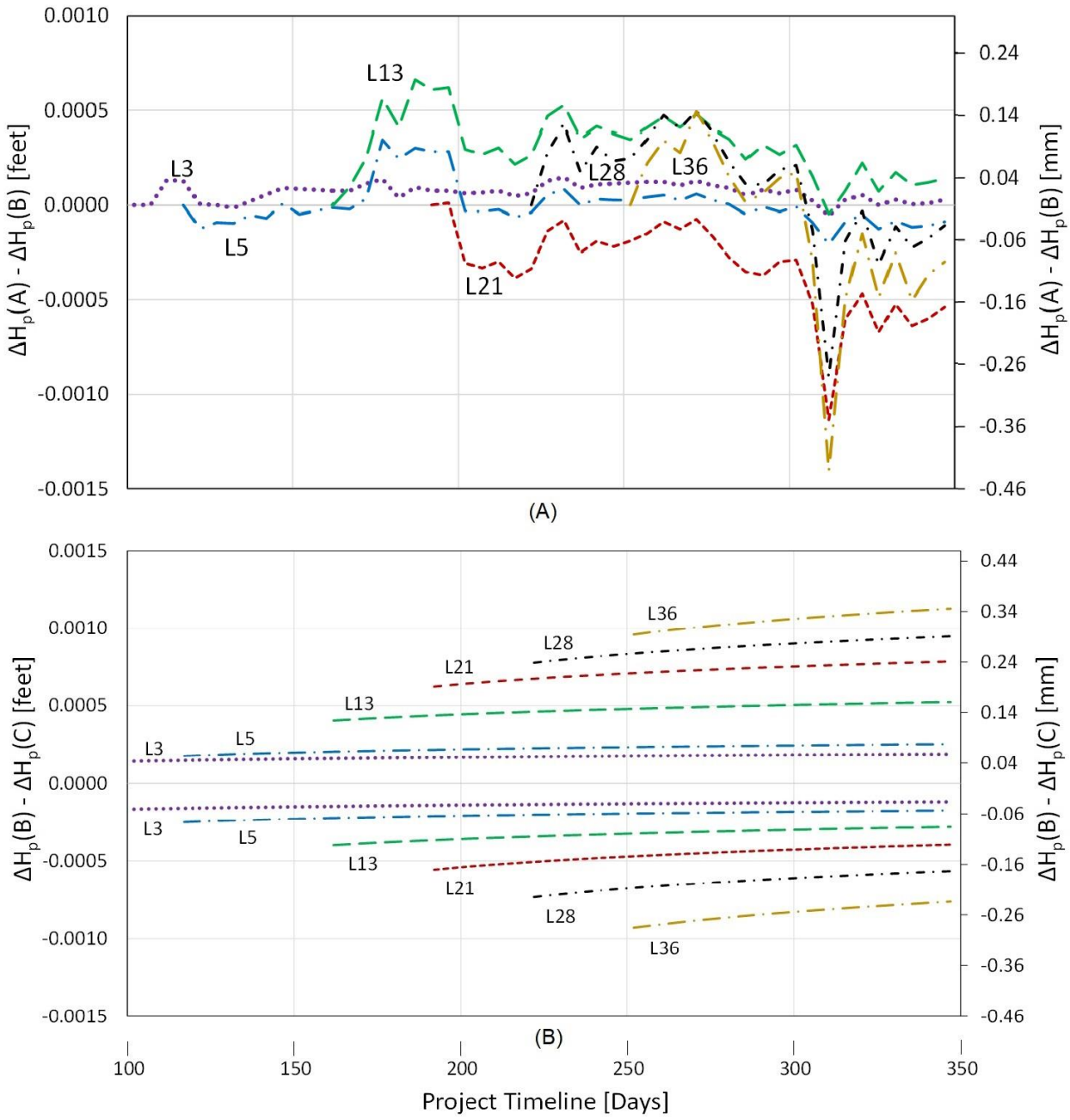

Figure 5.19 (A) Difference between Method A and B Estimations, and (B) Difference between Method B and C Estimations

Figure 5.19A illustrates differences between Method A and B shortening estimations. The only difference between the two methods is the CTE adjustment in Method B. The most substantial variation to note is around day 312 when a spike in gauge temperature on the order of 6°C occurred. Because Method A estimations do not adjust for temperature fluctuations, the readings registered an apparent strain reduction. The greatest affect was on Level 36 shortening, temporarily reflecting a reduction of approximately 0.0014 feet (0.43 mm). It is understandable that levels higher in the tower would experience greater effects since the shortening they experience is an accumulation of all lower levels.

Figure 5.19B illustrates differences between Method B and C shortening estimations. The only difference between the two methods is the approximate non-linearity adjustment in Method C, which includes a range of error based on a 95% confidence interval. The upper and lower bounds for each level in Figure 5.19B illustrate this range of error. Ranges for levels higher in the tower are greater because they accumulate all error below them. The fact that the upper and lower bounds for each level are approximately centered around zero indicates the non-linearity adjustments themselves had only a minor effect on the shortening estimations, and that the key benefit of Method C is a better understanding of the level of uncertainty that exists in the estimates. Although the error range of about ± 0.001 ft (± 0.30 mm) exhibited by Level 32 may be minor in survey terms, error ranges will continue to compound at higher tower levels, producing results of greater significance. Additionally, error range significance become more apparent when comparing differences between Methods A and C, which can be computed by summing corresponding data from Figures 5.19A and 5.19B ([A-B]+[B-C]=[A-C]). For example, the difference of -0.0014 feet (-0.43 mm) at Level 36 on day 312 from Figure 5.19A summed with the -0.0008 feet (0.24 mm) value from Figure 5.19B for the lower range of Level

36 on the same day, gives a total difference of -0.0022 feet (-0.67 mm), indicating Method A shortening estimations errors can become large when temperature fluctuations occur, particularly at higher levels in the tower.

5.5 Summary of Salesforce Tower Implementation

Lessons learned throughout the system implementation and measurement acquisition process indicated the need for a more thoroughly coordinated sensor installation plan well before core wall construction is set to begin. Strain gauges should be protected from damage during concrete placement, power systems should be in place so there is no delay in initiating the data logging process after an instrumented story is poured, and wiring should be laid out so that it will not interfere with other phases of construction.

Three shortening estimation methods that utilize strain gauge measurements acquired at intermittent levels were presented. Method A is the simplest of the three and is best suited for environments with mild temperature fluctuations (<10°C); Method B adjusts for errors associated with temperature fluctuations and is generally adequate for towers of moderate height (<60 stories); and Method C is the most complex of the three but adjusts for approximate non-linearity in concrete strain development between instrumented levels and provides a range of error in estimation results, which is particularly beneficial for taller towers (>60 stories).

A sample of conventionally surveyed measurements agreed with shortening estimation results. Although the strain-based elevation monitoring system imposed a larger up-front cost, the significant reduction in survey labor resulted in an estimated net reduction in monitoring costs of at least 10%. It is estimated that taller towers will experience greater relative benefit, with cost reductions of at least 30% for buildings on the order of 100 stories tall. In general, the strain-based elevation monitoring approach proved to be a practical and complimentary

measurement method during construction of the Salesforce Tower through both cost savings and increased efficiency.

CHAPTER VI

GUIDELINES FOR EFFECTIVE DEFORMATION MONITORING ADJACENT TO CONSTRUCTION ACTIVITY

6.1 Introduction

Deformation monitoring has been a rapidly evolving field. As such, construction specification authors may not have familiarity with particular technologies, systems, and methods. Insufficiently detailed specifications in conjunction with low bid contracts have led to monitoring systems that are subject to mismanagement and lack usable results even though they may loosely meet requirements. Catastrophic consequences have resulted in some cases and worthless outcomes in many others (Brownjohn, 2007; NAS, 2005).

A wide range of sensors, instruments, and system configurations have been utilized and developed to measure and report a number of metrics in a variety of conditions. This chapter focuses on specifications related to the use of Automated Motorized Total Stations (AMTS) to measure and identify anomalous behavior in structures adjacent to construction activity. AMTS systems have been used in deformation monitoring programs for many years and are advantageous due to their high accuracy potential and low cost impact as opposed to manual data collection methods (Blackwell and Bonham-Carter, 1993). However, these systems can be complex and are often incorrectly utilized when individuals who lack adequate experience and understanding attempt to implement and manage them. This review aims to identify trends in

specifications that lend to ineffective results and provide guidelines to increase the probability of success.

6.2 Monitoring Structures During Construction

The monitoring of structural deformations is one of the most effective ways to understand structural response, particularly due to external influence (Ding et. al., 2000). Deformations of a structure can be defined as a relative change in form or position over time with respect to its original state. Therefore, in order to effectively monitor structural deformations, relative movement at various points on a structure must be measured over time. Surveying procedures have provided an accurate means to measure points of movement and spatially relate them. This could be accomplished manually using a total station, but since deformation monitoring requires repeated measurements over time, costs could escalate. Additionally, the presence of human error in the process could result in reduced measurement accuracies. To get the best results, the monitoring system should be automated and autonomous (Kenchington, 2003). AMTS instrumentation offers the ability to monitor deformations continuously and accurately, particularly in urban environments when GNSS sensors may be ineffective due to obstructions.

Like traditional total stations, AMTS instruments simultaneously collect horizontal angles, zenith angles, and distance measurements. However, AMTS instruments also contain a feature frequently referred to as Automatic Target Recognition (ATR). ATR determines the horizontal and zenith angle deviations that exist between the current telescope alignment and the center of prism located within the field of view. The horizontal and zenith angles will adjust until the deviations are within a certain threshold, at which point the deviation values along with instrument's tilt compensation values are added to the telescope's positioned angles to determine the final angles to be used in the target's positional computation (Bayoud, 2007).

The development and advancement of this technology over the past two decades, including wireless communications for remote data review, has made AMTS systems an ideal monitoring solution for many projects. Although AMTS monitoring systems have been implemented in a variety of situations, the design of such systems and the analysis of the data it produces is not well documented, standardized, or regulated. Construction specifications are often vague and lack the necessary requirements to ensure the system is successfully implemented and produces meaningful results.

6.3 Monitoring Specifications Review

Construction specifications should provide specific criteria as to how a monitoring system is to be implemented and managed. What follows is a summary of a collection of construction specifications for a variety of AMTS deformation monitoring projects throughout the United States that have been publicly advertised within the past several years. The purpose is to examine what statements are made or not made, what is or isn't working, and what improvements may be considered.

A university in Ohio was seeking installation of an AMTS system to monitor deformations of several structures. Numerous detailed technical specifications were listed for the AMTS instrument, prisms, and processing software. The level of technical detail appeared to endorse a particular line of products. Outside of these requirements, there were only vague references to actual intended results and functionality of the system. A similarly structured specification package for a dam monitoring project in California also required the equipment to meet exact specifications but again neglected to describe results and functionality. The instrumentation specialist was also required to describe relevant work experience and demonstrate success on previous projects. In Washington, another dam monitoring project

required several detailed instrumentation specifications as well as references to confirm success of at least three similar projects within the last five years.

A railyard in Brooklyn required installation of an AMTS deformation monitoring system when work that may affect existing structures in the area was to commence, including demolition, excavation, dewatering, and pile driving. The specifications required that work be performed under the direction of a Professional Surveyor (P.S.) and that qualifications be submitted showing three successfully completed similar projects within the last five years. Much of the monitoring system design was left up to the project awardee and required that a work plan be submitted that detailed what was to be monitored and how. Some of the required elements of the work plan included the type of equipment proposed, the tolerances of the equipment, the calibration records of the equipment, the procedures for installation of the equipment, and the methods and frequency of measurements. Daily reports were to be submitted detailing the maximum levels of movement recorded. A minimum of two optical targets were to be installed and monitored on each foundation. The specifications also identified measurement displacement values at which alerts should be triggered. An alert threshold value of 0.25 inches (6.4 mm) would require that a message be sent to appropriate project representatives, and a maximum alert threshold value of 0.50 inches (12.7 mm) would require immediate suspension of work.

An airport in Minneapolis required structural deformation monitoring during an underground railway construction project. The specifications required that the AMTS system be provided, monitored, and maintained under the direction of an instrumentation specialist that has at least five years of comparable experience including at least three projects with web-based reporting. The AMTS instruments were required to have an accuracy of +/- 0.05 inches (1.3 mm) when measuring to prisms. A reference network of at least three prisms located outside the

zone of influence was also required. The project awardee would also be required to provide training sessions to appropriate personnel. The training should include a description of the monitoring system, a description of the alert system, and instruction on how to use the web-based platform. Alert threshold and maximum values were also specified at 0.20 inches (5.1 mm) and 0.40 inches (10.2 mm), respectively, and text messages were to be sent if either mark is reached.

A large excavation project in Seattle prompted a comprehensive deformation monitoring plan due to the project's proximity to adjacent buildings as well as a highway overpass. The specifications required that the AMTS monitoring system be implemented under the direction of a P.S. There was no reference to equipment specifications except that the measurements must be within a tolerance of +/-1/8 of an inch (3.2 mm). Monitoring prisms were required to be installed on settlement sensitive structures located within a horizontal distance equal to the depth of the excavation, and the measurements were to be collected hourly. Appropriate personnel were to be notified if adjacent building displacement measurements exceeded 0.5 inches (12.7 mm). The specifications required that baseline readings specific to the overpass be used to estimate effects of temperature and traffic on the displacement results. If triggered, an alert threshold value of 0.48 inches (12.2 mm) would require appropriate personnel to be notified the same day. Another alert threshold value of 0.96 inches (24.4 mm) would require appropriate personnel to be notified immediately. A maximum alert threshold value of 1.44 inches (36.6 mm) would require that construction activity be suspended, and a corrective action plan be submitted to resolve the observed deformations.

The development of a high-rise apartment building in Boston required deformation monitoring of a turnpike tunnel ramp directly adjacent to the construction site. The

specifications required that 18 monitoring points along the alignment of the ramp wall be measured twice per week by a P.S. who had a minimum of three years of experience performing similar surveys. While the system was not required to be automated, an AMTS system could be used in lieu of manual surveying. The specifications required that the measurements have an accuracy within +/- 1/8 inch (3.2 mm). An initial baseline survey was to be established one week prior to construction with reference points that have been established outside of the construction ZOI.

Existing structures required deformation monitoring surrounding a revitalization project in downtown Austin, Texas which included two high rise office buildings extending five stories below grade. The specifications required that a P.S. obtain baseline readings for all AMTS monitoring points. A total of six reference points was required to be established outside the excavation ZOI. It was also stated that the contractor was responsible for interpreting the data produced by the monitoring instrumentation. An alert value of 0.25 inches (6.4 mm) would require measurement review, an alert value of 0.75 inches (19.0 mm) would require that construction be halted, and repairs mitigated.

6.3.1 Specifications Review Summary

The following is a summary of the most common requirements identified during the review of construction specifications:

- Four of eight required that a P.S. have some involvement in the process
- Four of eight specified displacement alert values
- Three of eight contained measurement accuracy values
- Three of eight discussed reference control requirements
- Three of eight contained detailed equipment specifications

- Three of eight required some degree of experience in place of professional qualifications

The following is a summary of the less common requirements that were identified in only one of the eight construction specifications reviewed:

- Project awardee required to provide some degree of system training
- Monitoring system to be designed by the project awardee
- Monitoring data to be interpreted by the project awardee
- AMTS system presented as an option in lieu of manual surveying
- Baseline monitoring evaluation of temperature and traffic effects

The following is a summary of some items that were not identified in any of the construction specifications reviewed:

- No directives as to how the position of the instrument was to be determined
- No requirements for system testing
- None of the projects were structured as a Request for Qualifications for professional services

6.3.2 Specifications Review Discussion

One half of the specifications reviewed required that a P.S. have some involvement in the process. One of these four only required a P.S. be involved during the collection of baseline readings. Since the design, implementation, and operation of an AMTS system is based on the same theory and fundamentals of land surveying, the requirement that a professional oversee the process throughout is inherently obligatory. Additionally, licensed professionals are bound by a

code of ethics, an obligation to their profession that carries substantial weight when making decisions.

One half of the specifications reviewed provided displacement alert values that, when exceeded, would trigger either a data review or suspension of construction. The source of the chosen magnitudes was not specified. Since movement may vary between monitoring points, the application of a single threshold value to all locations may be problematic. For instance, a specified alert threshold may be too limiting at one location, which could result in a false alert, but not limiting enough at another, which could result in a missed alert.

Less than half of the specifications reviewed contained accuracy requirements. Even when provided, the accuracy requirements lacked detail and were specific to the instrument alone. For instance, a stated instrument accuracy of +/- 1/8 inch (3.2 mm) does not indicate if this is evaluated at one standard deviation or some other level of confidence. Although instrument specifications may be important, the accuracy of the data collected in the field during monitoring activities is more important than how the instrument may have performed in a laboratory test.

Less than half of the specifications reviewed discussed requirements associated with control references. The AMTS measurements and results are a product of the reference control network. Even the most stringent accuracy requirements and instrument specifications cannot make up for a poorly constructed control network. Problems with an inadequate control network may obscure movement of monitoring targets. Defective control references can generate unusable and meaningless results, and problems could be impossible to detect.

Less than half of the specifications reviewed provided detailed instrumentation and equipment specifications. As stated previously, although instrument specifications may be important, the accuracy of the data collected is the most important factor to consider. Three of the eight specifications reviewed allowed some degree of applicable work experience in place of professional qualifications. These generally required that bidders provide references of similar types of work that had been recently completed. As stated previously, four of the eight specifications reviewed required a P.S. be involved, leaving one project without any required qualifications. A lack of qualifications is likely to result in a purely low bid scenario. Green (2000) observed that *low-bid procurement of services and instruments almost always leads to low quality*.

One of the specifications reviewed required that some degree of training be provided to the owner. However, the training only included a basic overview of the system and how to view the measurement data. If the intent is to pass a monitoring project to the owner after it is operational, the training program should be thorough and indicate when a professional should be consulted over time.

One of the specifications reviewed required the project awardee to design the monitoring system while another required the project awardee to interpret the results. The monitoring system design and subsequent interpretation of results should be provided by professionals that have a thorough understanding of the needs of the project; as well as the knowledge and experience necessary to both design a comprehensive system and effectively interpret the data it generates. This should generally be handled by the project design engineer since they are most familiar with the project or by a separately contracted professional engineering services firm that is experienced and dedicated to the AMTS monitoring quality control and analysis process.

One of the specifications reviewed required the project awardee to interpret the monitoring results. This should be avoided for the same reasons the monitoring system should not be designed by the bidder.

One of the specifications reviewed presented an AMTS system as an option in lieu of manually surveying. This optional approach may be advantageous for smaller projects with shorter durations and low hazardous potential.

One of the specifications required that the baseline readings be evaluated for temperature and traffic effects. Environmental effects, particularly temperature, have the potential to substantially influence measurements. This evaluation should be a regular part of baseline measurement review.

None of the specifications reviewed stated how the instrument position was to be determined or verified. Since all monitoring point measurements are based on the instrument position and orientation, a thorough understanding if it's level of stability and potential movement is critical to obtain accurate results.

None of the projects required testing or system validation. Once systems are implemented, accuracies are verified, and alert thresholds are set, a process that demonstrates the effectiveness of the system should be completed. For instance, a test may be performed by manually displacing a monitoring prism and assessing the monitoring system results. The test may be considered successful if the system identifies the displacement and triggers an appropriate alert.

None of the projects reviewed had issued a Request for Qualifications (RFQ) for professional services but were instead all bid solicitations. Dunnicliff and Powderham (2001) concluded that professional service methods are *much more likely to result in the goal of*

securing reliable and high quality data versus low bid methods. Professional service versus low bid methods have long been debated and much of the research supports a shift towards having monitoring programs handled by professional service contracts. Whether it is a concern with cost or simply a lack of motivation to alter the status quo, a low bid process still appears to be the general standard. Dail and Volterra (2009) acknowledged that baseline data collection is often inadequate when handled by the contractor since there is generally insufficient lead time between when the project is awarded and when it is scheduled to begin. Additional time is also often necessary to secure agreements with neighboring property owners to mount instrumentation on their structures. It was also noted that the contactor generally considers monitoring as a *cost with little benefit*, that it is viewed as a nuisance, and that it is not in their best interest because it has the potential to slow or halt construction.

The American Society of Civil Engineers Hydropower Committee (ASCE, 2000) recognized and discussed the benefits of contracting monitoring separately from construction, stating: *The following are generally not true when the contract for instrumentation is between the owner and the general contractor: (1) Contract is issued to entity most familiar with instrumentation. (2) Technical issues involving instrumentation system are resolved directly between owner and instrumentation specialists. (3) Staff is skilled in instrumentation issues. (4) Instrumentation issues are given top priority. (5) No additional markup on instrumentation system cost. All the above five factors are generally true when the contract for instrumentation is between the owner and an instrumentation company.*

6.4 Monitoring Specification Recommendations

The following four sub-sections detail areas of recommended improvement when preparing monitoring program specifications.

6.4.1 Contract Structure and Oversight

The structure of the contact is critical to the successful execution of work. Propper oversight ensures the subsequent results are accurate and meaningful.

- It is recommended that the monitoring work be structured as a separate professional services style contract that is based on qualifications versus a bid solicitation that is generally based on cost. Licensed professionals are bound by a code of ethics, an obligation to their profession that carries substantial weight when making decisions. A Professional Surveyor (P.S.) that is experienced in deformation monitoring is likely most qualified to lead the system implementation and data acquisition process. A Professional Engineer (P.E.) that is experienced in deformation monitoring is likely most qualified to lead the system design, threshold determination, and interpretation of results. This recommended structure should help ensure the entire monitoring program is handled by qualified and experienced professionals.
- If the monitoring work must be included as part of the construction bid, it should at a minimum be accomplished under the oversight of a P.S. that is qualified and experienced in the field of deformation monitoring. Under this scenario, the monitoring system design, quality control review, and subsequent interpretation of results should be provided by professionals that have a thorough understanding of the needs of the project; as well as the knowledge and experience necessary to both design a comprehensive system and effectively interpret the data it generates. This should generally be handled

by the project design engineer since they are most familiar with the project or by a separately contracted professional engineering services firm that is experienced and dedicated to the AMTS monitoring quality control and analysis process.

6.4.2 System Protection, Stability, and Network Geometry

Careful consideration must be made when designing a system to ensure it is adequately protected and stable so that unplanned disturbances do not taint monitoring results. The reference network design is also critically important to the quality of the measurements.

- Require the design of the instrument pedestal to be stable, predictable, and in a location that will experience minimal disturbance.
- Require that the instrument be reasonably protected from environmental effects (e.g. direct sun light, moisture, dust, wind, vibrations, etc.).
- Require that the instrument be reasonably protected from vandalism (e.g. damage, theft, etc.)
- Require the design of the reference points to be reasonably stable, predictable, and in locations that will remain undisturbed throughout the project duration.
- Require that the reference network consist of no less than five points distributed in no less than three quadrants. A minimum of three points are necessary to derive error residual values and the other two can provide additional redundancy. In urban environments, instruments and reference prisms are often mounted to buildings to provide an elevated vantage point away from the congested street level. Due to the potentially numerous obstructions encountered in this type of environment, careful consideration should be made when deciding the location of the instrument relative to the reference points and project area. The reference points should be distributed in at least

three, if not all four quadrants. Distributing the angles in this fashion minimizes the amount of error that exists while computing the instrument's position. The reference prisms should also be set at a distance equal to or greater than the farthest monitoring point observation so that measurement errors are controlled within the bounds of the baselines. Ideally the instrument would be located outside the ZOI to minimize potential instrument disturbance. The reference prisms must be mounted outside the ZOI since they will be used as a basis of control and the means by which the instrument's location is determined and verified. In the event it is not possible to mount sufficient reference points outside the ZOI, additional instruments will be required to 'leapfrog' reference observations to a point outside the ZOI. This configuration should be avoided whenever possible as it will compound error in the reference network and increase the cost of instrumentation.

6.4.3 Baseline Acquisition, Accuracy Evaluation, and Thresholds

Accurate and complete baseline acquisition is necessary to understanding overall system accuracies and for defining threshold values. An approach, referred to herein as the Baseline Behavior Analysis (BBA) method, is recommended for these purposes. Baseline models are developed for each monitoring point in each orthogonal direction and statistically significant deviations from these models are used to identify anomalous behavior that may be a result of construction influence. In order to be sensitive enough to detect real movement, the model error must be limited. Construction monitoring specifications generally express real movement as no less than 0.020 feet (6.0 mm). Unless other values have been specified based on structural analysis or other considerations, a model with a minimum accuracy level of +/- 0.010 feet (3.0

mm) would be an appropriate default threshold capable of detecting movement of +/- 0.020 feet (6.0 mm).

- Require baseline observations to occur well in advance of construction for a duration long enough to capture a range of environmental fluctuations consistent with what will be experienced during construction. This may range anywhere from one week to multiple months depending on the location and duration of the project.
- Require that a BBA be performed that identifies accuracy results at a 95% level of confidence for each component of each monitoring point. If the minimum accuracy level of +/- 0.010 feet (3.0 mm) cannot be obtained, the measurements may require additional compensation for temperature or other environmental effects.
- Using the baseline model data, *log*, *review*, and *suspend* alert thresholds are recommended to be established at two, three, and four standard deviations from the mean, respectively, for each component of each monitoring point. A *log* alert would require that the magnitude, location, and time of the exceedance be reported and reviewed during the next regular monitoring system assessment. False alerts occur when a threshold is exceeded but is likely not the result of construction influence but rather measurement noise. False alerts in this range should statistically be limited to approximately 1 in 22 (4.55%). In other words, if measurements are taken hourly, one false alert would be expected on any given day. A *review* alert would require immediate notification of the exceedance to monitoring staff. False alerts in this range should statistically be limited to approximately 1 in 370 (0.27%). A *suspend* alert would require immediate notification to construction personnel to suspend operations in the vicinity of exceedance until

monitoring personnel provide a thorough review. False alerts in this range should statistically be limited to nearly zero, or about 1 in 16,000 (0.006%).

6.4.4 Measurement Corrections and System Verification

Since AMTS instruments utilize Electronic Distance Measurement (EDM) technology which uses electromagnetic energy to measure lengths, changes in atmospheric conditions must be considered since they impact wave velocity. Additionally, the instrument's position should be continuously reevaluated since changes in environmental conditions may shift the support pedestal and the center of the instrument may also become altered after repeated rotations. Periodic testing and verification of the system's effectiveness should also be performed to ensure appropriate results are reported as expected.

- Require that a meteorological sensor be installed in the vicinity of the instrument so that temperature, humidity, and atmospheric pressure values are measured automatically with each cycle of observations and refractivity corrections are updated and applied to the EDM. Temperature readings may also be necessary to identify and compensate for thermally induced measurement fluctuations.
- Require that the computed position of the instrument be verified prior to each monitoring cycle by observing a stable reference network.
- Require that the system be tested and validated utilizing a device such as a triaxial displacement gauge. The test may be performed by manually displacing a monitoring prism and assessing the monitoring system results. The test may be considered successful if the system identifies the displacement and triggers an appropriate alert.

6.5 Summary of Monitoring Specification Guidelines

AMTS has been identified as an effective means to monitor structures adjacent to construction activity. A review of a collection of construction specifications revealed several deficiencies that could be improved upon when developing a monitoring plan. Recommended areas of improvement include contract structure and oversight; system protection, stability, and network geometry; baseline acquisition, accuracy evaluation, and thresholds; and measurement corrections and system verification. The Baseline Behavior Analysis (BBA) method was introduced as a statistical approach to defining threshold values. The following chapter details how this approach may be implemented during AMTS monitoring activities.

CHAPTER VII

DEFINING AMTS MONITORING THRESHIOLDS BY ANALYZING BASELINE BEHAVIOR

7.1 Introduction

Construction of a new building in Brooklyn, New York required AMTS monitoring of an adjacent 40-story building during deep excavation operations. The monitoring program was included as part of the construction bid and did not require a qualified P.S. to manage the system and interpret the results. The construction specifications also lacked requirements related to reference point quantity and geometry, instrument stability, and threshold values. Although the monitoring system met the requirements of the construction specifications, contractor personnel experienced difficulties producing meaningful results. A post-construction review of the datasets was performed to identify some of the problems experienced and to demonstrate how the data may have been used more effectively.

Figure 7.1 illustrates the general layout of the monitoring system. Two AMTS instruments were mounted at the top of the excavation on opposite sides and two reference points (RPs) were installed per instrument, notated as RP-1A, RP-1B, RP-2A, and RP-2B. A total of six monitoring points (MPs) were installed on the adjacent building and excavation shoring. Measurement results from MP-1A and MP-1B are highlighted in this chapter.

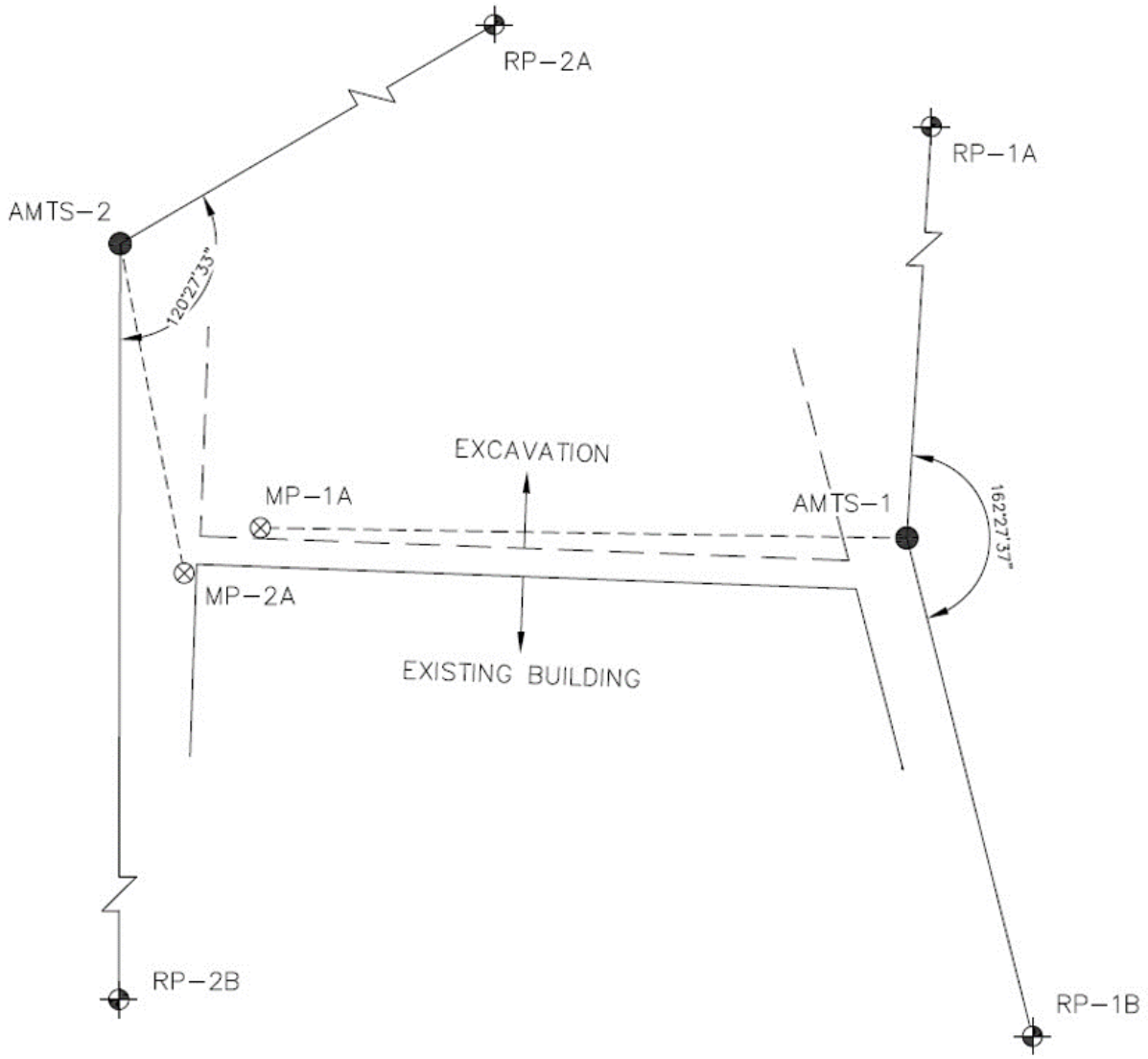

Figure 7.1 Project Layout Plan.

7.2 Establishing a Baseline

The two instruments observed their respective reference and monitoring prisms at a one-hour frequency. An approximate four-week baseline period was initially established, and the raw slope distance and temperature readings were reviewed. The measurements from AMTS-1

to RP-1A indicated a possible inverse relationship between slope distance and temperature (Figure 7.2). Although a temperature sensor was installed, it was apparent that atmospheric corrections were likely not applied to the EDM at the time of measurement. To investigate this further, the relationship between slope distance readings and temperature were evaluated for each reference point measurement and coefficients of determination were found to be 0.7065, 0.7463, 0.5401, and 0.7703 for RP-1A, RP-1B, RP-2A, and RP-2B, respectively.

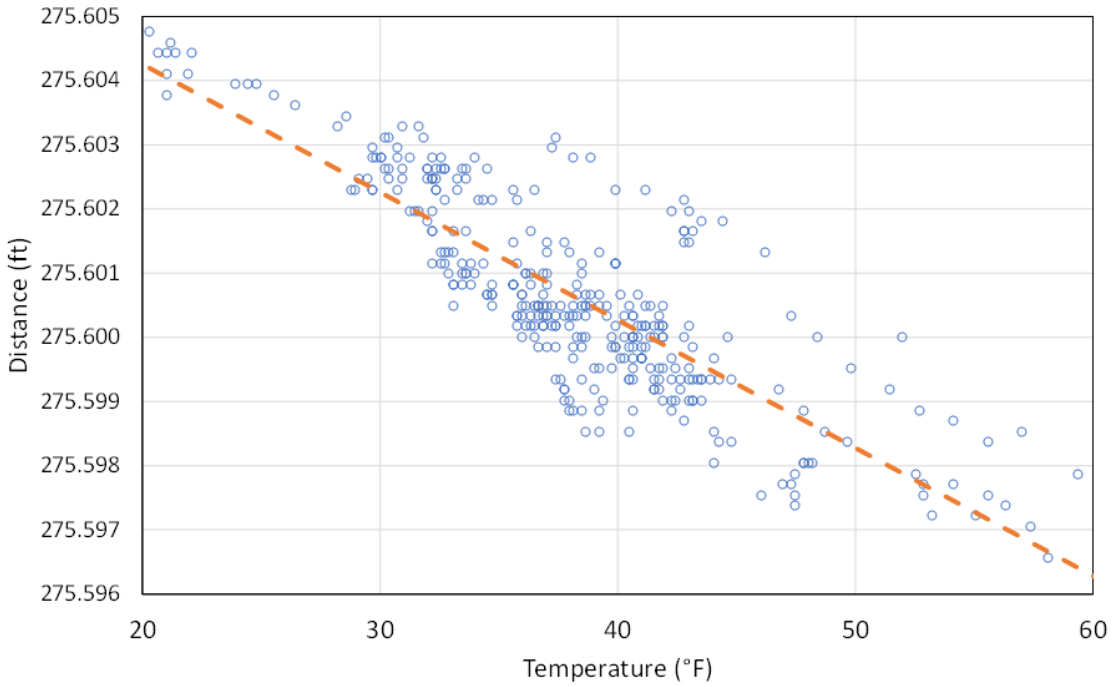

Figure 7.2 RP-1A Baseline Period Distance Measurements

7.2.1 Atmospheric Corrections

Slope distance adjustments were applied based on the refractivity index approximation originally derived by Barrell and Sears (1939) and still used by total station manufactures today

(Leica Geosystems, 2013). The adjustment takes into account ambient temperature, atmospheric pressure, and relative humidity. Since only a temperature sensor was installed at each instrument location, average regional atmospheric pressure and relative humidity values were applied to the adjustment computations. It was determined that the combined effects of atmospheric pressure and relative humidity fluctuations would only result in approximately 3 parts per million of measurement error as opposed to approximately 16 parts per million associated with temperature. Coefficients of determination between adjusted values of slope distance and temperature were reduced to 0.0844, 0.4211, 0.0138, and 0.1708 for RP-1A, RP-1B, RP-2A, and RP-2B, respectively. Any remaining apparent correlations may be associated with environmental variations along the EDM path or thermal movement of the structures supporting the instrument and reference prisms. The EDM path environmental variations may be approximated but would require additional meteorological sensors and specific knowledge of changing parameters, such as sun exposure, along the measurement length (Angus-Leppan and Brunner, 1980). Such parameters would be difficult to measure and would likely vary with time making this correction an unreasonable undertaking that may ultimately have minimal effect on the overall accuracy of the measurement.

7.2.2 Instrument Triangulation

The positions of the AMTS instruments were computed for each hourly cycle of measurements through a triangulation process where the reference point coordinates are held constant and the instrument's coordinates are trigonometrically computed using observed angles and distances. The associated changes in the northing, easting, and elevation components for each instrument position were then plotted. Figures 7.3 and 7.4 illustrate results for AMTS-1 in the easting and elevation components. The large fluctuations observed in the easting component

of AMTS-1 is likely due to the poor geometric orientation of the reference points related to the instrument and the lack of additional reference points necessary to accurately compute the instrument's position. RP-1A and RP-1B are nearly directly north and south of the instrument, resulting in a high level of variability in the easterly/westerly position solution. As discussed in the previous chapter, a minimum of three reference points are required in order to understand how much measurement error may be present, however, five reference points located in multiple quadrants are recommended for additional redundancy.

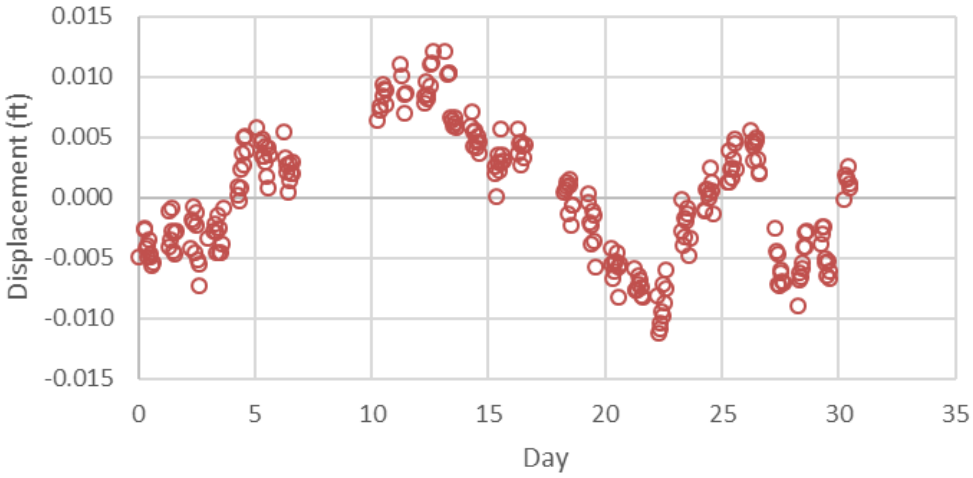

Figure 7.3 AMTS-1: Change in Computed Easting Coordinate.

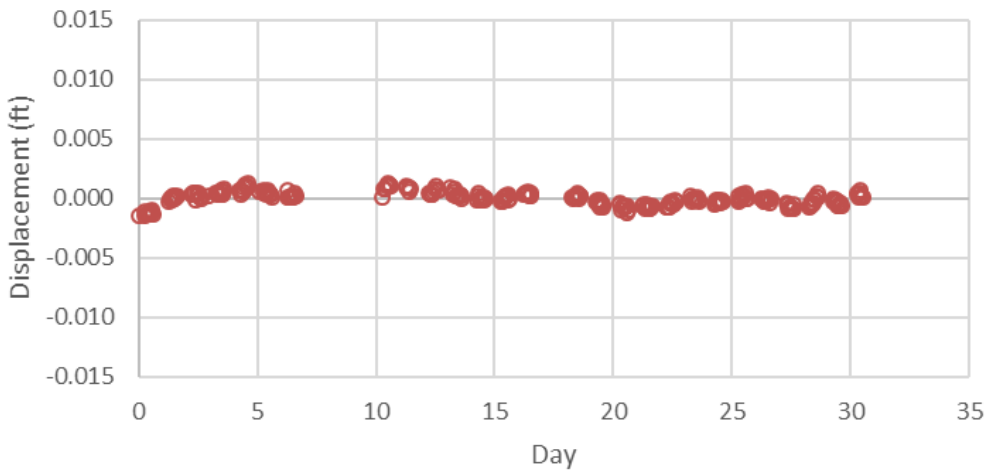

Figure 7.4 AMTS-1: Change in Computed Elevation Coordinate.

7.2.3 Baseline Behavior Analysis

The Baseline Behavior Analysis (BBA) method establishes a baseline mean from which to measure displacements, evaluates displacement deviations to define threshold values, and if needed, incorporates an adjustment to compensate for external influences. Adjustments are necessary when precisions within in the baseline dataset are low. The general form of the model, μ, is defined as:

$$\mu = \bar{y} + \hat{y} \tag{7.1}$$

Where, $\bar{y}$, denotes the mean value for each of the northing, easting, and elevation coordinates, defined as:

$$\bar{y} = \frac{1}{\eta}\sum_{i=1}^{\eta} y_i \tag{7.2}$$

Where y denotes an individual computed coordinate value and η the total number of measurements. Displacements from the model, D, for each measurement can be found by computing the difference between each individual value and the model:

$$D_i = y_i - \mu \tag{7.3}$$

Using measured horizontal angles, zenith angles, and slope distances, the coordinates of MP-1A, a monitoring prism mounted on the shoring system supporting the excavation, were computed for each hourly cycle of baseline measurements based on the triangulated position of AMTS-1. Standard deviations for the northing, easting, and elevation component displacements were computed as ± 0.0028 feet (0.85 mm), ± 0.0053 feet (1.62 mm), and ± 0.0018 feet (0.55 mm), respectively. As discussed in the previous chapter, a minimum displacement of 0.020 feet (6.0 mm) should be detectible, meaning the baseline model should be accurate within ± 0.010 feet (3.0 mm) at a 95% confidence level. The easting component does not meet this level of precision when evaluated at two standard deviations from the mean, requiring an adjustment to the model. Model errors may be reduced by compensating for potential influences on monitoring point behavior. For instance, the structure the monitoring point is mounted on may experience expansions and contractions caused by changes in ambient temperature. Since temperature was measured during the baseline period, a relationship could be investigated. A linear regression analysis was performed to evaluate the relationship between model displacements in the easting component with changes in temperature and a p-value near zero was accepted as an indication that a relationship was likely. The fundamental linear regression model equation for this analysis is represented as (Mendenhall and Sincich, 2012):

$$\hat{y} = \hat{\beta}_0 - \hat{\beta}_1 T \tag{7.4}$$

Where, $\hat{\beta}_0$ denotes the model constant; $\hat{\beta}_1$ the constant associated with the independent variable temperature; and T the value of temperature. Figure 7.5 illustrates the difference between the unadjusted and adjusted models.

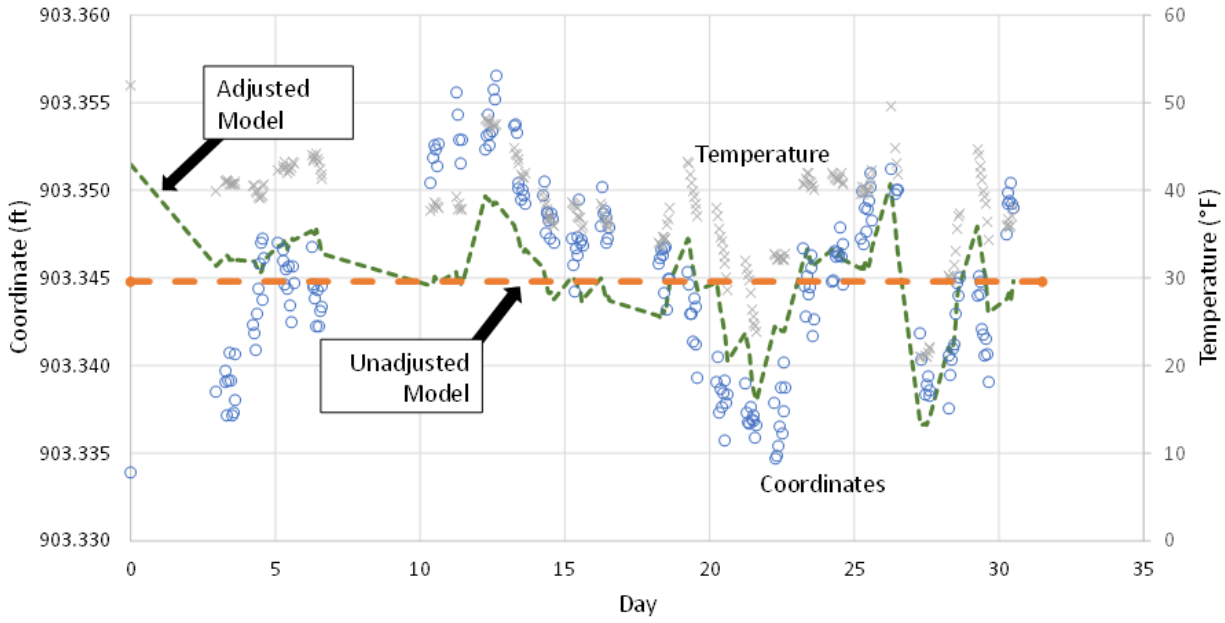

Figure 7.5 MP-1A: Baseline Easting Coordinates and Models

After recomputing displacements, the easting component standard deviation was reduced to ± 0.0043 feet (1.31 mm). This amounts to an error of approximately ± 0.0086 feet (2.62 mm) when evaluated at two standard deviations from the mean, producing a model of appropriate accuracy. It should be noted that the modeled temperature range was between approximately 20

and 50 degrees Fahrenheit (-7 and 10 degrees Celsius). The model would need to be reevaluated for any temperatures experienced outside of this range.

The position of MP-1 B, a prism mounted on the existing building adjacent to the excavation, was then computed for each hourly cycle of measurements and was based on the previously computed position of AMTS-2. Changes in the northing, easting, and elevation components were then determined and standard deviations were found to be ± 0.0040 feet (1.22 mm), ± 0.0021 feet (0.64 mm), and ± 0.0026 feet (0.79 mm), respectively. Errors in each component were found to be less than ± 0.010 feet (3.0 mm) when evaluated at two standard deviations from the mean, therefore no adjustments to the model were necessary for this position.

Finally, *log*, *review*, and *suspend* alert thresholds were established at two, three, and four standard deviations from the mean, respectively, for each component of each monitoring prism. As discussed in the previous chapter, a *log* alert would require that the magnitude, location, and time of the exceedance be reported and reviewed during the next regular monitoring system assessment; a *review* alert would require immediate notification of the exceedance to monitoring staff; and a *suspend* alert would require immediate notification to construction personnel to suspend operations in the vicinity of exceedance until monitoring personnel provide a thorough review. Figures 7.6 and 7.7 illustrate the baseline period position data with alert thresholds overlaid for the easting and elevation components of MP-1A.

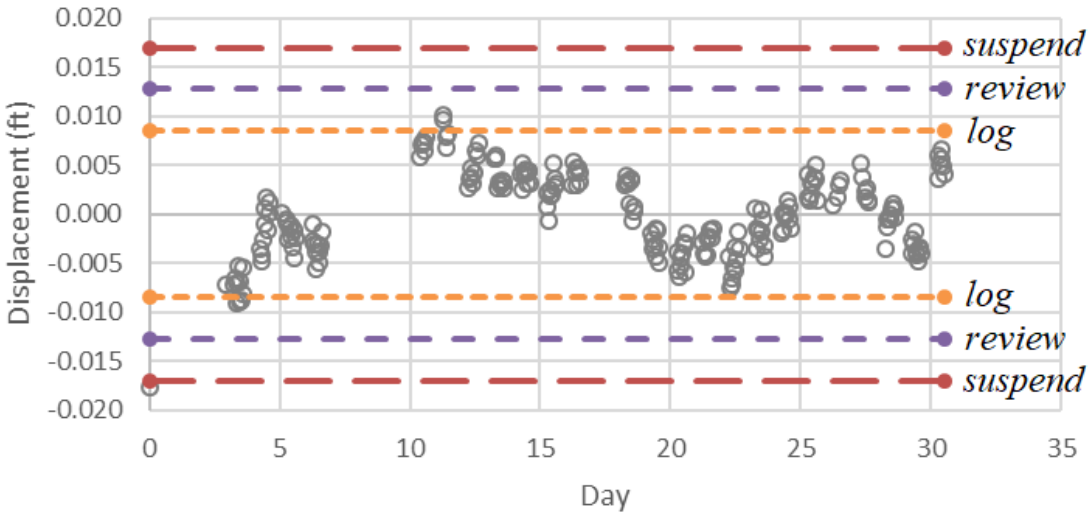

Figure 7.6 MP-1A: Baseline Model & Alert Thresholds for Easting Coordinate.

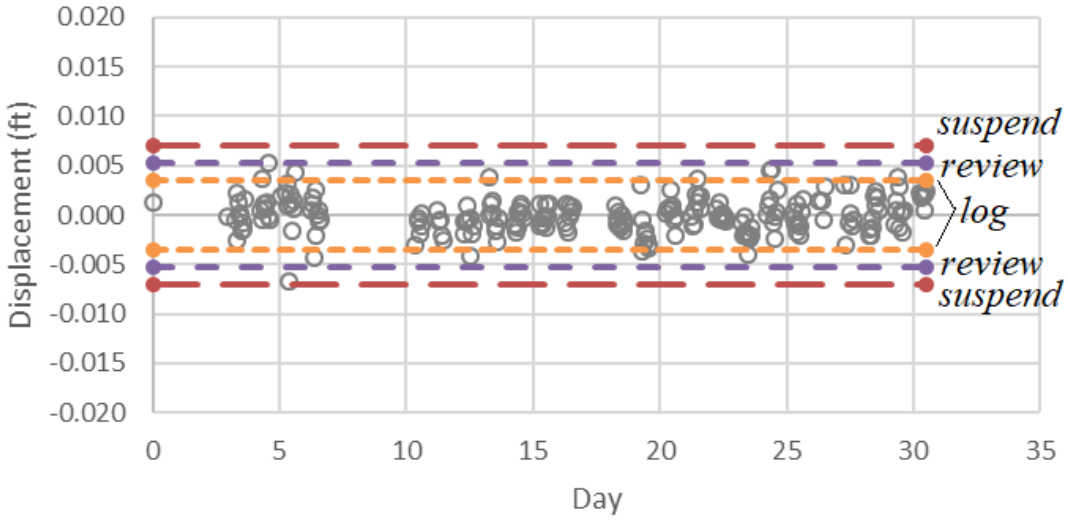

Figure 7.7 MP-1A: Baseline Model & Alert Thresholds for Elevation Coordinate.

7.3 Monitoring Data Evaluation

Data collected during a monitoring period of approximately 130 days was then evaluated against the threshold values that were defined during the baseline period. Trends indicating a drop in elevation and a slight shift to the northeast was identified in the MP-1A data. Figures 7.8 and 7.9 illustrate the monitoring period position data with alert thresholds overlaid for the northing and elevation components of MP-1A. The shift appears to stabilize approximately during the final 50 days of the monitoring period. A 10-day moving average line was also overlaid to illustrate data trends.

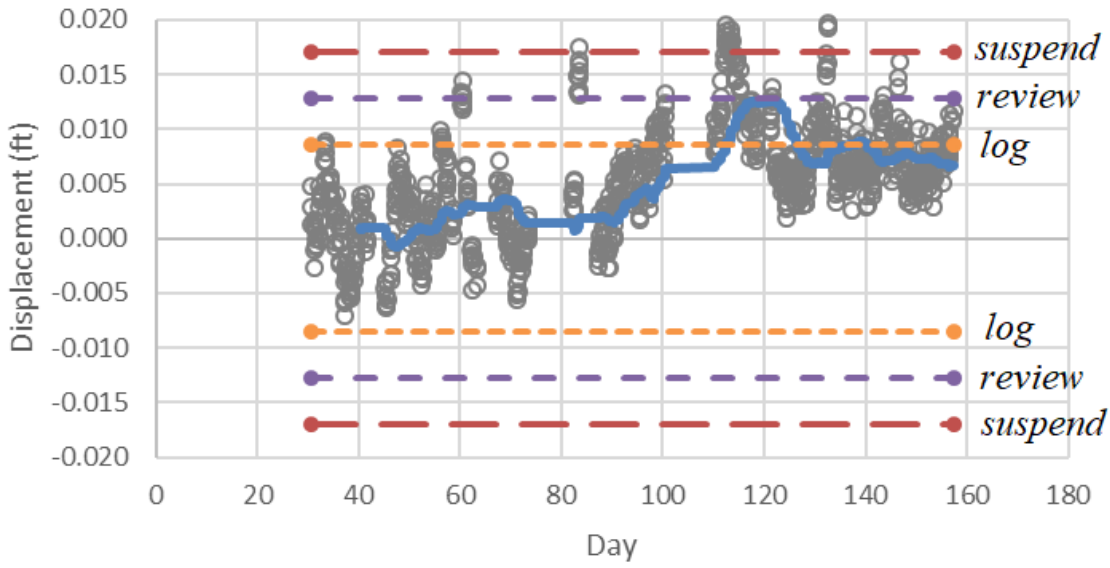

Figure 7.8 MP-1A: Monitoring Data & Alert Thresholds for Easting Coordinate.

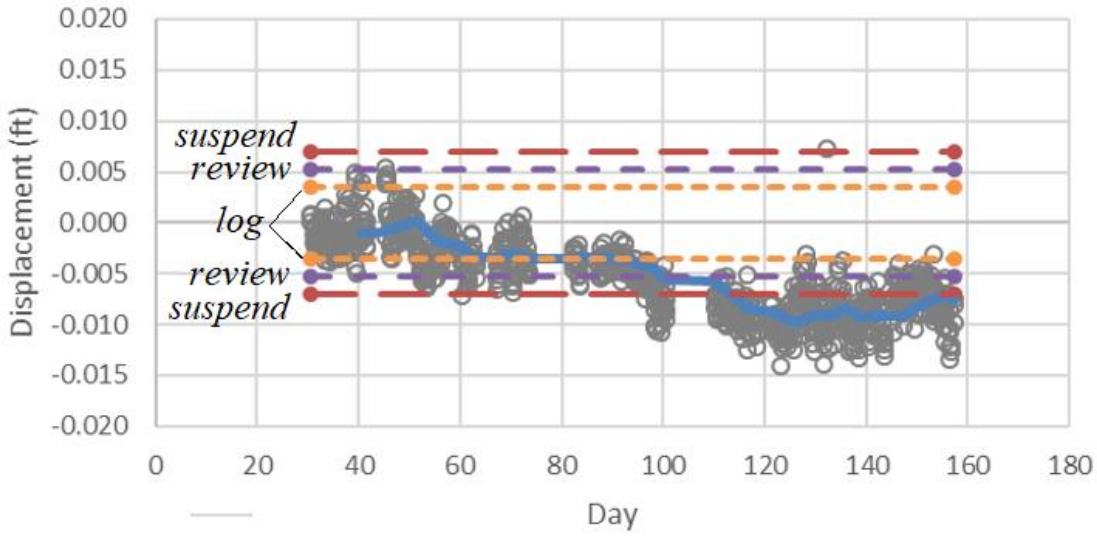

Figure 7.9 MP-1A: Monitoring Data & Alert Thresholds for Elevation Coordinate.

MP-1B indicated a near immediate drop in elevation at the beginning of the monitoring period. Figures 7.10 and 7.11 illustrate the monitoring period displacements with alert thresholds overlaid for the northing and elevation components of MP-1B. AMTS-2 and associated reference and monitoring points began to experience data collection problems soon after, but since no redundant reference points were implemented, there was no way to validate the potential movement. Additionally, AMTS-2 provided little usable data since inadequate reference observations were obtained and positions were not able to be computed after only 25 days into the monitoring period. This may have been a result of blocked or damaged prisms that could have been corrected if investigated properly at the time.

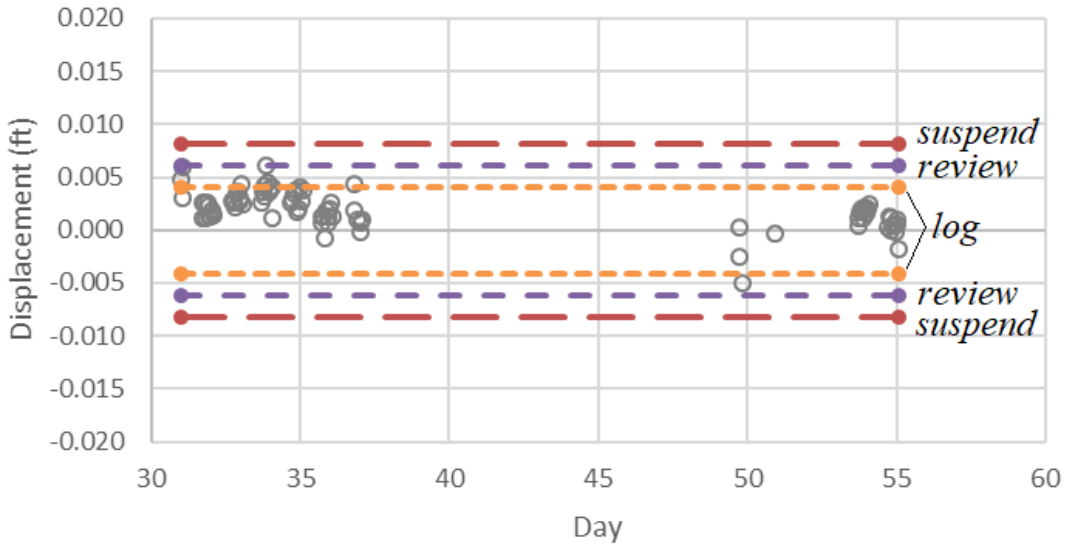

Figure 7.10 MP-1B: Monitoring Data & Alert Thresholds for Easting Coordinate.

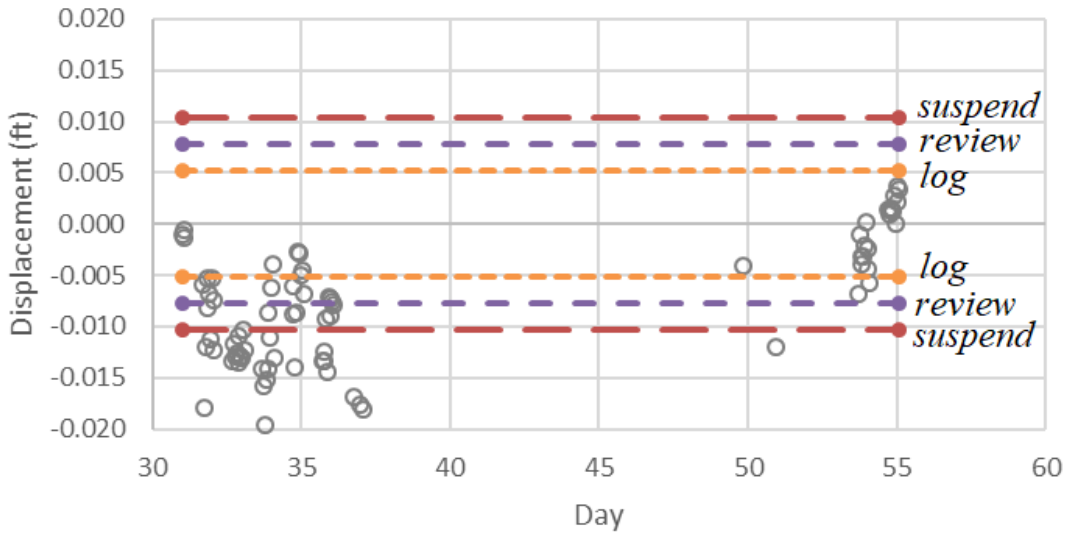

Figure 7.11 MP-1B: Monitoring Data & Alert Thresholds for Elevation Coordinate.

7.4 Summary of Baseline Behavior Analysis

AMTS derived structural deformation monitoring data acquired during excavation operations for a project in Brooklyn, NY was reviewed. Due to vague monitoring specifications and inexperienced monitoring personnel, deficiencies in control network and data acquisition processes were identified. The BBA method has been presented as a means to identify anomalous behavior in structures adjacent to construction activity. Although construction personnel were not alerted during excavation, a post-project review of the data using the BBA method indicates operations should have been suspended around 100 days into the monitoring period to investigate the apparent shift in the shoring structure.

Future research may consider the implementation of other independent variables in the BBA methods, such as gravity loads, due to traffic on a bridge or equipment on a building, and lateral loads, such as wind on a tower or fluid pressures on a dam. Studies may also be dedicated toward the detection of trends prior to threshold exceedance by analyzing displacement velocities and accelerations.

CHAPTER VIII

SUMMARY, CONCLUSIONS, AND RECOMMENDATIONS

8.1 Summary

A variety of structural monitoring applications and methods have been presented in this dissertation. Performance, in-service, and construction monitoring categories have been discussed along with examples of each category. A new performance monitoring approach utilized during construction of the Salesforce Tower project in San Francisco was presented. The primary contribution of this work is that a practical and implementable approach to estimating elevation changes throughout a multi-story reinforced concrete core wall tower during construction while utilizing strain measurements acquired at intermittent levels was presented. Additionally, specification and procedure recommendations related to in-service and construction monitoring activities was discussed and a framework that utilizes baseline data to define threshold values was presented.

8.2 Conclusions

The strain-based elevation monitoring system was successfully implemented during construction of the Salesforce Tower. The approach required strain development estimations between sensors and three methods of varying complexity were used. Although the system imposed a larger up-front cost, the significant reduction in survey labor resulted in an estimated net reduction in monitoring costs of at least 15%. It is estimated that taller towers will

experience greater relative benefit, with cost reductions of at least 40% for buildings on the order of 100 stories tall.

There are several limitations to the strain-based elevation monitoring approach. Because strain gauges only capture behavior at a specific point within a wall, the measurements must be extrapolated to represent the behavior of the entire wall. Because strain variations exist throughout a wall, what is measured may not accurately represent the wall as a whole. For instance, drying shrinkage strains will vary across the wall section, generally leading to the gauge registering a lower strain than what actually exists at the wall surface. Prediction modeling is also limited by environmental conditions, loads, and construction sequencing that will inevitably fluctuate. Data acquisition and quality is also limited by gauge damage and disturbance.

A method that analyzes baseline AMTS measurements was successfully applied to data acquired during an excavation project in Brooklyn, NY. Results of the post-construction analysis clearly identified deficiencies that may not have been apparent to the contractor during construction. The approach may be utilized during construction on projects that similarly utilize AMTS to monitor structural deformations.

Limitations to this approach primarily revolve around the fact that conditions experienced during the baseline period will not exactly represent conditions experienced during the monitoring period. Model adjustments also assume a direct relationship with an independent variable when other unmeasured factors could be influencing the results.

8.3 Recommendations

Future research may explore adjustments to strain measurements based on expected strain variations within a given wall. For instance, measurements could be compensated for variations in drying shrinkage strain through a wall section based on environmental conditions and concrete aging. Implementing strain-based monitoring systems on a variety of towers in different climates should better identify circumstances where each model presented is most applicable. Strain development results from a variety of large volume to surface ratio members can also improve prediction modeling. Because sensors were damaged during the Salesforce Tower project, better techniques to protect strain gauge sensors should be explored.

Improvement upon and standardization of the development of construction monitoring specifications should be further pursued to ensure monitoring systems are properly designed, implemented, and managed throughout the construction process. Implementation of a baseline behavior analysis method in a variety of settings can better identify optimal variables to consider. Although ambient temperature was exclusively considered during review of the Brooklyn project, a variety of variables, including gravity and lateral loads, may be similarly incorporated. Optimal baseline period durations can also be investigated based on what is being monitored and what primary influences are expected.

REFERENCES

Abdelrazaq, A. (2012). Validating the structural behavior and response of Burj Khalifa: synopsis of the full scale structural health monitoring programs. *International Journal of High-Rise Buildings*, *1*(1), 37-51.

Alba, M., Fregonese, L., Prandi, F., Scaioni, M., & Valgoi, P. (2006). *International archives of photogrammetry, remote sensing, and spatial information sciences. 36*(5). 6-11.

Al-Manaseer, A., & Prado, A.. (2015). Statistical comparisons of creep and shrinkage prediction models using RILEM and NU-ITI databases. *ACI Materials Journal*, *112*(1), 125.

American Society of Civil Engineers [ASCE]. (2021). *ASCE's 2021 infrastructure report card.* Washington D.C. 2021. http://www.infrastructurereportcard.org/. Accessed September 2022.

American Concrete Institute [ACI] Committee 209. (2008) Guide for modeling and calculating shrinkage and creep in hardened concrete (ACI 209.2 R-08). *American Concrete Institute*.

American Concrete Institute [ACI] Committee 212. (2016) Report on chemical admixtures for concrete (ACI 212.3 R-16). *American Concrete Institute.*

American Society of Civil Engineers [ASCE] Hydropower Committee. (2000). *Guidelines for instrumentation and measurements for monitoring dam performance*. American Society of Civil Engineers. ISBN 978-0784405314.

Angus-Leppan, P.V., & Brunner, F.K. (1980). Atmospheric temperature models for short-range EDM. *The Canadian Surveyor*, *34*(2), 153-165.

Asadi, I., Shafigh, P., Hassan, Z.F.B.A., & Mahyuddin, N.B. (2018). Thermal conductivity of concrete–A review. *Journal of Building Engineering*, *20*, 81-93.

Ashkenazi, V., Dodson, A.H., Moore, T., & Roberts, G.W. (1997). Monitoring the movements of bridges by GPS. *Proceedings of the 10th International Technical Meeting of the Satellite Division of The Institute of Navigation*, 1165-1172, Kansas City, MO, September 16-19.

Attewell, P.B., Yeates, J., & Selby, A.R. (1986). *Soil movements induced by tunnelling and their effects on pipelines and structures*. Chapman and Hall. ISBN 0216918766.

Baker, W.F., Korista, D.S., Novak, L.C., Pawlikowski, J., & Young, B. (2007). Creep and shrinkage and the design of supertall buildings - a case study: the Burj Dubai Tower. *ACI Special Publication, 246*, 133-148.

Bakoss, S.L., Burfitt, A.J., & Cridland, L. (1977). Measurement of strains in concrete members with vibrating wire strain gauges. *Australian Road Research, 7*(3), 20-26.

Bao, Y., Guo, W., Wang, G., Gan, W., Zhang, M., & Shen, J.S. (2018). Millimeter-accuracy structural deformation monitoring using stand-alone GPS: case study in Beijing, China. *Journal of Surveying Engineering, 1*, 05017007.

Barrell, H., & Sears, J.E. (1939). The refraction and dispersion of air and dispersion of air for the visible spectrum. *Philosophical Transactions of the Royal Society of London. Series A, Mathematical and Physical Sciences, 238*(786), 1-64.

Batten, M., Powrie, W., Boorman, R., & Leiper, Q. (1999). Use of vibrating wire strain gauges to measure loads in tubular steel props supporting deep retaining walls. *Institution of Civil Engineers-Geotechnical Engineering, 137*(1), 3-13.

Bazant, Z. P. (1988). *Mathematical modeling of creep and shrinkage of concrete*. 99-215. John Wiley and Sons. ISBN 0 471920576.

Bazant, Z.P. & Baweja, S. (2000) Creep and shrinkage prediction model for analysis and design of concrete structures: model B3. *ACI Special Publications, 194*, 1-84.

Bazant, Z.P., Jirasek, M., Hubler, M.H., & Carol, I. (2015). RILEM draft recommendation: TC-242-MDC multi-decade creep and shrinkage of concrete: material model and structural analysis. model B4 for creep, drying shrinkage and autogenous shrinkage of normal and high-strength concretes with multi-decade applicability. *Materials and Structures, 48*(4), 753-770.

Bazant, Z.P., Kim, J.K., Wittmann, F.H., & Alou, F. (1987). Statistical extrapolation of shrinkage data—Part II: bayesian updating. *ACI Materials Journal, 84*(2), 83-91.

Bazant, Z.P., & Li, G. (2008). Unbiased statistical comparison of creep and shrinkage prediction models. *ACI Materials Journal, 105*(6), 610-621.

Bazant, Z.P., & Najjar, L.J. (1972). Nonlinear water diffusion in nonsaturated concrete. *Materials and Structures, 5*(1), 3-20.

Bazant, Z.P., & Wang, T. (1984). Spectral analysis of random shrinkage stresses in concrete. *Journal of Engineering Mechanics, 110*(2), 173-186.

Beer, F.P., Johnston, E.R., Jr., & DeWolf, J.T. (2006). *Mechanics of materials (4)*, 46-62. McGraw-Hill. ISBN 0-07-298090-7.

Beresford, F. D. (1970). Measurement of time-dependent behaviour in concrete buildings. *Proceedings of the Fourth Australian Building Research Congress Sydney,* Sydney Australia, 23–26.

Berwanger, C. (1971). The modulus of concrete and the coefficient of expansion of concrete and reinforced concrete at below normal temperatures. *ACI Special Publication, 25*, 191-234.

Blackwell, G.H., & Bonham-Carter, G.F. (1993). Remote robotic real time slope monitoring with motorized total station survey instruments. *Proceedings of APCOM XXIV: International Symposium on the Application of Computers and Operations Research in the Mineral Industries*, 493-500, Montreal, Quebec, Canada, October 31-November 3.

Boscardin, M.D., & Cording, E.J. (1989). Building response to excavation-induced settlement. *Journal of Geotechnical Engineering, 115*(1), 1-21.

Brady, E. A. (1985). Movements of reinforced concrete buildings. *Australian Surveyor, 32*(8), 602-614.

Brownjohn, J., Rizos, C., Tan, G.H., & Pan, T.C. (2004). Real-time long-term monitoring and static and dynamic displacements of an office tower, combining RTK GPS and accelerometer data. *Proceedings of the 1st FIG International Symposium on Engineering Surveys for Construction Works and Structural Engineering,* TS1.9.1-TS1.9.15, Nottingham, UK, June 28- July 1.

Brownjohn, J. M. (2007). Structural health monitoring of civil infrastructure. *Philosophical Transactions of the Royal Society A: Mathematical, Physical and Engineering Sciences*, *365*(1851), 589-622.

Celebi, M. (2000). GPS in dynamic monitoring of long-period structures. *Soil Dynamics and Earthquake Engineering*, *20*(5-8), 477-483.

Comité Euro-International du Béton [CEB] (1999) *Structural concrete – textbook on behaviour, design and performance. Updated Knowledge of the CEB/FIP Model Code 1990, 2,* 37-52, Fédération Internationale du Béton.

Choi, S.W., Kim, Y., Kim, J.M., & Park, H.S. (2013). Field monitoring of column shortenings in a high-rise building during construction. *Sensors*, *13*(11), 14321-14338.

Cronin, A. (2020, October 6). Chief Surveyor, RSC Concrete, New York. Personal interview.

Council on Tall Buildings and Urban Habitat [CTBUH] Skyscraper Center. (2022, July 25). *Skyscraper Database.* https://web.archive.org/web/20221025163759/https://www.skyscrapercenter.com/buildings

Dail, E.B., & Volterra, J.L. (2009). Instrumentation and monitoring trends in New York City and beyond. *Geotechnical Instrumentation News*, 27(3), 31-34.

Ding, X., Ren, D., Montgomery, B., & Swindells, C. (2000). Automatic monitoring of slope deformations using geotechnical instruments. *Journal of Surveying Engineering, 126*(2), 57-68.

Domosh, M. (1988). The symbolism of the skyscraper: case studies of New York's first tall buildings. *Journal of Urban History, 14*(3), 320-345.

Duffy, M., Hill, C., Whitaker, C., Chrzanowski, A., Lutes, J., & Bastin, G. (2001). An automated and integrated monitoring program for Diamond Valley Lake in California. *Proceedings of the 10th FIG Symposium on Deformation Measurements,* 1-21, Orange, CA, March 19-22, 19.

Dunnicliff, J., Powderham, A., & MacDonald, M. (2001). Recommendations for procurement of geotechnical instruments and field instrumentation services. *Geotechnical News, 19*(3), 30-35.

Eschmann, C., & Wundsam, T. (2017). Web-based georeferenced 3D inspection and monitoring of bridges with unmanned aircraft systems. *Journal of Surveying Engineering, 143*(3), 04017003.1-04017003.10.

Fintel, M., Ghosh, S.K., & Iyengar, H. (1987) *Column shortening in tall structures - prediction and compensation.* Portland Cement Association. ISBN 0-89312-083-9.

Fragomeni, S., Whaikawa, H., Boonlualoah, S., & Loo, Y.C. (2014). Axial shortening in an 80-storey concrete building. *Proceedings of the 23rd Australasian Conference on the Mechanics of Structures and Materials, 2,* 1231-1236, Southern Cross University, Lismore, NSW, December 9-12.

Gardner, N. J. (2004). Comparison of prediction provisions for drying shrinkage and creep of normal strength concretes. *Canadian Journal of Civil Engineering, 31*(5), 767-775.

Gardner, N.J., & Lockman, M.J. (2001). Design provisions for drying shrinkage and creep of normal-strength concrete. *ACI Materials Journal, 98*(2), 159-167.

Gaxiola-Camacho, J.R., Vazquez-Ontiveros, J.R., Guzman-Acevedo, G.M., Bennett, R.A., Reyes-Blanco, J.M., & Vazquez-Becerra, G.E. (2021). Real-time probabilistic structural evaluation of bridges using dynamic displacements extracted via GPS technology. *Journal of Surveying Engineering, 147*(2), 04021002.

Geymayer, H. G. (1968). Strain meters and stress meters for embedment in models of mass concrete structures. *Technical Report No. 6-811 US Army Corps of Engineers, 1,* Office, Chief of Engineers U.S. Army, Vicksburg, Mississippi.

Ghilani, C.D. (2018) *Elementary surveying: an introduction to geomatics* (15), 347-348. Pearson. ISBN 9780134604657.

Goel, R., Kumar, R., & Paul, D.K. (2007). Comparative study of various creep and shrinkage prediction models for concrete. *Journal of Materials in Civil Engineering*, 19(3), 249-260.

Green, G. E. (2000). Geotechnical instrumentation practice problems, and future trends. *Geotechnical News*, *18*(2), 36-42.

Greulich, G., & Rober, C. (1988). Monitoring of high-rise buildings. *Journal of Surveying Engineering*, *114*(1), 26-36.

Gribniak, V., Kaklauskas, G., Kliukas, R., & Jakubovskis, R. (2013). Shrinkage effect on short-term deformation behavior of reinforced concrete–when it should not be neglected. *Materials & Design*, *51*, 1060-1070.

Hajek, P., & Fiala, C. (2018). Advanced concrete structures for the sustainable- and resilient-built environment. *ACI Special Publication, 326*, 69.1-69.8.

Habrah, A., & Abu-Tair, A. (2017). The reliability of the ACI 209R-92 method in predicting column shortening in high-rise concrete buildings. *Proceedings of the International Sustainable Buildings Symposium*, 396-412, Dubai, UAE, March 15-17.

Ha, T., & Lee, S. (2016). Construction of complex RC tall building considering time-dependent properties of concrete and construction sequence. *Proceedings of the 2016 Structures Congress.* Jeju Island, Korea, August 28-September 1.

Hameed, A., Fernando, G.F., Hetherington, J.G., Brown, R.D., Leng, J., & Barnes, R.A. (2002). Investigation of strain transfer to a sensor protection system embedded in concrete using finite element analysis. *Materials and Structures*, *35*(9), 557-563.

Harwin, J. M. (1979). A review of survey control of tall buildings, tunnels and shafts. *Australian Surveyor*, *29*(5), 348-352.

Hayes, D.M., Sparks, I.R., & van Cranenbroeck, J. (2006). Core wall survey control system for high rise buildings. *Proceedings of Shaping the Change XXIII FIG Congress*, 1-12, Munich, Germany, October 8-13.

Heiman, J.L., Bakoss, S.L., Burfitt, A.J., & Cridland, L. (1980). Measured and predicted axial strains and deformations in a column of a tall reinforced concrete building. *Transactions of the Institution of Engineers of Australia, Civil Engineering. 22*(3), 193-201.

Hubler, M.H., Wendner, R., & Bazant, Z.P. (2015). Comprehensive database for concrete creep and shrinkage: analysis and recommendations for testing and recording. *ACI Materials Journal*, *112*(4), 547-558.

Im, S.B., Hurlebaus, S., & Kang, Y.J. (2013). Summary review of GPS technology for structural health monitoring. *Journal of Structural Engineering*, *139*(10), 1653-1664.

Kaalberg, F.J., Braakman, S., & Cook, D.K. (2003). Amsterdam Noord/Zuidlijn: one of the largest settlement monitoring projects in Europe. *Proceedings of the 6th Symposium Field Measurements in Geomechanics,* Oslo, Norway, September 15-18, 769-774.

Kang, S., Choi, J., Kim, H., & Kim, I. (2011). Prediction and compensation of column shortening for Bitexco Financial Tower. *Proceedings of the CTBUH 2011 World Conference,* 812-818, Seoul, Korea, October 10-12.

Kaplan, R.M., Chambers, D.A., & Glasgow, R.E. (2014). Big data and large sample size: a cautionary note on the potential for bias. *Clinical and Translational Science, 7*(4), 342-346.

Kenchington, A. (2003). *Monitoring building structures*: *automatic and autonomous monitoring*, 96-137. Springer. ISBN 0-203-16886-0.

Kim, H., & Cho, S. (2005) Column shortening of concrete cores and composite columns in a tall building. *The Structural Design of Tall and Special Buildings, 14*(2), 175-190.

Kim, H., Jeong, S., Shin, S. (2012). Column shortening analysis of tall buildings with lumped construction sequences. *The Structural Design of Tall and Special Buildings, 21*(10), 764-776.

Kim, J.K., & Lee, C.S. (1998). Prediction of differential drying shrinkage in concrete. *Cement and Concrete Research, 28*(7), 985-994.

Klemczak, B., & Knoppik-Wrobel, A. (2014) Analysis of early-age thermal and shrinkage stresses in reinforced concrete walls. *ACI Structural Journal, 111*(2), 313-322.

Koutsoftas, D.C., Frobenius, P., Wu, C.L., Meyersohn, D., & Kulesza, R. (2000). Deformations during cut-and-cover construction of Muni Metro Turnback project. *Journal of Geotechnical and Geoenvironmental Engineering, 126*(4), 344-359.

Kropacek, M., Cajka, R., & Mynarcik, P. (2019). Volume changes of concrete in interaction with sliding joint. *Proceedings of the 13th International Conference, Modern Building Materials, Structures, and Techniques,* 387-393, Vilnius, Lithuania, May 16-19.

Kwak, E., Detchev, I., Habib, A., El-Badry, M., & Hughes, C. (2013). Precise photogrammetric reconstruction using model-based image fitting for 3D beam deformation monitoring. *Journal of Surveying Engineering, 139*(3), 143-155.

Lawrence, A.M., Tia, M., Ferraro, C.C., & Bergin, M. (2012). Effect of early age strength on cracking in mass concrete containing different supplementary cementitious materials: experimental and finite-element investigation. *Journal of Materials in Civil Engineering, 24*(4), 362-372.

Leica Geosystems. (2019). *Leica Geosystems innovative vertical alignment system keeps 432 Park Ave. plumb*. https://web.archive.org/web/20221129192945/https://leica-geosystems.com/-/media/files/leicageosystems/case-studies/monitoring/innovative%20vertical%20alignment%20system%20keeps%20432%20park%20ave%20plumbnts.ashx

Leica Geosystems. (2013). *Leica MS50/TS50/TM50–User Manual*. https://web.archive.org/web/20221028091618/http://docs.onepointsurvey.com/pdf/Leica-MS50-TS50-TM50-user-manual.pdf

Leica Geosystems (2007). *Leica TPS1200+: A telescope with opto-mechanical design, white paper*. https://web.archive.org/web/20220204070655/https://www.gefos-leica.cz/ftp/White_papers/Total_stations/Leica_TPS1200+_Whitepaper_0709_762676_en.pdf

Li, M., Koks, E., Taubenbock, H., & Vliet, J.V. (2020). Continental-scale mapping and analysis of 3D building structure. *Remote Sensing of Environment, 245*, 111859.

Li, X., Ge, L., Ambikairajah, E., Rizos, C., Tamura, Y., & Yoshida, A. (2006). Full-scale structural monitoring using an integrated GPS and accelerometer system. *GPS Solutions*, *10*(4), 233-247.

Li, X., Rizos, C., Peng, G.D., Ge, L. (2004). Integration of GPS, accelerometer and optical fiber sensors for structural deformation monitoring. *Proceedings of the 17th International Technical Meeting of the Satellite Division of The Institute of Navigation,* 211-224, Long Beach, CA, September 21-24.

Lienhart, W., Ehrhart, M., & Grick, M. (2017). High frequent total station measurements for the monitoring of bridge vibrations. *Journal of applied geodesy*, *11*(1), 1-8.

Liu, S., & Wang, Z. (2008). *Landslides and engineered slopes: choice of surveying methods for landslides monitoring*, 1211-1216. Taylor & Francis Group. ISBN 978-0-415-41196-7.

Lovse, J.W., Teskey, W.F., Lachapelle, G., & Cannon, M.E. (1995). Dynamic deformation monitoring of tall structure using GPS technology. *Journal of Surveying Engineering*, *121*(1), 35-40.

Lowry, Ben. (2018, June 20). Instrumentation Specialist, Sensemetrics, Colorado. Personal interview.

Lu, Q., & Lee, S. (2017). Image-based technologies for constructing as-is building information models for existing buildings. *Journal of Surveying Engineering, 31*(4), 04017005.1-04017005.14

Luo, Y., Chen, J., Xi, W., Zhao, P., Li, J., Qiao, X., Liu, Q. (2017). Application of a total station with RDM to monitor tunnel displacement. *Journal of Performance of Constructed Facilities, 31*(4), 04017030.1-04017030.11.

Markic, T., Amin, A., & Kaufmann, W. (2018). Stress field solution for strip loaded reinforced concrete blocks. *Engineering Structures*, *171*, 911-920.

Matar, S.S., & Faschan, W.J. (2017). A structural engineer's approach to differential vertical shortening in tall buildings. *International Journal of High-Rise Buildings, 6*(1), 73-82.

McFarland, D.A., & McFarland, H.R. (2015). Big data and the danger of being precisely inaccurate. *Big Data & Society*, *2*(2), 1-4.

McGee, Nathan. (2018, July 10). Instrumentation Specialist, Sensemetrics, California. Personal interview.

Mendenhall, W., & Sincich, T. (2012) *Regression analysis: a second course in statistics* (Vol. 7), 166-182. Pearson. ISBN 0-321-69169-5.

Moss, R.M., & Matthews, S.L. (1995). In-service structural monitoring. a state-of-the-art review. *Structural Engineer*, *73*(2), 23-31.

National Archives of Singapore [NAS]. (2005). https://web.archive.org/web/20221129194804/https://www.nas.gov.sg/archivesonline/data/pdfdoc/20050513987.pdf

Neild, S.A., Williams, M.S., & McFadden, P.D. (2005). Development of a vibrating wire strain gauge for measuring small strains in concrete beams. *Strain, 41*(1), 3-9.

Neville, A.M. (2011). *Properties of concrete (5th Ed.)*. Pearson Education Limited.

Niknezhad, D., Kamali-Bernard, S., & Mesbah, H. (2017). Self-compacting concretes with supplementary cementitious materials: shrinkage and cracking tendency. *Journal of Materials in Civil Engineering*, *29*(7), 04017033.1-04017033.11.

Oh, S. (2020, October 26). Solutions Engineer, Sensemetrics, Vancouver, BC. Personal interview.

Paiovici, R., Bucuresti, S., & Ionescu, S. (2004). About concrete consolidation and vibration. *The Annals of University of Galati Fascicle XIV Mechanical Engineering,* 71-76. ISSN 1224-5615.

Pan, Z., Lu, Z., & Fu, C.C. (2011). Experimental study on creep and shrinkage of high-strength plain concrete and reinforced concrete. *Advances in Structural Engineering*, *14*(2), 235-247.

Peronto, J., Sinn, R., & Huizinga, M. (2017). Vertical shortening considerations in the 1 km tall Jeddah Tower. *International Journal of High-Rise Buildings*, *6*(1), 21-31.

Potocki, F. P. (1958). Vibrating-wire strain gauge for long-term internal measurements in concrete. *The Engineer*, *206*, 964-967.

Price, G., Longworth, T.I., & Sullivan, P.J.E. (1994). Installation and performance of monitoring systems at the Mansion House. *Proceedings of the Institution of Civil Engineers-Geotechnical Engineering, 107*(2), 77-87.

Psimoulis, P.A., & Stiros, S.C. (2008). Experimental assessment of the accuracy of GPS and RTS for the determination of the parameters of oscillation of major structures. *Computer-Aided Civil and Infrastructure Engineering, 23*(5), 389-403.

Quirion, M., & Ballivy, G. (2000). Concrete strain monitoring with Fabry-Pérot fiber-optic sensor. *Journal of Materials in Civil Engineering, 12*(3), 254-261.

Raziq, N., & Collier, P. (2007). GPS deflection monitoring of the West Gate Bridge. *Journal of Applied Geodesy, 1*(1), 35-44.

Resop, J.P., & Hession, W.C. (2010). Terrestrial laser scanning for monitoring streambank retreat: Comparison with traditional surveying techniques. *Journal of Hydraulic Engineering, 136*(10), 794-798.

Roberts, G.W., Meng, X., & Dodson, A.H. (2004). Integrating a Global Positioning System and Accelerometers to Monitor the Deflection of Bridges. *Journal of Surveying Engineering, 130*(2), 65-72.

Roberts, W.S., Heywood, R.J., & McKenzie, C.K. (2003). Protecting heritage masonry structures from explosive blasts. *Australian Journal of Civil Engineering, 1*(1), 67-76.

Roy, D.S., & Gouvin, P. (2007). Applications and limitations of automated motorized total stations. *Proceedings of the 7th FMGM 2007: Field Measurements in Geomechanics*, 1229-1240, Boston, MA, September 24-27.

Schindler, A.K., & Folliard, K.J. (2005). Heat of hydration models for cementitious materials. *ACI Materials Journal, 102*(1), 24-33.

Sellevold, E.J., & Bjontegaard, O. (2006). Coefficient of thermal expansion of cement paste and concrete: mechanisms of moisture interaction. *Materials and Structures, 39*(9), 809-815.

Soil Instruments, Ltd. 2018. (2022, November 20). https://web.archive.org/web/2/http://www.itmsoilsupport.com/manuals/Man142_Vibrating_Wire_Embedment_Strain_Gauge.pdf

Stein, K. (2020, October 17). Sr. Project Manager, BKF Engineers, California. Personal interview.

Stiros, S.C., Vichas, C., Skourtis, C. (2004). Landslide monitoring based on geodetically derived distance changes. *Journal of Surveying Engineering, 130*(4), 156-162.

Sullivan, R. (2020, October 2) Principal Surveyor, Psomas, California. Personal interview.

Swamy, R.N., & Arumugasaamy, P. (1978). Deformations in service of reinforced concrete columns. *ACI Special Publication, 55*, 375-408.

Tejedor, C. (2021, June 24). FIU professor: collapsed Surfside building showed signs of subsidence in '90s. *FIU News.* https://web.archive.org/web/2/https://news.fiu.edu/2021/fiu-professor-collapsed-surfside-building-showed-signs-of-subsidence-in-90s-era-space-radar-data

Turcry, P., Loukili, A., Haidar, K., Pijaudier-Cabot, G., & Belarbi, A. (2006). Cracking tendency of self-compacting concrete subjected to restrained shrinkage: experimental study and modeling. *Journal of Materials in Civil Engineering*, *18*(1), 46-54.

van Cranenbroeck, J., Hayes, D., Oh, S.H., & Haider, M. (2009). Core wall control survey – state of the art. *Proceedings of the 7th FIG Regional Conference,* 19-22, Hanoi, Vietnam, October 19-22.

van Oosterhout, G. P. C. (2003). Recent Dutch experiences in developing structural monitoring systems to shield driven tunnels. *HERON*, *48*(1), 65-78.

Wagner, N., Largent, M., Curran, H., & Murphy, D. (2022). Foundation performance of the Millennium Tower in San Francisco, California: one-dimensional settlement analysis. *Geo-Congress 2022: Site and Soil Characterization, Computational Geotechnics, Risk, and Lessons Learned,* 359-373, ISBN (PDF) 9780784484036.

Watson, C., Watson, T., and Coleman, R. (2007). Structural monitoring of cable-stayed bridge: analysis of GPS versus modeled deflections. *Journal of Surveying Engineering*, *133*(1), 23-28.

Weissgerber, F., Colin-Koeniguer, E., Nicolas, J., & Trouve, N. (2017). 3D monitoring of buildings using TerraSAR-X InSAR, DInSAR and PolSAR capacities. *Remote Sensing*, 9(10), 1010.4-1010.24.

Whitlow, R.D., Haskins, R., McComas, S.L., Crane, C.K., Howard, I.L., & McKenna, M.H. (2019). Remote bridge monitoring using infrasound. *Journal of Bridge Engineering, 24*(5), 04019023.

Whitlow, R.D., Howard, I.L., Jordan, A.M., McComas, S.L., McKenna, M.H. (2020). Infrastructure Structural Health Monitoring via Infrasound. *Proceedings of Structures Congress 2020,* Apr 05-08, St. Louis, MO, 239-250.

Wolf, P.R. (2002). Surveying and mapping: history, current status, and future projections. *Journal of Surveying Engineering*, *128*(3), 79-107.

Yang, K., Yan, L., Huang, G., Chen, C., & Wu, Z. (2016). Monitoring building deformation with InSAR: experiments and validation. *Sensors*, *16*(12), 2182.1-2182.16.

Yu, F., & Gupta, N. (2005). An efficient model for improving performance of vibrating-wire instruments. *Measurement, 37*(3), 278-283.

Zebker, H.A., & Villasenor, J. (1992). Decorrelation in interferometric radar echoes. *IEEE Transactions on Geoscience and Remote Sensing*, *30*(5), 950-959.

Zhang, J., Huang, Y., Qi, K., Gao, Y. (2012). Interior relative humidity of normal-and high-strength concrete at early age. *Journal of Materials in Civil Engineering*, *24*(6), 615-622.

Zou, D., Liu, T., Teng, J., Du, C., & Li, B. (2014). Influence of creep and drying shrinkage of reinforced concrete shear walls on the axial shortening of high-rise buildings. *Construction and Building Materials*, *55*, 46-56.